

1
2
3
4
5
6
7
8
9
10
11
12
13
14
15
16

Atmospheric gas-phase composition over the Indian Ocean

Susann Tegtmeier¹, Christa Marandino², Yue Jia¹, Birgit Quack², Anoop S. Mahajan³

¹Institute of Space and Atmospheric Studies, University of Saskatchewan, Saskatoon, Canada

²GEOMAR Helmholtz Centre for Ocean Research Kiel, 24105 Kiel, Germany

³Center for Climate Change Research, Indian Institute of Tropical Meteorology, Pune,
411016, India

1 Abstract

2
3 The Indian Ocean is coupled to atmospheric dynamics, ~~transport~~ and chemical composition via
4 several unique mechanisms, such as the seasonally varying monsoon circulation. During the
5 winter monsoon season, high pollution levels are regularly observed over the entire northern
6 Indian Ocean, while during the summer monsoon, clean air dominates the atmospheric
7 composition, leading to distinct chemical regimes. The changing atmospheric composition over
8 the Indian Ocean can interact with oceanic biogeochemical cycles and impact marine
9 ecosystems, resulting in potential climate feedbacks.

10 Here, we review current progress in detecting and understanding atmospheric gas-phase
11 composition over the Indian Ocean and its local and global impacts. The review ~~takes into~~
12 ~~account~~ considers results from recent Indian Ocean ship campaigns, satellite measurements,
13 station data and information on continental and oceanic trace gas emissions. The distribution
14 of all major pollutants and greenhouse gases shows pronounced differences between the
15 landmass source regions and the Indian Ocean with strong gradients over the coastal areas.
16 Surface pollution and ozone are highest during the winter monsoon over the Bay of Bengal and
17 the Arabian Sea coastal waters due to air mass advection from the Indo-Gangetic Plain and
18 continental outflow from Southeast Asia.

19 We observe, however, that unusual types of wind patterns can lead to pronounced deviations
20 of the typical trace gas distributions. For example, the ozone distribution maxima shift to
21 different regions under ~~different~~ wind scenarios that differ from the typical seasonal transport
22 patterns. The distribution of greenhouse gases over the Indian Ocean shows many similarities
23 when compared to the pollution fields, but also some differences of the latitudinal and seasonal
24 variations resulting from their long lifetimes and biogenic sources. Mixing ratios of greenhouse
25 gases such as methane show positive trends over the Indian Ocean, but long-term changes of
26 pollution and ozone, and in particular how they are driven by changing emissions and transport
27 patterns, require further investigation in the future. Although we know that changing
28 atmospheric composition and perturbations within the Indian Ocean affect each other, the
29 impacts of atmospheric pollution on oceanic biogeochemistry and trace gas cycling is severely
30 understudied. We highlight potential mechanisms, future research topics and observational
31 requirements that need to be explored in order to fully understand such interactions and
32 feedbacks ~~between the ocean and atmosphere~~ in the Indian Ocean region.

34 1. Introduction

35 Over the Indian Ocean, intense anthropogenic pollution from Southeast Asia mixes with
36 pristine oceanic air. The interplay of the polluted continental and the clean oceanic air masses,
37 and the resulting atmospheric composition are determined by distinct seasonal circulation
38 patterns. The large-scale monsoon circulations in combination with anthropogenic emissions
39 from southern Asia lead to seasonally contrasting chemical regimes over the Indian Ocean. As
40 the anthropogenic emissions include relatively large contributions from biofuel/biomass
41 combustion and incomplete industrial burning, the atmospheric composition during polluted
42 periods shows unique characteristics when compared to other regimes. The complex mixture
43 of chemical constituents and large-scale transport patterns can have a profound influence on
44 oceanic processes, stratospheric composition, and neighbouring regions such as the
45 Mediterranean and Africa. ~~Here, we review~~ This article provides a review of the recent progress
46 in ~~detecting and our~~ understanding of the atmospheric gas-phase composition over the Indian
47 Ocean and ~~its local and global impact~~ how it impacts the ocean and upper atmosphere. This
48 article is part of the special issue ‘Understanding the Indian Ocean system: past, present and
49 future’.

1

2 1.1 Region

3 The Indian Ocean is the world's third largest ocean covering 19.8% of the water on the Earth's
4 surface. In contrast to the Pacific and Atlantic Oceans, it does not stretch from pole to pole, but
5 is enclosed on three sides by major landmasses and an archipelago. The Indian Ocean is centred
6 on the Indian Peninsula, which also forms the northern border together with Iran, Pakistan, and
7 Bangladesh. In the west, the Indian Ocean is bounded by East Africa and the Arabian Peninsula,
8 while the eastern and southern boundaries are set by Southeast Asia, Australia, and the Southern
9 Ocean.

10 The countries bordering the Indian Ocean ~~include a wide variety of races, cultures, and~~
11 ~~religions. They~~ are home to one-third of the world's population accounting for approximately
12 2.5 billion people (Roser et al., 2013). The economies of many Indian Ocean countries are
13 expanding rapidly, with India being the fastest growing major economy in the world. Similarly,
14 many Indian Ocean countries show a rapid population growth, which is expected to further
15 increase in the future. Given the quickly growing populations and industries, the Indian Ocean
16 is becoming a pivotal zone of strategic political competition. At the same time, the Indian Ocean
17 hosts a large variety of marine ecosystems including coral reefs, seagrass beds, and mangrove
18 forests. Anthropogenic activities along the coastlines and climate change threaten biodiversity
19 in the Indian Ocean, which contains 25% of the Earth's biodiversity hotspots (Mittermeier et
20 al., 2011).

21 Growing populations also lead to rapidly increasing anthropogenic emissions. Burning
22 conditions are often poorly controlled, as for instance during biofuel burning in cook-stoves,
23 and fossil fuel burning in vehicles (Li et al., 2017). Together with burning of coal and other
24 fossil fuels for energy production, this leads to large emissions of man-made trace species
25 including greenhouse gases and ozone precursors (e.g., Lawrence, 2004). In addition, primary
26 aerosols, such as soot and dust, and precursors of secondary aerosols are released in relatively
27 large amounts. As a result, air pollution is a serious health issue in many Indian Ocean countries,
28 leading to increases in respiratory and cardiovascular problems (Rajak and Chattopadhyay,
29 2019). The intense pollution has also been linked to regional weather impacts, such as changes
30 of rainfall patterns and decreasing crop harvests (e.g., Bollasina et al., 2011, Li et al., 2016).

31 1.2 Seasons

32 Seasonal changes of atmospheric transport patterns are the main driver of Indian Ocean
33 chemical regimes and lead to periods of ~~strong-intense~~ anthropogenic pollution alternating with
34 periods of clean oceanic air. The South Asian monsoon circulation, the strongest monsoon
35 system in the world, dominates the regional meteorology of the Indian subcontinent. The
36 seasonal reversal of the winds is coupled to a strong annual cycle of precipitation with very wet
37 summer and dry winter conditions (Chang, 1967). Being the dominant driver of the annual
38 cycle of rainfall, the South Asian monsoon controls the water and food security of the region
39 and, thus, the well-being and prosperity of large populations.

40 The monsoon system also has a strong impact on the atmospheric composition over the Indian
41 Ocean. ~~The winter monsoon from November to March is characterized by a strong north-~~
42 ~~easterly flow that spreads regional pollution from Southeast Asia over the entire northern Indian~~
43 ~~Ocean (Lelieveld et al., 2001). During the winter monsoon from December to February,~~
44 ~~c~~ontinental aerosols as well as man-made trace species and their reaction products dominate
45 the chemical regime (Lelieveld et al., 2001). ~~During this time, a~~ layer of air pollution is visible
46 on satellite pictures as a haze of brown colour hanging over much of South Asia and the Indian
47 Ocean. This so-called Indian Ocean brown cloud has been suggested to impact regional climate

1 by masking greenhouse gas induced surface warming (Ramanathan et al., 2005) and to affect
2 monsoon rainfall.

3 In contrast, clean air dominates the atmospheric composition over the Indian Ocean during the
4 summer monsoon from June to September, leading to a completely different chemical regime.
5 Atmospheric pollutant levels over the Indian Ocean are low and typical open ocean background
6 conditions can be observed (Lawrence and Lelieveld, 2010). ~~The surface circulation is
7 accompanied by heavy rainfall over the Indian subcontinent and an anticyclonic circulation,
8 centred at 200 to 100 hPa.~~ While boreal summer ~~surface~~ conditions prevent the anthropogenic
9 pollution from spreading across the Indian Ocean, the an anticyclonic circulation, centred at
10 200 to 100 hPa, offers an efficient pathway for continental pollution into the global upper
11 troposphere and lower stratosphere (e.g., Randel et al., 2010; Lelieveld et al., 2018).

12 Finally, during the monsoon transition periods from April to May and September to October,
13 ~~zonal flows dominate the surface transport patterns. While this allows for the offshore pollution
14 is less strong, some continental due to weaker air masses transport~~ from Southeast Asia and
15 Africa ~~to be transported~~ over the Indian Ocean, ~~the offshore pollution is in general less strong
16 during the transition periods compared to the winter monsoon conditions~~ (Sahu et al., 2006).
17 ~~Strong spatial and temporal variations of trace gas distributions resulting from transitioning
18 transport regimes have been reported during these periods (e.g., Mallik et al., 2013).~~

19

20 1.3 Early work

21 The largest international scientific study exploring the impact of South Asian emissions on the
22 composition of the atmosphere over the Indian Ocean, the Indian Ocean Experiment
23 (INDOEX), took place during the winter monsoon 1999, with some pilot campaigns
24 conducted during 1996–1997. During the multiplatform field campaign, surprisingly high
25 pollution was detected over the entire northern Indian Ocean all the way to the Intertropical
26 Convergence Zone (ITCZ). Scientific studies revealed that the nature of the pollution was
27 considerably different from that in Europe or North America, with strongly enhanced carbon
28 monoxide concentrations related to widespread biofuel use and agricultural burning (e.g.,
29 Lelieveld et al., 2001). Other large pollution sources based on fossil fuel combustion and
30 biomass burning were linked to high loads of sunlight-absorbing aerosols with potential
31 consequences for the regional atmospheric energy balance (Ramanathan et al., 2002). A few
32 years before INDOEX, the Joint Global Ocean Flux Study (JGOFS) India investigated the
33 factors controlling carbon fluxes in the Arabian Sea and led to estimates of CO₂ emissions to
34 the atmosphere for this region (Sarma et al., 2003).

35

36 The INDOEX findings, presented in many scientific publications, have drawn attention to this
37 region and several projects and campaigns followed over the next decade. The Bay of Bengal
38 Experiment (BOBEX) research cruise during February to March 2001 detected high ozone and
39 pollution levels over the Bay of Bengal and linked them to transport from the continent (Naja
40 et al., 2004; Lal et al., 2006). The southern Indian Ocean was explored during the Pilot
41 Expedition to the Southern Ocean (PESO) research cruise from January to April 2004, which
42 revealed much cleaner air masses with smaller aerosol loadings in the region south of the ITCZ
43 (Pant et al., 2009). Other research cruises such as the Bay of Bengal Processes Studies (BOBPS)
44 during September to October 2002, investigated oceanic productivity and nutrients in relation
45 to air-sea exchange of climate active gases (Sardessai et al., 2007). A detailed overview of
46 research cruises, island measurements and aircraft campaigns investigating the atmosphere over
47 the Indian Ocean is given in Lawrence and Lelieveld (2010). The authors provide a

1 comprehensive review of the state of the art at this time by bringing together observational and
2 modelling studies.

3 **1.4 Scope and organization of this study**

4 Here we will focus on recent progress in the field by giving an overview of results obtained
5 after 2010. We will synthesize the current understanding of Indian Ocean gas phase
6 atmospheric composition and explore how it is driven by emission sources, transport, and
7 chemistry. Our region of interest encloses the Indian Ocean from 30°S to its northern
8 continental borders and across its whole longitudinal range. It also includes neighbouring land
9 mass such as parts of East Africa, the Arabian Peninsula, South Asia, Southeast Asia, and
10 Australia as depicted in Figure 1. This review focuses on three groups of atmospheric gases 1)
11 ozone and pollutants - carbon monoxide (CO), nitrogen oxides (NO_x), sulphur dioxide (SO₂),
12 ammonia (NH₃) and mercury; 2) greenhouse gases - methane (CH₄), nitrous oxide (N₂O),
13 carbon dioxide (CO₂) and carbonyl sulphide (COS) and 3) volatile organic compounds (VOCs)
14 and short-lived biogenic gases - dimethylsulphide (DMS), isoprene and halogen compounds.
15

16 Section 2 provides an overview of the physical processes in the atmosphere and ocean that are
17 relevant for the atmospheric composition. Section 3 will introduce all campaigns and
18 measurements that are the basis for scientific studies published after 2010 and are discussed
19 here. Regional sources and sinks of greenhouse gases, pollution and biogenic trace gases will
20 be given in Section 4. Short introductions to all gases listed above, including their role in the
21 atmosphere, can also be found in section 4. The focus of section 5 is on our current knowledge
22 of the atmospheric composition over the Indian Ocean and how it is driven by physical
23 processes and by regional sources. We will present a synthesis of the scientific progress made
24 after 2010 in Section 6, where we will also discuss the global and local impacts of the Indian
25 Ocean atmospheric composition. An outlook and a summary of current knowledge gaps are
26 given in Section 7. A key for all abbreviations used in this paper is provided in Appendix A.
27
28
29

30 **2 Physical processes**

31 **2.1 Atmospheric processes**

32 The South Asian monsoon circulation dominates the transport patterns and regional
33 meteorology over the Indian Ocean. Strong seasonal circulation changes give rise to three main
34 meteorological regimes: the summer monsoon from June to September, the winter monsoon
35 from November to March and the transition periods from April to May and from the end of
36 September to October. Surface flow patterns as well as seasonal transport regimes are described
37 in the following subsections, while ~~(for more details about the summer and winter monsoons~~
38 and a discussion of intraseasonal and ~~interannual variability~~, please see can be found in the
39 supplementary materials section A).

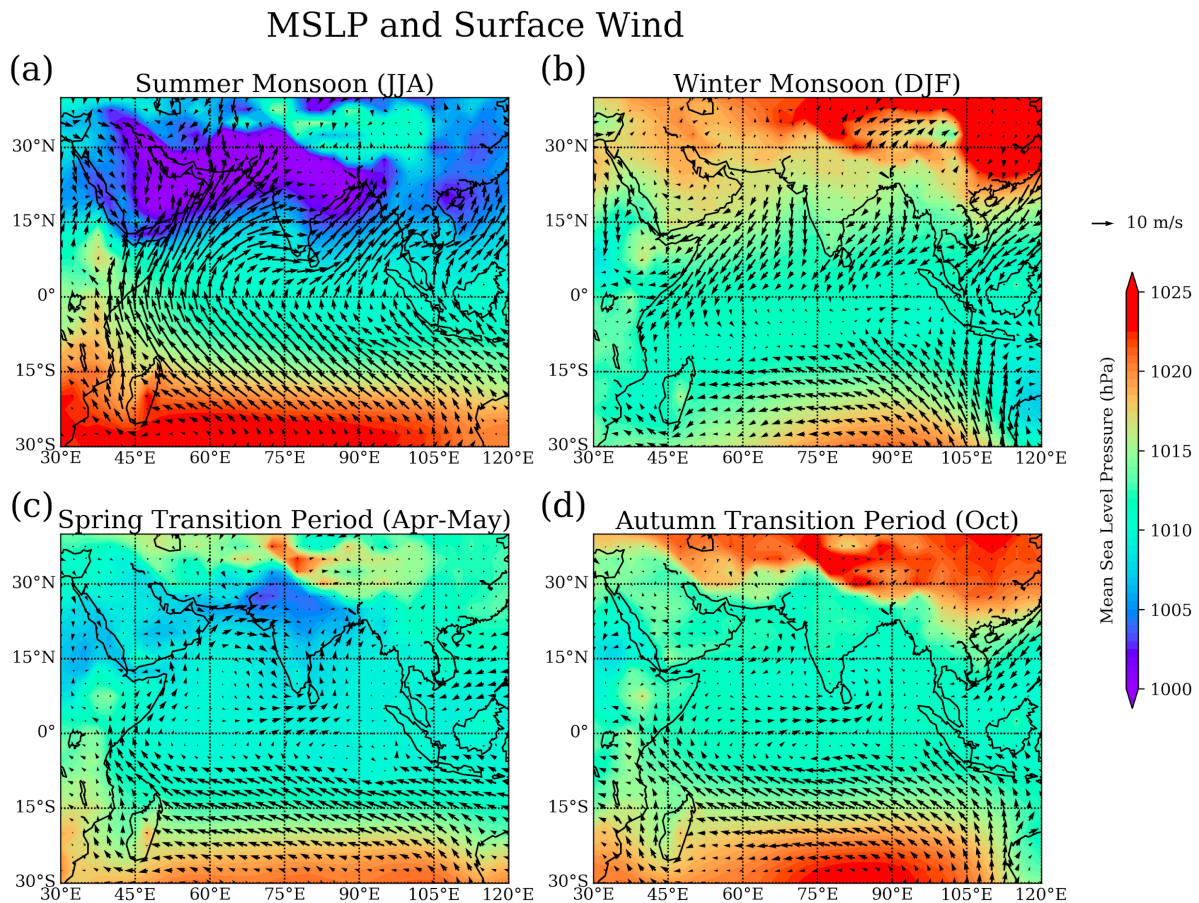
40 **Near-surface flow patterns**

41 A detailed picture of the near-surface flow patterns is provided in Fig. 1 in the form of seasonal
42 mean surface wind fields and sea level pressure derived from 2018/2019 ERA-Interim
43 reanalysis data. Seasonal mean plots here and in the rest of the paper are shown for core
44 monsoon and transition periods, i.e., June to August (JJA) for the summer monsoon, December
45 to February (DJF) for the winter monsoon, April to May (Apr-May) for the boreal spring
46 transition period and October (Oct) for the boreal autumn transition period. The equatorial and
47 northern Indian Ocean (north of 10°S) are dominated by seasonally reversing monsoon winds
48 (Schott and McCreary, 2001; Schott et al., 2009). Southeast winds occur during the summer

1 monsoon with the low-pressure system of the ITCZ shifted north of 15°N (Fig. 1a), while
 2 northwest winds occur during the winter monsoon with the low-pressure belt situated south of
 3 the equator (Fig. 1b). Over the southern Indian Ocean (south of 10°S), steady southeast trades
 4 prevail during all seasons, but reach further northward during the northern summer.

5 The seasonally reversing monsoon winds and inter-hemispheric pressure gradients over the
 6 equatorial Indian Ocean are a striking feature different from the other tropical oceans, where
 7 sustained easterly winds are found along the equator. In contrast, equatorial winds over the
 8 Indian Ocean are westerlies during the monsoon transition periods (Fig. 1c and 1d) and show a
 9 weak westerly annual mean component (Lamb and Hastenrath, 1979). These equatorial
 10 westerlies are driven by an interplay of an eastward pressure gradient along the equator, the
 11 latitudinal position of the flow recurvature and the strength of the trade winds (Hastenrath and
 12 Polzin, 2004). ~~During the autumn transition period, the equatorial westerlies are the surface
 13 manifestation of a zonal-vertical circulation cell between the regions of ascending motion over
 14 Indonesia and subsidence over equatorial East Africa (Hastenrath, 2000). Interannual variations
 15 of the zonal circulation lead to enhanced subsidence and decreased rainfall at the coast of East
 16 Africa during years of intense circulation with accelerated surface westerlies.~~

17



18
 19 **Figure 1.** Mean surface level pressure (MSLP) and surface wind for (a) summer monsoon 2018 (June –
 20 – August), (b) winter monsoon 2018/2019 (December – February), (c) spring transition 2018 (April –
 21 May) and (d) autumn transition 2018 (October) periods from ERA-Interim.

22
 23 **Summer and winter monsoon**
 24 During the summer monsoon, steady onshore winds transport air from the ocean over to the
 25 continent, where it ~~rises due to buoyancy and orographic forcing. The resulting results in~~ deep

1 convection ~~is characterised by massive cirrus anvil clouds~~ and the well-known Indian summer
2 monsoon rains. Air masses experiencing fast upward transport in convective updraughts
3 converge in the upper troposphere forming a high-pressure system. The associated anticyclone
4 circulation is tied to the outflow of the deep convection and is situated directly over the highly
5 polluted southern Asia. As a result, distinct tracer anomalies have been observed in the
6 anticyclone indicating strong upward transport of pollution from the surface (e.g., Randel et al.,
7 2010). Given the dynamical confinement of tropospheric tracers and aerosols in the anticyclone,
8 the Asian monsoon system provides a potentially efficient pathway from the surface to the
9 tropical upper troposphere and lower stratosphere. However, a significant fraction of the
10 pollution can be removed from the airmass before entering the stratosphere due to lightning
11 driven OH reactions in monsoonal convection (Lelieveld et al., 2018).

12 During the winter monsoon, the prevailing north-easterly winds reverse the meteorological
13 situation. There is little rain over southern Asia marking this as the ‘dry season’ and the missing
14 convection chemically disconnects the surface layer from the upper troposphere
15 (Kunhikrishnan et al., 2004). Instead, pollution outflow occurs in the marine boundary layer
16 (MBL) via offshore winds towards the northern Indian Ocean down to the equator. Primary
17 MBL flow channels have been identified in the western Arabian Sea, the eastern Arabian Sea
18 just off the Indian west coast, the western Bay of Bengal and Southeast Asia (Krishnamurti
19 1997a; 1997b; Verver et al., 2001).

20 Winter monsoon flow patterns are further complicated by effects of the land-sea breeze, which
21 lofts coastal air masses above the MBL (Simpson and Raman, 2004). The associated offshore
22 flow above the MBL transports air masses over the coastal oceans where they constitute the so-
23 called ‘elevated layer’. Due to the relatively rapid outflow, the elevated layer provides an
24 additional effective mechanism for pollution transport from the continents towards the Indian
25 Ocean (Lawrence and Lelieveld, 2010). As a result, outflow during the winter monsoon occurs
26 in two distinct layers, namely the pollutant plume within the MBL (up to 800–1000m) and the
27 elevated layer (1–3km). Once over the northern Indian ocean, the north-easterly trade winds
28 transport the air masses towards the ITCZ, typical within 7–10 days (Ethe´ et al., 2002).
29 Similarly, over the southern Indian Ocean, south-easterly winds transport pristine boundary
30 layer air masses northwards. At the ITCZ, these trade wind flows converge, and associated
31 convection transports the air upwards into the upper troposphere (Iyengar et al., 1999).

32 Over the western part of the tropical Indian Ocean, the ITCZ has been observed to occur
33 simultaneously in two bands on either side of the equator forming the so-called double ITCZ
34 (Meenu et al., 2007). ~~Signatures of the double ITCZ are present practically~~ throughout the year
35 ~~with the largest frequency occurrence in November (~85%) and December (~62%).~~ Based on
36 cloud characteristics and outgoing longwave radiation, the most preferred latitudes for the
37 northern and southern bands of the ITZC were found to be around 5°N and 7.5°S to 10°S.

38 **Intraseasonal and interannual variability**

39 ~~Intraseasonal variability can impact atmospheric transport patterns over the Indian Ocean with~~
40 ~~the dominant mode being the eastward propagating Madden-Julian Oscillation (MJO).~~
41 ~~Equatorially trapped, baroclinic oscillations in the tropical wind field propagate slowly~~
42 ~~eastward across the Indian Ocean, Maritime Continent, and West Pacific with an intraseasonal~~
43 ~~cycle of 30–60 days (Madden and Julian, 1972). A typical MJO event exhibits large-scale~~
44 ~~convection anomalies where enhanced convection and rainfall develop over the western Indian~~
45 ~~Ocean with suppressed convection further east over the western Pacific (Zhang, 2005). The~~
46 ~~eastward propagation of the convection and circulation anomalies depends on the season and is~~
47 ~~strongest during the winter monsoon. The summer monsoon shows a north-eastward~~
48 ~~propagation of the anomalies into Southeast Asia in addition to the eastward propagation along~~
49 ~~the equator (Waliser, 2006). Among the many impacts of the MJO, strong interactions with~~

1 ocean surface fluxes of mass, heat, and momentum have been observed (e.g., Matthews et al.,
2 2010).

3 Similarly, modes of tropical interannual variability, such as the irregular oscillation of sea
4 surface temperatures known as the Indian Ocean Dipole (IOD), play a role for Indian Ocean
5 meteorology. The positive phase of the IOD is characterised by positive sea surface temperature
6 anomalies in the western part of the Indian Ocean accompanied by negative anomalies in
7 eastern part (Saji et al., 1999). The initial cooling off the coast of Sumatra–Java leads to a
8 positive feedback mechanism via suppressed local convection, anomalous easterly winds, a
9 shoaling thermocline and stronger upwelling, which in turn reinforce the initial cooling with a
10 peak from September to November (Cai et al., 2014). Extreme positive IOD events can also
11 impact the equatorial ocean by inducing a north–westward extension of the south–easterly trades
12 and drying along the equatorial Indian Ocean (Webster et al., 1999).

13 The dominant mode of interannual climate variability of the Pacific, the El Niño–Southern
14 Oscillation (ENSO), can also impact Indian Ocean sea surface temperatures via anomalous
15 wind stress forcing (Latif and Barnett, 1995). In addition, ENSO modulates the depth of the
16 Indian Ocean thermocline and contributes to changes in salinity due to shifts in rainfall and
17 evaporation. The potential impact of ENSO on the IOD is currently under discussion (Stuecker
18 et al., 2017 and references therein).

19 **2.2 Oceanic transport**

20 The physical oceanography of the equatorial and southern Indian Ocean, including currents,
21 thermohaline circulation, sea surface temperature (SST), salinity, and upwelling events, does
22 not experience the influence of the seasonal monsoon cycle, however, that of the northern
23 Indian Ocean displays the seasonal changes. Below we will outline the major features of the
24 equatorial and southern Indian Ocean first (Fig. 2) and then describe the influence of the
25 seasonal monsoon on the physical processes in the northern Indian Ocean (Fig. 2). For this
26 review, we concentrate on how physical oceanography affects salinity, SST, and biological
27 productivity, as they play a major role in controlling air–sea exchange and atmospheric
28 composition. For more details about general Indian Ocean physical processes, please see Schott
29 et al. (2009) and references therein. The physical oceanography of the northern Indian Ocean
30 reflects the seasonal changes of the monsoon cycle, including impacts on currents, thermohaline
31 circulation, sea surface temperature (SST), salinity, and upwelling events, while the equatorial
32 and southern Indian Ocean do not experience this influence (Fig. 2). For more details about
33 general Indian Ocean physical processes, please see Schott et al. (2009) and references therein,
34 as well as Phillips et al. (2021) from this issue and supplementary material B. In the following
35 sections, we concentrate on how physical oceanography affects salinity, SST, and biological
36 productivity, which in turn play a major role in controlling air–sea exchange and atmospheric
37 composition, in particular for biogenic trace gases such as bromoform, DMS, and isoprene.

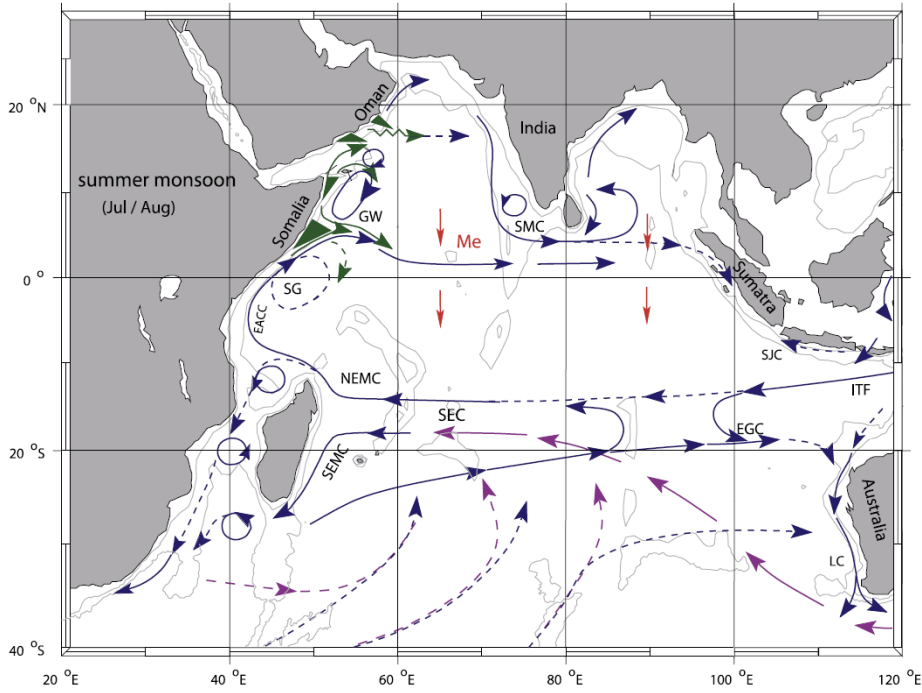
38 **Southern Indian Ocean**

39 The South Equatorial Current (SEC) in the Indian Ocean carries water masses entering through
40 the Indonesian passages, with a relative salinity minimum in the Indian Ocean environment,
41 via broad zonal inflow westward. Driven by the Southeast Trades, the SEC supplies the western
42 boundary currents east of Madagascar. Part of the throughflow water in the SEC forms the
43 northern East Madagascar Current (EMC), which partly passes in southward moving eddies
44 through the Mozambique Channel and merges into the Agulhas (Ridderinkhof and de Ruijter,
45 2003; Schouten et al., 2003).

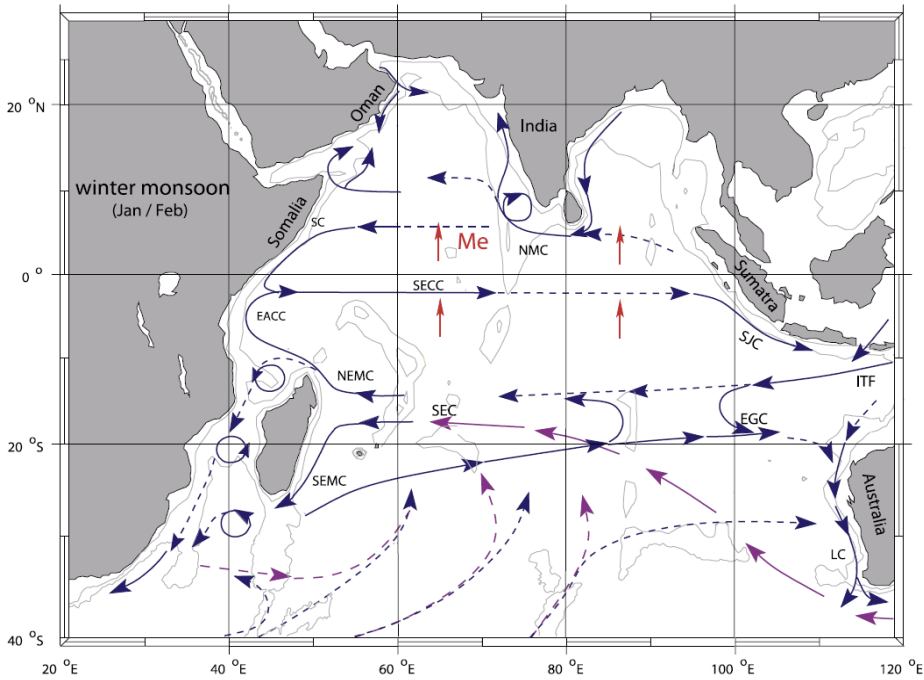
46 Data from satellite altimetry suggest that the eastward South Indian Countercurrent (SICC) is
47 already present in the Mozambique Basin, southwest of Madagascar (Siedler et al., 2006). The

1 eastward frontal SICC coincides with the thermohaline front that separates the saline
2 subtropical surface water from the fresher tropical surface water in the EMC in summer
3 (Palastanga et al., 2007). The variability of SST and salinity is high in the warm waters south
4 to south-east of Madagascar, likely due to eddy activity and upwelling. There is year-round
5 coastal upwelling along the southern stretch of the oligotrophic EMC and in the shallower
6 region just to the south of Madagascar, which leads to enhanced phytoplankton growth (Quartly
7 et al., 2006). All productivity further from the island in bands of relatively high variability along
8 25°S and along the EMC are due to a combination of local upwelling caused by eddies and,
9 more importantly, the advection of upwelled coastal waters around eddy features. The
10 anticyclones moving through the region wrap both the warm EMC waters and the nutrient-rich
11 upwelled waters into well-defined arcs. Occasionally strands of chlorophyll-rich water can
12 stretch 500 km or more eastward, which are caused by the combined effects of both cyclonic
13 and anticyclonic eddies (Quartly et al., 2006). The southward flowing EMC, as part of the
14 bifurcated SEC, and the SEC form the western and northern boundary currents of the South
15 Indian subtropical gyre, where saline surface water is formed, as there is more evaporation than
16 precipitation in this region (Schott et al., 2009). The south-eastern Indian Ocean shows the
17 strongest interannual to decadal variability of upper-ocean salinity in the Indian Ocean.
18 Seasonality of the mixed layer salinity in the south-eastern tropical Indian Ocean is influenced
19 by the annual cycles of the Indonesian Throughflow and the Leeuwin Current transports,
20 freshwater forcing, and eddy fluxes (Zhang et al., 2016).

21 Open ocean upwelling associated with the Seychelles dome, a thermocline ridge in the southern
22 tropical gyre can occur between 5 and 10°S, along the northern edge of the southeast trades,
23 where Ekman divergence occasionally appears to be strong enough to upwell subsurface waters
24 into the mixed layer (Schott et al., 2009). In this region, the South Equatorial Countercurrent
25 (SECC) flows eastward year-round, fed by the East African Coastal Current (EACC) and
26 forming the northern flank of the southern Indian Ocean tropical gyre. Low sea surface height
27 is the signature of the Indian Ocean's tropical gyre, bounded in the north by the SECC, to the
28 south by the SEC, and at the western boundary by the EACC.



1



2
3

4 **Figure 2.** Schematic representation of identified oceanic currents during the summer monsoon (a) and
 5 winter monsoon (b). Current branches indicated are the South Equatorial Current (SEC), South
 6 Equatorial Countercurrent (SECC), Northeast and Southeast Madagascar Current (NEMC and SEMC),
 7 East African Coastal Current (EACC), Somali Current (SC), Southern Gyre (SG) and Great Whirl (GW)
 8 and associated upwelling wedges (green shades), Southwest and Northeast Monsoon Currents (SMC
 9 and NMC), South Java Current (SJC), East Gyrals Current (EGC), and Leeuwin Current (LC). The
 10 subsurface return flow of the supergyre is shown in magenta. Depth contours shown are for 1000 m and
 11 3000 m (grey). Updated representations are from SMC01; red vectors (Me) show directions of
 12 meridional Ekman transports. ITF indicates Indonesian Throughflow (from Schott et al., 2009, copyright
 13 2009 by the American Geophysical Union, reproduced with permission).

14

15 **Northern Indian Ocean**

1 During the summer monsoon, the northward flowing Somali Current is supplied by the SEC
2 and EACC. Once the Somali Current crosses the equator, a part of it turns offshore around 4°N
3 and another part returns across the equator as a part of the southern gyre. A northern gyre occurs
4 north of the Equator and occasionally a third gyre can be observed in many summer monsoons
5 (Schott et al., 2009). These gyres influence the stability of the atmospheric planetary boundary
6 layer, impacting surface wind stress and heat fluxes (Vecchi et al., 2004). Furthermore, the
7 Southwest Monsoon Current flows towards the east, south of Sri Lanka, then turns to flow
8 toward the north, bringing saltier Arabian Sea water into the Bay of Bengal (Jensen, 2003). In
9 contrast, the Somali Current flows southward during the winter monsoon to meet the northward
10 flowing EACC. They supply water for the eastward flowing SECC. The Northeast Monsoon
11 Current flows toward the west, bringing fresher Bay of Bengal water into the Arabian Sea
12 (Schott et al., 2009). In addition, model studies have suggested that Bay of Bengal water flows
13 across the equator in the eastern basin in the winter monsoon (Han and McCreary, 2001; Jensen,
14 2003).

15 Unique to the Indian Ocean are strong eastward ocean surface jets during the inter monsoon
16 period, called Wyrtki Jets. They are produced by the semi-annual westerly equatorial winds and
17 are important because they carry warm upper layer waters toward the east, which increases sea
18 level and mixed layer depth in the east and decreases them in the west. These semi-annual
19 westerlies are the reason for another unique Indian Ocean feature, namely the eastward
20 Equatorial Undercurrent that is only present for a part of the year (i.e. February–June) when
21 the winds have an easterly component (Schott et al., 2009; Reppin et al., 1999).

22 Salinity, SSTs and productivity

23 On seasonal time scales, freshwater input due to rainfall and river discharge is important ~~for~~ to
24 the salinity balance in the Bay of Bengal ~~and~~, ~~while~~ horizontal advection related to the monsoon
25 plays a dominant role in the north Indian Ocean (Rao and Sivakumar 2003; Da-Allada et al.,
26 2015). In the southwestern tropical Indian Ocean, the seasonal cycle of the mixed layer salinity
27 in the south-central Arabian Sea is mainly due to meridional advection driven by the monsoon
28 winds, while freshwater flux due to precipitation may play an important role in the southwestern
29 tropical Indian Ocean is a major control on the salinity (Da-Allada et al., 2015). The Rrainfall
30 over the Indian Ocean shows a general migration to the summer hemisphere following sunlight
31 and warm SSTs, highlighting their strong coupling. Conversely, latent heat loss caused by cool,
32 dry air from the Asian continent leads to strong wintertime cooling in the northern Arabian Sea.
33 The strong summertime cooling in parts of the Arabian Sea instead is a combined result of
34 latent heat loss caused by the strong south-westerly winds and upwelling/offshore advection
35 from the Somali and Omani coasts. In addition, the general distribution of rainfall is similar to
36 that for SST, highlighting the strong coupling between the two. Wintertime cooling in the
37 northern Arabian Sea is strong because of latent heat loss caused by cool, dry air from the Asian
38 continent. Interestingly, there is strong summertime cooling in parts of the Arabian Sea as a
39 result of upwelling and offshore advection from the Somali and Omani coasts and due to latent
40 heat loss caused by the strong south-westerly winds. During boreal summer, upwelling induced
41 cooling off Somalia prevents atmospheric convection from the western Arabian Sea. From the
42 eastern Arabian Sea to the South China Sea, north of the Equator, high SSTs promote
43 atmospheric deep convection (Schott et al., 2009).

44 The oceanic upwelling caused by strong monsoonal winds ~~in the Indian Ocean lead to ocean~~
45 upwelling, supplying nutrients to the surface layer, where they support elevated rates of
46 primary productivity. This occurs mainly in the Arabian Sea, the Somali Basin, along the Indian
47 coast and the northern Bay of Bengal, especially during summer months. The seasonal reversals
48 in the boundary currents of the northern Indian Ocean, including the seasonal switching from
49 upwelling to downwelling circulations, have important biogeochemical and ecological impacts

1 ~~that and include seasonal switching from upwelling to downwelling circulations, and~~
2 ~~modification of~~ primary productivity, nutrient stoichiometry, oxygen concentrations and
3 phytoplankton species composition (Hood et al., 2017). ~~In addition, transient upwelling due~~
4 to seasonal variations of currents and mesoscale variability can give rise to episodically high
5 levels of primary production throughout the Indian Ocean coastal waters.

6 **2.3 Long-term changes**

7 **Indian Ocean warming**

8 The Indian Ocean has warmed steadily over the past century, with an SST increase of 1°C
9 during 1951–2015, markedly higher than the global average SST warming of 0.7°C, over the
10 same period (Du and Xie, 2008; Han et al., 2014; Krishnan et al., 2020). Overall, this Indian
11 Ocean-averaged warming rate is broadly consistent across observational products (Dong et al.
12 2014; Yao et al., 2016) and historical simulations from the Coupled Model Intercomparison
13 Project - Phase 5 (CMIP5). It can be largely attributed to anthropogenic forcing rather than
14 natural external forcing, such as volcanic and solar variations, ~~which have much weaker effects~~
15 (e.g., Dong et al., 2014). It has been shown that the basin wide warming due to increasing
16 greenhouse gases is slowed down by the indirect effects of anthropogenic aerosol (Dong and
17 Zhou, 2014). In addition to anthropogenic forcing, the sustained warming over the Indian Ocean
18 warm pool region is caused by local ocean–atmosphere coupled mechanisms, with their relative
19 roles being debated (e.g., Dong et al., 2014; Du and Xie, 2008; ~~Rao et al., 2012; Swapna et al.,~~
20 ~~2014~~).

21 ~~Some studies suggest that the warming is induced by the increase in downward longwave~~
22 ~~radiation due to greenhouse gases, and then amplified by the water vapor feedback and~~
23 ~~atmospheric adjustment (Du and Xie, 2008). Other studies argue that the SST trend is linked to~~
24 ~~the changes in ocean heat transport and wave-induced thermocline depth (Li et al., 2003) or to~~
25 ~~a decrease in the upwelling related to a slowdown of the wind-driven Ekman pumping (Alory~~
26 ~~and Meyers, 2009). Li et al. (2018) showed that the prevailing warming of the western to~~
27 ~~central Indian Ocean for 2000–2014 was largely induced by equatorial easterly winds, Ekman~~
28 ~~downwelling off the equator, and north-easterly wind trends over the west Asia–East Africa~~
29 ~~coastal region.~~ The importance of the Indian Ocean in the global ocean heat budget was not
30 recognised until the hiatus period at the beginning of the 21st century, during which the abrupt
31 increase of the upper Indian Ocean heat content served as a major sink of the excessive heat
32 entering the Earth system (~~Cheng et al., 2015; Nieves et al., 2015; Lee et al., 2015~~).

33 The Indian Ocean warming is not spatially homogeneous in both models and observations. The
34 western tropical Indian Ocean has been warming for more than a century, at a rate faster than
35 any other region of the tropical oceans and is the largest contributor to the overall trend in the
36 global mean SST (Roxy et al., 2014). ~~For the time period 1901–2012, summer SSTs of the~~
37 ~~western Indian Ocean experienced anomalous warming of 1.28°C, while the total Indian Ocean~~
38 ~~warm pool only saw an increase of 0.78°C. In addition to the overall warming trend, positive~~
39 ~~IOD events, with positive sea surface temperature anomalies in the western part of the Indian~~
40 ocean, have increased markedly since 1950, while negative IOD-events have reduced (Cai et
41 al., 2009). The warming of the generally cool western Indian Ocean against the rest of the
42 tropical warm pool region (Roxy et al., 2014, 2015) and corresponding changes of the zonal
43 SST gradient (Saha et al., 2014) have been both proposed as plausible explanations for the
44 observed decrease of Indian monsoon rainfall over the last three decades. In addition, they have
45 the potential to alter the marine food webs in this biologically productive region.

46 The Indian Ocean warming is projected to further increase over the course of the 21st century
47 in response to unabated greenhouse gas emissions. By the end of the 21st century, strongest
48 warming in the Arabian Sea and western equatorial Indian Ocean is consistently projected in

1 CMIP models, which could yield more Arabian Sea cyclones, ~~more extreme IOD events and~~
2 further decrease monsoonal rains (Gopika et al., 2020). ~~The mean SST distribution is projected~~
3 ~~to resemble more positive IOD events, although some change in frequency is expected in the~~
4 ~~future in response to greenhouse gas warming (Cai et al., 2014). Modelling studies also suggest~~
5 ~~that the predicted stronger warming of the northern Indian ocean compared to the southern~~
6 ~~Indian Ocean is most likely overestimated due to internal climate variability, observational~~
7 ~~biases and uncertainties (Gopika et al., 2020).~~
8

9 **Summer monsoon and precipitation**

10 There are large uncertainties related to variability in the South Asian summer monsoon in a
11 changing climate. Several studies debate whether the monsoon is weakening or strengthening,
12 as well as the mechanisms driving the changes (Roxy et al., 2015). According to a review by
13 Singh et al. (2019a), both observational and modelling studies have determined that the
14 potentially weakened monsoon is due to a combination of forcings, such as land use and
15 irrigation changes, ~~and~~ increased greenhouse gas ~~and as well as~~ anthropogenic aerosols
16 ~~concentrations. Many of the studies have determined that, due to this combination of forcings,~~
17 ~~oceanic warming plays a central role in altering the monsoon, but it is currently argued if~~
18 ~~oceanic warming weakens the monsoon over the Indian Ocean or if the weakened monsoon has~~
19 ~~accelerated the warming (Rao et al. 2012; Swapna et al. 2014). Roxy et al. (2015) provide~~
20 compelling evidence that Indian Ocean warming potentially weakens the land-sea thermal
21 contrast and dampens the summer monsoon Hadley circulation, leading to reduced rainfall over
22 parts of South Asia.

23 The Indian Ocean is one of the greatest moisture sources accounting for nearly one-third of the
24 total net transport of water toward the continents (Bengtsson, 2010). Both remote and local SST
25 anomalies can induce hydrological cycle changes over the Indian ocean affecting local and
26 remote precipitation. An increase in evaporation is due to the robust warming of SSTs during
27 recent decades, via changes of the near surface specific humidity gradient, near-surface wind
28 and the turbulent exchange coefficient (Yu, 2007; Richter and Xie, 2008). ~~Accompanied by~~
29 ~~atmospheric circulation changes, water vapor can be redistributed and affect local and remote~~
30 ~~precipitation.~~

31 Han et al. (2019) show that the moisture sources (evaporation minus precipitation) in the
32 tropical central-eastern and south-western Indian Ocean experienced a significant increase
33 during boreal summer between 1979 to 2016. ~~During those decades, the enhanced east-west~~
34 ~~thermal gradient in the Pacific strengthened the Walker Circulation, leading to a westward shift~~
35 ~~in convection and thus weakened convection and ascent over the tropical central-eastern Indian~~
36 ~~Ocean. Enhanced moisture sources over these regions led to strengthened wind in the lower~~
37 ~~troposphere over the south-western Indian Ocean, which is associated with an enhanced land-~~
38 ~~sea thermal gradient under global warming (Han et al., 2019). In addition, there has been a~~
39 significant reduction in the annual frequency of tropical cyclones and their associated rainfall
40 over the northern Indian Ocean since the middle of the twentieth century (Krishnan et al., 2020).
41 In contrast, the frequency of very severe cyclonic storms during the autumn transition~~post-~~
42 ~~monsoon~~ season has increased significantly during the last two decades. At the same time, an
43 enhanced rainfall contribution has occurred due to a higher precipitation efficiency (Singh et
44 al., 2016; 2019b) possibly leading to a dry atmosphere. Further changes of the Indian summer
45 monsoon rainfall are expected for the future, however current model projections give
46 contradicting results (e.g., Roxy et al., 2015; Zou and Zhou, 2013).

47

1 A significant reduction in the Indian summer rainfall over most of the Indian states during the
2 second half of the twenty-first century is projected by some modelling studies (Ramanathan et
3 al., 2005; Roxy et al., 2015). Other modelling studies project an increase in rainfall during the
4 East Asian summer monsoon region at the end of the twenty-first century (e.g., Zou and Zhou,
5 2013; Kitoh et al., 2013), with a large increase in rainfall over the ocean (Chen and Bordoni,
6 2016) and a slight increase in precipitation over central India (Asharaf and Ahrens, 2015). The
7 contradicting results indicate that the projection of the Indian summer monsoon rainfall is still
8 a key challenge for global and regional climate models. Enhanced evaporation variability,
9 which, in turn, intensifies the variability of Indian monsoon rainfall (Meehl and Arblaster,
10 2003) and a weakening in the monsoonal circulation are opposing effects, which remain a topic
11 of debate (Asharaf and Ahrens, 2015).

12 The mechanisms that alter regional precipitation vary at different time scales. A fast response
13 to an increase in CO₂ concentration before SST changes occurs at shorter time scales and is
14 associated with changes in large-scale wind patterns in the atmosphere. Changes in surface
15 wind are expected to be moderate for the first half of the 21st century, with a noticeable decline
16 of wind speed over the tropical Indian Ocean due to reduced thermal land-sea contrasts. The
17 southern extratropical region and Southern Ocean, on the other hand, show a significant
18 strengthening of the wind fields by the end of the twenty-first century (Mohan and Bhaskaran,
19 2019). Not well represented ocean-atmosphere feedback and coarse model resolutions,
20 however, are known to lead to large uncertainties in model estimates of wind speed changes
21 (Annamalai et al. 2017; Mohan and Bhaskaran, 2019).

22 Salinity and productivity

23 Du et al. (2015) noted freshening in the south-eastern tropical Indian Ocean starting the mid-
24 1990s. Idealised model experiments suggest that multidecadal changes of subsurface ocean
25 salinity during 1950–2000 were due to a result of an amplification of the mean surface salinity
26 pattern and isopycnal migration related due to the ocean surface warming (Lago et al. 2016).
27 However, the enhanced precipitation in the Maritime Continent and the strengthening of the
28 Indonesian Throughflow are thought to be the likely causes of the freshening trend in the south-
29 east Indian Ocean since early 2000s, rather than local Ekman pumping and freshwater flux
30 anomalies (Llovel and Lee 2015; Hu and Sprintall, 2017). Du et al. (2015) noted a contrasting
31 sea surface salinity trend pattern characterised by freshening in the south-eastern tropical Indian
32 Ocean and salinification in the western tropical Pacific starting in the mid-1990s, which is
33 attributed to a strengthening trend of the Indo-Pacific Walker circulation combined with ocean
34 advection processes.

35 While Behrenfeld et al. (2006) indicate a reduction in net primary productivity over most of the
36 tropics as a result of surface thermal stratification, they have suggested an increase in primary
37 productivity for the western Indian Ocean from 1998 to 2004. Recent biogeochemical
38 simulations of the Arabian Sea ecosystem also predict that a projected intensification of
39 monsoon winds strongly increases the ecosystem productivity, thereby amplifying the oxygen
40 biological consumption and intensifying the oxygen minimum zone (OMZ) at depth (Lachkar
41 et al., 2018). At the same time, the near-surface will experience increased ventilation due to the
42 predicted stronger winds. On the contrary, a review in this issue summarizes evidence
43 indicating a significant, but small, reduction in primary production in the northern Indian Ocean
44 (Löscher et al., 2021). Included, is a study using chlorophyll data and Earth system model
45 simulations over a larger region of the western Indian Ocean, which points out an alarming
46 decrease of up to 20% in marine phytoplankton during the past six decades (Roxy et al., 2016).
47 The authors suggest that this decrease is driven by enhanced ocean stratification due to the rapid
48 warming in the Indian Ocean, which suppresses nutrient mixing from subsurface layers. Gregg
49 and Rousseaux (2019) also conclude from the assimilation of ocean colour satellite data (1998–

1 -2015) into an ocean biogeochemical model, that the decline in global ocean primary
2 productivity of 2.1% per decade is mainly driven by the northern and equatorial Indian Ocean.
3 Any changes to biological processes have the potential to alter trace gas cycling in the surface
4 ocean.
5 Reduced production by large, fast-growing diatoms along with chlorophytes characterizes this
6 decline, while cyanobacteria and coccolithophores benefit in the model.
7

8 3. Campaigns, station data and satellite measurements

9 ~~Physical processes in the Indian Ocean are captured better now than in previous decades due to~~
10 ~~the deployment of Argo floats and moored tropical buoy arrays, as well as the application of~~
11 ~~satellite instruments (Hermes et al., 2019). Tropospheric composition over the Indian Ocean,~~
12 ~~on the other hand, is still poorly sampled. In order to investigate oceanic emissions, chemical~~
13 ~~transformation and transport of key substances, accurate atmospheric measurements are~~
14 ~~needed.~~ A few Indian Ocean coastal or island stations have been operated as part of long-term
15 scientific measurement programmes or operational air quality networks providing limited area
16 observations. In addition, ~~intensive~~ ship and aircraft campaigns have been conducted for
17 detailed investigations of atmospheric processes during short episodes. These data can be
18 complemented by satellite observations of the tropospheric composition, which provide the
19 large-scale picture for a number of substances, albeit often with limited vertical resolution and
20 reduced accuracy for individual measurements. In this section, we will give an overview of
21 campaigns, station data and satellite measurements that have been applied to study the
22 atmospheric composition over the Indian Ocean over the last decade.

23 3.1 Campaigns and station data

24 Over the last decades, chemical, physical, and biogeochemical processes occurring in and above
25 the Indian Ocean have been explored during various field campaigns.~~In the 21st century, several~~
26 ~~new attempts have been made to explore the processes occurring in and above the Indian Ocean,~~
27 ~~which span several disciplines including oceanography, atmospheric chemistry and physics,~~
28 ~~and biogeochemistry.~~ Here, ~~we will introduce~~ all the campaigns that have contributed to the
29 recent progress in the field and led to publications after 2010. ~~General information on the time~~
30 ~~periods, regions and objectives of the campaigns is~~ are summarized in Table 1. It should be
31 noted that the ICARB multi-platform field experiment consisted of three phases, with the first
32 phase exploring post winter monsoon composition in 2006 (ICARB), a second phase taking
33 place during the winter monsoon 2008/2009 (referred to as W_ICARB) supplemented by
34 aircraft measurements and a third phase during the winter monsoon of 2018 (referred to as
35 ICARB-218).

36 ~~The southern Indian Ocean was explored during the PESO cruise in 2004, with measurements~~
37 ~~south of the ITCZ highlighting the clean air masses dominated by pristine oceanic conditions.~~
38 ~~Since then, a series of campaigns, the Indian Southern Ocean Expeditions (ISOEs), were~~
39 ~~initiated, with key components including hydrodynamics, biogeochemistry, air-sea interactions,~~
40 ~~and more recently trace gases in the MBL. Since the inception of ISOE, 11 expeditions have~~
41 ~~been carried out with trace gas emissions being one of the key objectives since ISOE-8 in 2014.~~

42 ~~Efforts during the multi-platform field experiment ‘Integrated Campaign for Aerosols, gases~~
43 ~~and Radiation Budget’ (ICARB) have focused on the northern Indian Ocean, Arabian Sea and~~
44 ~~Bay of Bengal with the cruise tracks designed to cover maximum areas of these regions. The~~
45 ~~experiment consisted of a first phase exploring post winter monsoon composition in 2006~~
46 ~~(ICARB), a second phase taking place during the winter monsoon 2008/2009 (referred to as~~
47 ~~W_ICARB) and a third phase during the winter monsoon of 2018 (referred to as ICARB-218).~~

All ICARB campaigns focused on the physico-chemical properties and radiative effects of aerosols and trace gases and how they are affected by polluted continental air mass transported over the oceans by the various wind regimes.

Since 2014, several campaigns focused on the South Asian summer monsoon time period have taken place. The Organic VSLs and their air-sea exchange from the Indian Ocean to the Stratosphere (OASIS) campaign in 2014 aimed at analysing the impact of oceanic gases on the remote stratospheric ozone chemistry. In 2015, the Oxidation Mechanism Observations (OMO) aircraft campaign addressed the “self-cleaning capacity” of the atmosphere by focusing on oxidation mechanisms and radical chemistry. During the OMO campaign, air pollutants such as non-methane volatile organic compounds (NMVOC), oxidized volatile organic compounds (OVOC) and nitrogen oxides were measured over continental regions (South Asia, Arabian Peninsula, and east Africa) as well as over the Mediterranean and the Indian Ocean. In a similar region, the Air Quality and climate change in the Arabian Basin (AQABA) shipborne campaign, was carried out in 2017, during which non-methane hydrocarbons (NMHCs) were measured.

The 2nd International Indian Ocean Expedition program (IIOE-2) was launched in 2015 with the goal to advance the understanding of interactions between geologic, oceanic, and atmospheric processes of the Indian Ocean region, and the impact on other Earth components and socio-economic activities. The scientific program organizes collaborative research investigating the Indian Ocean from coastal environments to the deep sea. Campaigns conducted within IIOE-2, focus on the ocean but also help characterise related atmospheric processes at a wide spectrum of spatial and temporal scales.

In addition to dedicated campaigns, some island and coastal stations have conducted long-term measurements that provide valuable information about the atmospheric composition over the Indian Ocean.

Table 1. Summary of campaigns in the Indian Ocean for the 21st century.

Campaign	Time	Region	Objective	Reference
ARMEX (Arabian Sea Monsoon Experiment)	2002 Jun – Aug	Arabian Sea	Study of reactive halides released from sea salt aerosols and their role in ozone chemistry	Ali et al., 2009
PESO (Pilot Expedition to the Southern Ocean)	2004 Jan – Apr	Southern Indian Ocean	Multi-disciplinary expeditions to understand the forcing mechanisms behind widely geographically separated climate change.	Pandey et al. (2006)
ISOE 1-11 (1st-11th Indian Southern Ocean Expedition)	Since 2004	Southern Indian Ocean	Identify role and response of Southern Ocean to the regional and global climate variability (emissions of trace gases since ISOE 8)	ISOE Reports Mahajan et al. (2019a, b) Inamdar et al. (2020)
ICARB (Integrated Campaign for Aerosols, gases and Radiation Budget)	2006 Mar – May; 2008/09 Dec – Jan; 2018	Indian mainland, northern Indian Ocean, Bay of Bengal	Characterize the physico-chemical properties and radiative effects of atmospheric aerosols and trace gases over the Indian landmass and the adjoining oceanic regions.	Moorthy et al. (2008) David et al., 2011

	Jan -- -Feb			
Sagar Kanya cruise during the CTCZ (Continental Tropical Convergence Zone) experiment	2009 Jul -- Aug	Bay of Bengal	Understanding the gaseous atmospheric boundary layer composition over the Bay of Bengal during the summer monsoon season	Girach et al. (2017)
Campaign aboard the Ocean Research Vessel Sagar Kanya (SK-277)	2010 Oct -- -Nov	Bay of Bengal	Analyze atmospheric composition over the Bay of Bengal and how it is driven by air mass origin from Indian Ocean, Southeast Asia, and the Indian subcontinent	Mallik et al. (2013)
OASIS (Organic VLSLs and their air sea exchange from the Indian Ocean to the Stratosphere)	2014 Jul -- - Aug	West Indian Ocean	Investigate oceanic emissions of very short-lived substances and their transport and chemistry from the tropical Indian Ocean to the atmosphere, in particular to the stratosphere	Fiehn et al. (2017) Zavarsky et al. (2018b)
OMO (Oxidation Mechanism Observations aircraft campaign)	2015 Jul -- Aug	Indian Ocean and the Mediterranean	Identify atmospheric impacts of associated air pollution emissions at regional and global scales during the South Asian summer monsoon	Lelieveld et al. (2018)
IIOE-2 (Second International Indian Ocean Expedition)	2015 -- - 2020	Indian Ocean	Advance Indian Ocean initiatives and projects addressing emerging scientific issues of the Indian Ocean in the 21st century	Hood et al., 2016
AQABA (Air Quality and climate change in the Arabian BASin)	2017 Jul -- -Aug	Mediterranean and Arabian Peninsula	Study air quality and climate change in the Arabian Basin	Bourtsoukidis et al., 2019

1
2
3

4 CO₂ surface flask measurements from the Cape Rama site on the Indian coastline have been
5 used to analyse the distribution and variability of CO₂ over this region for 2009--2012 (Nalini
6 et al., 2018). Measurements of CH₄, another important greenhouse gas, and the pollutant CO
7 are available from ground-based in situ cavity ring-down spectroscopy analysers and Fourier
8 transform infrared spectrometers at two sites on Reunion Island in the southern Indian Ocean
9 (Zhou et al., 2018). These multi-annual time series (2011--2017) allowed to investigate the
10 impact of emissions from biomass burning in Africa and South America on atmospheric
11 pollutant levels over the Indian Ocean. CO surface data are also available from the
12 NOAA/ESRL Global Monitoring Division network station in Mahé (Wai et al., 2014).

1 In situ tropospheric ozone measurements have been collected from 2003 to 2007 from balloon-
2 borne electrochemical concentration cell sensors launched above Ahmedabad in western India
3 (Lal et al., 2014). The continuous dataset enabled studies of the impact of transport processes
4 on the seasonal cycle and on the vertical distribution of ozone. The observation site in
5 Trivandrum situated on the southwest coast of India collected measurements of nitrogen oxides
6 with a chemiluminescence NO_x analyser from 2007 to 2009 (David and Nair, 2011).

7 **3.2 Satellite measurements**

8 Satellite measurements of atmospheric composition over the Indian Ocean have provided
9 valuable information over the last decades that allowed for studies of the overall distribution
10 and long-term changes of key substances. Most instruments used today apply passive remote
11 sensing with observations being mainly done in nadir geometry. Here we will give a short
12 overview of satellite instruments that provide measurements used in scientific studies of the
13 Indian Ocean atmosphere. In addition, we have compiled plots of the seasonal CO, NO₂ and
14 CH₄ surface distribution for this review article and will describe the respective satellite
15 measurements more in detail.

16 **Ozone and ~~p~~ollutants from OMI and TROPOMI**

17 The Ozone Monitoring Instrument (OMI) is a key instrument onboard NASA's Aura satellite.
18 OMI is a nadir-viewing, wide-field-imaging spectrometer that measures backscattered
19 radiances at a spectral resolution of 0.42–0.63 nm (Levelt et al., 2006). Its wide field-of-view
20 of 114° with a swath width of 2600 km yields daily global coverage with a spatial resolution of
21 13 km×24 km (Liu et al., 2010). OMI measures ozone profiles as well as other key air quality
22 components such as NO₂, SO₂, and aerosol characteristics. In this article, we use the OMI
23 tropospheric NO₂ column product from 2003 to 2020 to analyse long-term changes over
24 different coastal and open ocean regions of the Indian Ocean (Section 6.2).

25 The TROPospheric Monitoring Instrument (TROPOMI) is a nadir-viewing imaging
26 spectrometer on board the Copernicus Sentinel-5 Precursor satellite, which was launched in
27 October 2017 for a mission of seven years. The satellite has a sun-synchronous orbit achieving
28 near full-surface coverage on a daily basis. The TROPOMI instrument contains four
29 spectrometers with three covering the ultraviolet-near infrared and one for the shortwave
30 infrared range. Key atmospheric species observed by TROPOMI include ozone, NO₂, SO₂, CO
31 and aerosol properties. The TROPOMI tropospheric NO₂ column product (Boersma et al.,
32 2018) shows improved spatial resolution over previous. The NO₂ retrieval algorithm is based
33 on the NO₂ DOMINO retrieval previously used for OMI spectra with improvements made for
34 all retrieval steps. In this article, we use the TROPOMI Level 2 NO₂ tropospheric column data
35 product to show its distribution and seasonal variations (Section 5.1).

36 **Pollutants (CO) from MOPITT**

37 The Measurements of Pollution in the Troposphere (MOPITT) instrument is onboard NASA's
38 Earth Observing System Terra spacecraft, measuring tropospheric CO since March 2000. The
39 satellite is in a sun-synchronous polar orbit of 705 km allowing the instrument to make
40 measurements in a 612 km cross-track scan with a footprint of 22 km × 22 km providing global
41 coverage every 3 days. The MOPITT measurements provide vertical profiles and total columns
42 of CO, which are useful to analyse the distribution, transport, sources and sinks on a global
43 scale. CO retrieval products are generated with an iterative optimal-estimation-based retrieval
44 algorithm based on the MOPITT calibrated radiances and a priori knowledge of CO variability.
45 The recently released version 8 (V8) products benefit from updated spectroscopic information
46 used in the radiative transfer model and improved methods for radiance bias corrections (Deeter
47 et al., 2019). In this article, we use MOPITT V8 Level 3 monthly data ([Near and Thermal](#)

1 Infrared Radiances, JIR) with day and night retrievals averaged to analyse the seasonal variation
2 of surface CO distribution (Section 5.1).

3 **Greenhouse gases (CH₄ and CO₂) from AIRS and GOSAT**

4 ~~The Atmospheric Infrared Sounder (AIRS) provides measurements of temperature and water~~
5 ~~vapor through the atmospheric column along with a number of trace gases, surface and cloud~~
6 ~~properties. The instrument is mounted on the sun-synchronous, near polar orbiting NASA~~
7 ~~satellite, AQUA, and measures the brightness temperature of infrared radiation emitted by the~~
8 ~~Earth's surface and atmosphere. CO₂ measurements from AIRS (XCO₂, ~2 ppm accuracy)~~
9 ~~show a good coverage over the Indian Ocean mid-tropospheric region and have been used in~~
10 ~~studies by Nayak et al. (2011) and Nalini et al. (2018). The AIRS retrieval algorithm is a~~
11 ~~sequential retrieval, in which the quality of the CH₄ retrievals strongly depends on the AIRS~~
12 ~~temperature and moisture profiles as well as surface temperature and emissivity products in~~
13 ~~previous steps. In this article, we use AIRS version 6 level 3 data to depict the seasonal variation~~
14 ~~of surface CH₄ distribution.~~

15 The Greenhouse Gases Observing Satellite (GOSAT/Ibuki) is a sun-synchronous polar orbit
16 satellite that measures CO₂ and CH₄ from the stratosphere to the Earth's surface. The retrieval
17 precision for CO₂ is smaller than 3.5 ppm (Yoshida et al., 2011) utilising the Thermal and Near
18 Infrared Sensor for Carbon Observation – Fourier Transform Spectrometer, which operates in
19 the shortwave and thermal emission bands. The GOSAT Level 3 product at a horizontal
20 resolution of 2.5° × 2.5° has data gaps over the globe including a major portion of the Indian
21 region during the monsoon season due to its limitation in retrieving CO₂ in the presence of
22 clouds. This is rectified in the level 4 product that uses the Atmospheric Tracer Transport Model
23 to incorporate ground-based observations and achieves a better distribution of CO₂ over the
24 Indian Ocean (Nalini et al., 2018).

25 Observations from the Thermal and Near-infrared Sensor for carbon Observation-Fourier
26 Transform Spectrometer (TANSO-FTS) onboard GOSAT in the thermal infrared (TIR) provide
27 CH₄ profile information. While the sensitivity of TIR CH₄ observations is relatively low near
28 the surface, the GOSAT/TANSO-FTS TIR instrument has been shown to have sufficient
29 sensitivity to provide CH₄ information at the top of the boundary layer for the Indian
30 subcontinent and Indian ocean region (Belikov et al., 2021). In this article we use
31 GOSAT/TANSO-FTS CH₄ Version 1 (Level 2 V1) CH₄ data at 800 hPa averaged over 2009–
32 2014 to analyse the seasonal variation of surface CH₄ distribution (Section 5.2).

34 **Pollutants (NO_{x2}) from GOME and SCIAMACHY**

35 The Global Ozone Monitoring Experiment (GOME) is a UV/Visible spectrometer on the
36 European polar sun-synchronous orbiting satellite ERS-2, launched in April 1995. It measures
37 in 230–800 nm wavelength range, with a spectral resolution of 0.2–0.4 nm, and obtains global
38 coverage at the equator after 3 days (Burrows et al. 1999). Problems with tape storage on ERS-
39 2 led to the replacement of GOME by the Scanning Imaging Absorption Spectrometer for
40 Atmospheric Chartography (SCIAMACHY), which was launched in 2002 on the European
41 ENVISAT platform. It measures in the spectral range 240–2380 nm (Bovensmann et al., 1999).
42 Both instruments provide measurements of the mean columnar amount of tropospheric NO₂
43 and allowed to study its variations and long-term changes over the Indian subcontinent (Ghude
44 et al., 2013; Mahajan et al., 2015a).

47 **4. Regional sources and sinks**

1 Atmospheric composition over the Indian Ocean is known to be impacted by the trace gas
2 outflow from the surrounding continental land masses, long range transport and regional
3 oceanic air-sea fluxes (Lawrence and Lelieveld, 2010). Here, we describe the distribution,
4 seasonality and trends of continental and oceanic trace gas emissions important for the
5 atmospheric composition over the Indian Ocean. Our study region includes East Africa, the
6 Middle East, South Asia, East Asia, and Southeast Asia and is depicted in Fig. 3.

7 We use the latest versions of the Emissions Database for Global Atmospheric Research
8 (EDGAR), in order to present continental pollution and greenhouse gas emissions over the last
9 two decades. For air pollutants, EDGAR v5.0_AP for the period 1970–2015 is available
10 (Crippa et al., 2020) and for greenhouse gases EDGAR v5.0_GHG for the period 1970–2015
11 (Crippa et al., 2019) can be used. The EDGAR datasets include continental emissions from the
12 energy sector (i.e., power industry), industrial processes (i.e., manufacturing, industrial
13 combustion), the transport sector (i.e., road transport, aviation), residential sources (small-scale
14 combustion and waste treatment), and agriculture. Exhausts from ship engines as one of the
15 major sources of air pollution over the open ocean are also included in the EDGAR emissions.
16 The datasets are given at a high spatial resolution of $0.1^\circ \times 0.1^\circ$. The results shown in this
17 section focus on the main pollutants CO, NO_x, and SO₂, and the greenhouse gases CH₄, N₂O,
18 and CO₂. We also briefly discuss mercury emissions. The most recent year for which data is
19 given (year 2015 for both air pollutants and greenhouse gases) is used here to present emissions
20 strength and patterns representative for the last decade. Emission changes are calculated for the
21 time period 2000–2015 and are shown in relative terms compared to the emissions in 2000.
22 Emissions are averaged over East Africa, the Middle East, South Asia, East Asia, and Southeast
23 Asia for a direct comparison of the regional contributions and the text and tables.

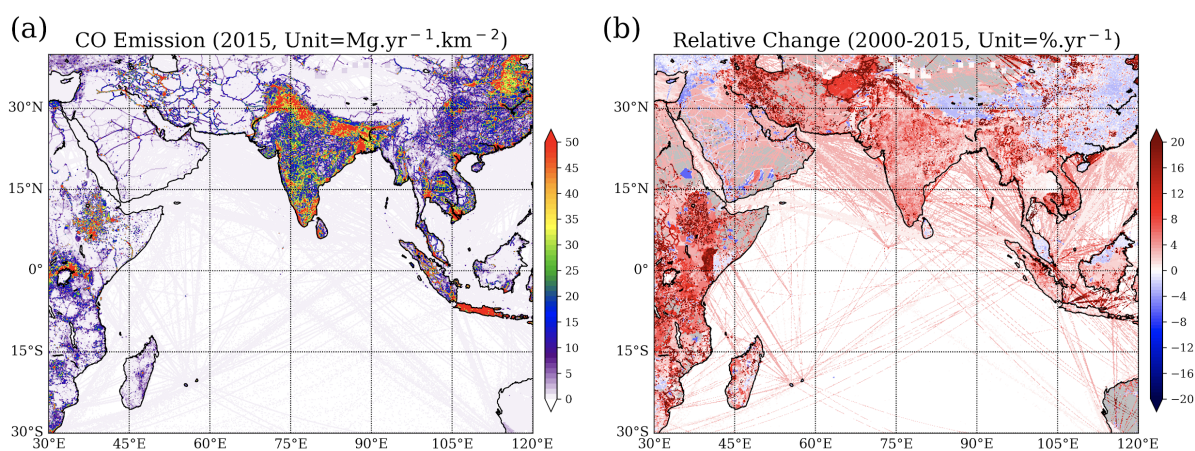
24 The ocean is an important source and sink to/from the atmosphere for many of the same gases
25 mentioned above, as well as other climate- and chemically active compounds, such as DMS,
26 isoprene, and halogen species. Below we will describe the net ocean fluxes of CO, CH₄, CO₂,
27 N₂O, [VOCs](#), DMS, isoprene, and bromoform (CHBr₃) as obtained from recent publications,
28 placing special attention on monsoon related variability.

29 **4.1 Pollutants**

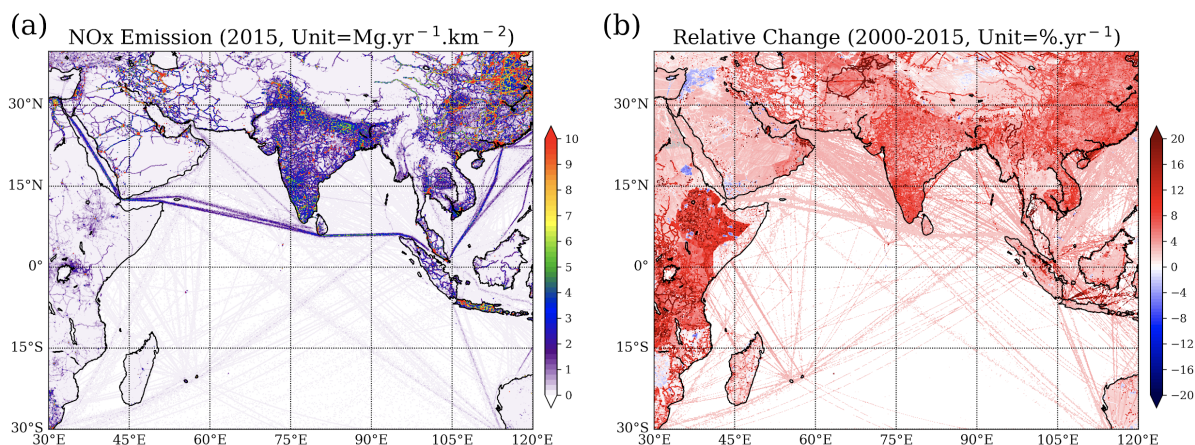
30 Among atmospheric pollutants, CO is considered to be one of the most important gases as it is
31 highly toxic at elevated concentrations. Due to its intermediate lifetime of a few months
32 (Seinfeld and Pandis, 2006), CO is much more variable in the troposphere than other
33 atmospheric constituents with longer lifetimes and often used as a transport tracer. CO has an
34 indirect radiative effect, since it scavenges the hydroxyl radical (OH), the cleaning agent of the
35 atmosphere that otherwise would destroy the greenhouse gases CH₄ and O₃ (Daniel and
36 Solomon, 1998). Another important pollutant is the family of the nitrogen oxides (NO_x)
37 consisting of nitrogen dioxide (NO₂) and nitrogen oxide (NO). Tropospheric NO_x acts as a
38 precursor for a number of harmful secondary air pollutants such as ozone and particulate matter
39 and plays a role in the formation of acid rain. Breathing in raised levels of NO₂ can cause
40 respiratory problems independently of negative health effects of other secondary pollutants.
41 Once transported into the stratosphere, reactive odd-nitrogen species destroy ozone, in
42 particular in the middle stratosphere near the ozone maximum (Portmann et al., 2012). SO₂ is
43 another key component of gaseous air pollution. As for NO₂, exposure to SO₂ can harm the
44 human respiratory system. In addition, SO₂ can react with other compounds in the atmosphere
45 to form small particles that contribute to particulate matter pollution. If oxidised within airborne
46 water droplets, SO₂ produces sulphuric acid, which can be transported by wind over many
47 hundreds of kilometres and deposited as acid rain. Atmospheric ~~ammonia~~ (NH₃) is a pollutant
48 which plays an important role in the formation of particulate matter, as well as in acidification
49 and eutrophication of ecosystems (Lelieveld et al., 2015; Bauer et al., 2016).

1 The distributions of CO, NO_x, and SO₂ emissions are shown in Figures 3, 4 and 5, respectively.
2 One of the common features of the spatial distribution of these emissions is that they generally
3 coincide with the population distribution, such that high emissions appear in the densely
4 populated areas. In East Asia, high-emission areas include northern China, the Yangtze River
5 delta, Sichuan Basin, Korea, and Japan (not shown in the Figure). In South Asia, high emissions
6 are distributed throughout northern India, Nepal, the southern point of India, and Bangladesh.
7 In Southeast Asia, high emissions appear around some major cities including Bangkok, Hanoi,
8 and Ho Chi Minh City, as well as Java. Similar to Southeast Asia, high-emission regions in
9 East Africa are also around major cities like Kampala, Nairobi, and Addis Ababa. In the Middle
10 East, high-emission regions are distributed around the Persian Gulf. Among the different source
11 regions, East Asia and South Asia are main emitters. In 2015, the two regions accounted for
12 41% (East Asia) and 27% (South Asia) of the total CO emissions discussed here. East Asia is
13 also a large emitter of NO_x (54%) and SO₂ (57%).

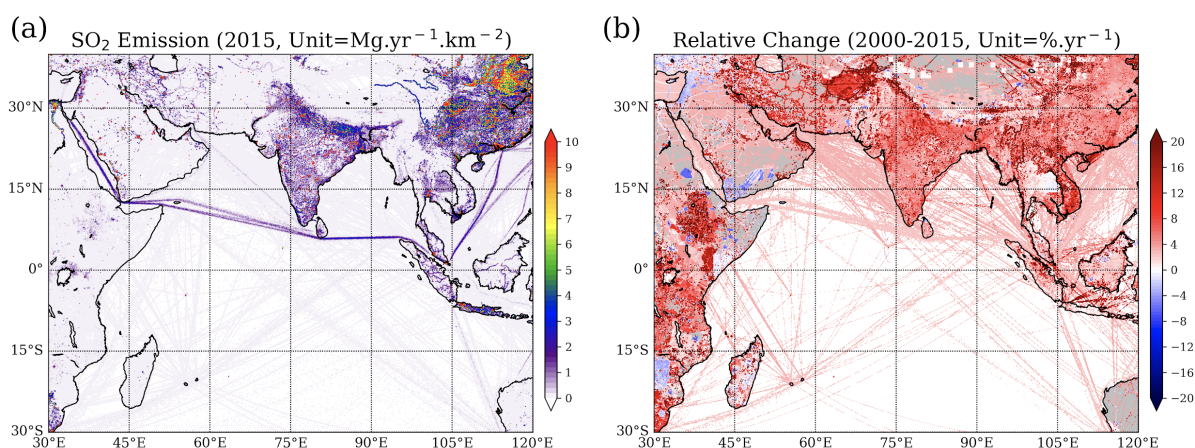
14 It is well known that pollution sources from Asia are characterized by inefficient combustion
15 processes during biofuel and fossil fuel burning. For instance, the burning of biofuels such as
16 wood, dung, and agricultural waste accounts for 18% of all CO emissions in Southeast Asia.
17 Globally it only accounted for ~9% of all CO emissions in 2015, highlighting the role of biofuel
18 burning in regions around the Indian Ocean. Inefficient combustion processes also occur during
19 fossil fuel burning at lower temperatures and result in relatively low NO_x emissions and higher
20 CO/CO₂ ratios, when compared to other industrialized areas around the globe. The incomplete
21 fossil fuel combustion from the residential sector and road transportation are the two main
22 sources contributing to the CO production, accounting for 29.5% and 29.0% of all CO
23 emissions in our study region in 2015.



24
25 **Figure 3.** Annual mean CO emissions for 2015 (a) and relative change with respect to 2000 (b) from
26 EDGAR V5.0_AP.



1
2 **Figure 4.** Same as Figure 3, but for NO_x.



3
4 **Figure 5.** Same as Figure 3, but for SO₂.

5
6 NO_x emissions mainly stem from high temperature combustion. Energy production,
7 manufacturing industries and road transportation caused 30.7%, 25.8%, and 25.6% of all NO_x
8 emissions in our study region in 2015, respectively. Manufacturing industries and energy
9 (electricity ~~production~~ and heat production) are also the two main contributors to the SO₂
10 emissions, accounting for 41% and 40%, respectively, of all SO₂ emissions in our study region
11 in 2015. As per the 2000 Asian emission inventory, India has the second highest SO₂ emission
12 (14%) after China (65%) with coal-burning power plants contributing to around half (47%) of
13 the emissions in India ([Kurokawa et al., 2013](#)[Ohara et al., 2007](#)). About 40% of the thermal
14 plants in India are located over the Indo-Gangetic Plains causing relatively high SO₂ emissions
15 from this region (Fig. 5; Aswini et al., 2020). In addition, ship traffic leads to anthropogenic
16 NO_x and SO₂ emissions directly over the open ocean with emissions concentrated along the
17 major shipping lanes (e.g., Franke et al., 2009). In general, NO_x ship emissions can lead to
18 substantial ozone enhancements and in turn to higher OH concentrations (Endresen et al.,
19 2003).

20 Over the period 2000-2015, the emissions of all pollutants increased in almost all regions
21 around the Indian Ocean, with CO emissions changing from 275.9 Tg yr⁻¹ to 350.3 Tg yr⁻¹, NO_x
22 from 35.3 Tg yr⁻¹ to 58.3 Tg yr⁻¹, and SO₂ from 41.8 Tg yr⁻¹ to 61.1 Tg yr⁻¹. Between 2000 and
23 2015, CO emissions increased particularly along the Mekong River, north of the Persian Gulf,
24 in Afghanistan and East Africa, while CO emissions in most regions of East Asia decreased

1 despite a comparably low overall increase (15%, Table 2, Fig. 3b). NO_x emission increases
 2 show a different pattern and are relatively high in most regions around the Indian Ocean, with
 3 peaks in East Asia, South Asia and East Africa (Fig. 4b) SO₂ emission changes show a similar
 4 distribution as the NO_x changes, with peaks along the Mekong River and in East Africa (Fig.
 5 5b). Ship traffic in the Indian ocean has seen the largest increase worldwide between 1992 and
 6 2012, especially on well-defined shipping lanes, such as the Red Sea-Arabian Gulf-Asia route
 7 or the Asia-Cape Town route (Tournadre, 2014). The overall increase of the pollutant emissions
 8 shows pronounced variations from region to region (Table 2) with the highest rate of all three
 9 pollutants emission increases found in South Asia.

10 In particular, for the time period after 2012, satellite measurements have shown pronounced
 11 regional SO₂ and NO₂ pollution changes. A decrease of SO₂ pollution from the North China
 12 Plain has been noted since 2011 as a result of government efforts, while SO₂ and NO₂ emissions
 13 from India have continued to grow at a fast rate (Krotkov et al., 2016). Recent emission
 14 estimates suggest that during 2013–2017, anthropogenic emissions from China decreased by
 15 23 % for CO, 21 % for NO_x, and 59 % for SO₂ over this period as a consequence of the
 16 implementation of active clean air policies (Zheng et al., 2018).

17
 18 **Table 2.** Emissions of CO, NO_x, and SO₂ from different regions in 2015 and their increase with respect
 19 to 2000.
 20

	Emission in 2015 (Increase with respect to 2000)				
	East Africa	Middle East	South Asia	East Asia	Southeast Asia
CO	26.48 Tg yr ⁻¹ (40%)	16.76 Tg yr ⁻¹ (18%)	93.97 Tg yr ⁻¹ (50%)	144.21 Tg yr ⁻¹ (15%)	68.91 Tg yr ⁻¹ (25%)
NO _x	0.89 Tg yr ⁻¹ (76%)	7.27 Tg yr ⁻¹ (65%)	12.47 Tg yr ⁻¹ (101%)	31.39 Tg yr ⁻¹ (56%)	6.28 Tg yr ⁻¹ (54%)
SO ₂	0.43 Tg yr ⁻¹ (67%)	7.55 Tg yr ⁻¹ (54%)	13.09 Tg yr ⁻¹ (120%)	34.63 Tg yr ⁻¹ (29%)	5.42 Tg yr ⁻¹ (40%)

21
 22
 23 Unfortunately, measurements of oceanic CO emissions from the Indian Ocean are sparse. We
 24 only know of unpublished data sets (D. Arevalo-Martinez, personal communication) from one
 25 GEOMAR campaign (OASIS) and a series of NASA-SAGA cruises
 26 (www.saga.pmel.noaa.gov, eastern open Indian Ocean, summer 1987). Net fluxes covering the
 27 northern to southern extent of the Indian Ocean range from ~0.1 to ~1.4 Mg km⁻² yr⁻¹, as CO is
 28 always supersaturated in the surface ocean (Conte et al., 2019 and references therein), and
 29 values are similar to ship emissions but considerably smaller than continental emissions (Fig.
 30 3). CO is produced in the surface ocean from organic material photochemistry and biological
 31 processes (Conte et al., 2019). Available data from the western Indian Ocean suggests that the
 32 most significant meridional gradients occur due to open ocean upwelling at 5°S–10°S. CO
 33 emissions are high from 5°–15°S, but to the north and south of this region, emissions decrease
 34 to zero with seasonal variations occurring due to upwelling changes. In the eastern Indian
 35 Ocean, seasonal variability is expected in association with surface productivity changes in the
 36 Seychelles–Chagos Thermocline Ridge. However, here no seasonal cycle can be detected in

1 available measurements, and it is not clear if this is a real feature or caused by the lack of data.
2 Additional variability is expected in coastal regions, since large amounts of seasonally
3 discharged runoff supply terrestrial organic material that serves as a precursor to CO marine
4 photoproduction.

5 The atmospheric pollutant mercury is transported around the globe as gaseous elemental
6 mercury, eventually oxidizing to divalent mercury. The latter is known to deposit to the surface
7 from where it can be taken up into food webs and be transformed to highly toxic species
8 endangering humans and ecosystems (Selin et al., 2007). Atmospheric mercury is released from
9 anthropogenic activities, such as coal-fired power plants, metal smelting, and waste incineration
10 (Pacyna et al., 2005; Streets et al., 2005). Emissions associated with artisanal and small-scale
11 gold mining account for almost 38% of the global total emission (UN-Environment, 2019).
12 Mercury is also emitted from the oceans, soils, terrestrial vegetation, and biomass burning.
13 These ‘natural’ emissions include some anthropogenic fraction related to the recycling of
14 previously deposited mercury (Mason and Sheu, 2002). Based on 2015 inventories, Asia is
15 responsible for a large part of the emissions (49%), which primarily stem from East and
16 Southeast Asia. While emissions in North America and the European Union have shown
17 moderate decreases, increased economic activity, notably in Asia, and the use and disposal of
18 mercury-added products have led to a global increase of approximately 20% between 2010 and
19 2015 (UN-Environment, 2019).

20 For NH₃, East Asia and South Asia are the two main contributors, which account for 38.9% and
21 32.3% of the total emissions, respectively (not shown here). From 2000 to 2015, emissions of
22 NH₃ in the regions around the Indian Ocean documented by EDGAR increased by 22.5%.
23 Agricultural activities dominate the ammonia emissions, with about 56.7%, 18.4% of the
24 emissions from the sectors of direct soil emission and manure management. Besides, long-term
25 satellite measurements (van Damme et al., 2018) show other hotspots of ammonia emission not
26 well represented in EDGAR inventory, most of which are associated with either high-density
27 animal farming or industrial fertilizer production.

28 4.2 Greenhouse gases

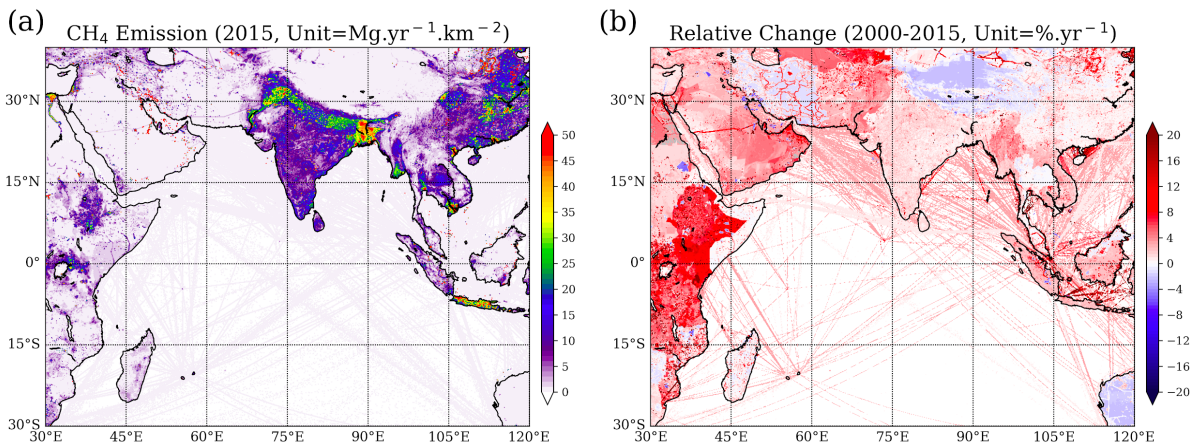
29 CO₂ concentrations have been increasing steadily over the last decades reaching a new annual
30 global mean record high in 2019~~8~~ of 409.8 ± 0.1 ppm ~~407.4 ± 0.1 ppm~~ (Blunden and Arndt,
31 2020~~19~~). Due to its high atmospheric abundance and long atmospheric lifetime, CO₂ is the most
32 important of Earth’s long-lived greenhouse gases. In addition to its impact on climate, CO₂ is
33 responsible for ocean acidification as it produces carbonic acid when it dissolves in the ocean.
34 CH₄ is also a very effective greenhouse gas and the second-largest contributor to anthropogenic
35 radiative forcing since preindustrial times after CO₂. In the troposphere, CH₄ acts to reduce the
36 atmosphere’s oxidizing capacity. It has a relatively short atmospheric lifetime of about 12.49
37 years (Myhre et al., 2013~~Prather et al., 2012~~) and exhibits a strong seasonal cycle as well as a
38 distinct gradient across the equator. Despite its relatively low atmospheric concentrations, N₂O
39 is the third anthropogenic greenhouse gas after CO₂ and CH₄ in terms of radiative forcing (Ciais
40 et al., 2014). Due to its long atmospheric lifetime of about 116 years (Prather et al., 2015) and
41 large infrared absorption capacity per molecule, N₂O is a much more efficient greenhouse gas
42 than CO₂ with a global warming potential of 265 over a 100-year time span. In the stratosphere,
43 reaction with O(¹D) leads to the production of NO (Seinfeld and Pandis, 2006), which is
44 involved in chemical ozone depletion. As a consequence, N₂O has been estimated to be the
45 main emitted ozone-depleting substance of the 21st century (Ravishankara et al., 2009; Butler
46 et al., 2016).

47 Anthropogenic greenhouse gas emissions in the regions surrounding the Indian Ocean generally
48 correspond to economic activities. As the largest emerging economies, East Asia and South

1 Asia are the main emitters of CH₄ (Fig. 6) and N₂O (Fig. 7) with emission centres in the Indo-
2 Gangetic Plain, northern China and Java. In 2015, East Asia and South Asia accounted for 37%
3 and 26% of the total CH₄ emission, as well as 43% and 26% of the total N₂O emission discussed
4 here. Among the regions surrounding the Indian Ocean, East Asia is also the largest CO₂ emitter
5 causing 68% of the total CO₂ emissions in our study region in 2015 (Fig. 8).

6 Atmospheric CH₄ has anthropogenic and natural sources, with the latter including natural
7 wetlands, livestock, termites, hydrates and forest fires. Anthropogenic sources account for the
8 majority of all emissions and can be split into biogenic and non-biogenic sectors. Almost a
9 quarter (23%) of the CH₄ emissions in our study region stems from enteric fermentation
10 (livestock farming), which acts as the primary source in South Asia and East Africa. Rice
11 cultivation in Asia is responsible for 19% of CH₄ emissions in our study region causing a
12 systematic seasonal pattern with peak emissions during the fully-grown stage in September and
13 October (Pathak et al., 2005). Other main sources of CH₄ are solid fuels (17%), mainly from
14 East Asia and Southeast Asia, and oil and gas production (14%), mainly from the Middle East.

15 N₂O emissions are linked to the biogeochemical cycle of nitrogen and are thus impacted by
16 anthropogenic use of fertilizer and industrial activities that lead to the atmospheric deposition
17 of reactive nitrogen (e.g., Davidson, 2009). More than half of the N₂O emissions in our study
18 region (56%) are directly from managed soils and can be quite heterogeneous with spatial
19 patterns revealing hot spots in agricultural areas in China and the Indo-Gangetic Plains (Ito et
20 al., 2018; Fig. 7). Furthermore, the N₂O emissions from managed soils are characterized by a
21 pronounced seasonal cycle and interannual variability, primarily in response to meteorological
22 conditions and nitrogen inputs. In particular, N₂O emissions are correlated with soil moisture
23 (Raut et al., 2015), leading to strongly enhanced emissions in South Asia during summertime
24 when high precipitation events occur.



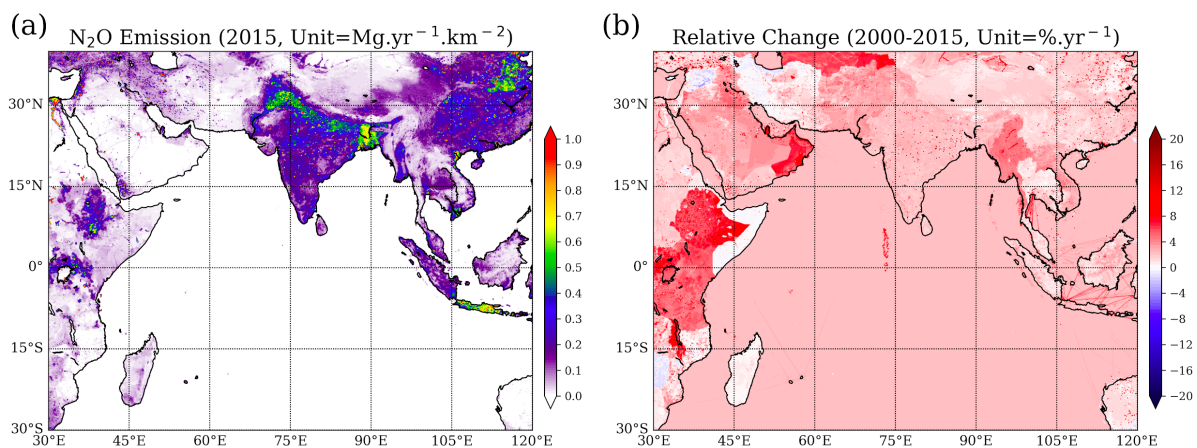
25
26 **Figure 6.** Annual mean CH₄ emissions for 2015 (a) and relative change with respect to 2000 (b) from
27 EDGAR V5.0_GHG.

28
29 Similar to the air pollutants discussed above, the overall CH₄ and N₂O emissions increased
30 significantly over the period 2000–2015 from 135.7 Tg yr⁻¹ to 182.4 Tg yr⁻¹ and from 2.80 Tg
31 yr⁻¹ to 3.51 Tg yr⁻¹, respectively. Increasing CH₄ emission in South Asia (Fig. 6b) have been
32 linked to increased rice cultivation area, natural wetlands, and warmer climate (Tian et al.,
33 2015). Increasing N₂O emissions (Fig. 7b) are believed to stem from intensified crop production
34 and nitrogen fertilizer use as well as higher air temperatures (Raut et al., 2015). While not being
35 the main emitter, East Africa is the region with the fastest increase of CH₄ and N₂O emissions
36 among the regions discussed here (Fig. 6b and 7b, Table 3). A recent study suggested that east
37 African wetlands could account for up to a third of the spike in global CH₄ emissions between

1 2010 and 2016, with most of this coming from the South Sudanese wetland, one of the largest
 2 freshwater ecosystems in the world (Lunt et al., 2019).

3 **Table 3.** Emissions of CH₄, N₂O, and CO₂ from different regions in 2015 and their increase in respect
 4 to 2000.

	Emission in 2015 (Increase respect to 2000)				
	East Africa	Middle East	South Asia	East Asia	Southeast Asia
CH ₄	12.33 Tg yr ⁻¹ (50%)	21.47 Tg yr ⁻¹ (50%)	47.65 Tg yr ⁻¹ (24%)	68.08 Tg yr ⁻¹ (34%)	32.83 Tg yr ⁻¹ (38%)
N ₂ O	0.36 Tg yr ⁻¹ (51%)	0.20 Tg yr ⁻¹ (21%)	0.91 Tg yr ⁻¹ (36%)	1.52 Tg yr ⁻¹ (15%)	0.52 Tg yr ⁻¹ (26%)
CO ₂	69.3 Tg yr ⁻¹ (137%)	2062.30 Tg yr ⁻¹ (93%)	2565.10 Tg yr ⁻¹ (125%)	13041.02 Tg yr ⁻¹ (127%)	1430.79 Tg yr ⁻¹ (79%)



5
 6 **Figure 7.** Same as Figure 6 but for N₂O

7
 8 For CO₂, the majority of the emissions in our study region stem from East Asia related to two
 9 main sectors: electricity and heat production (41%) and manufacturing industries (23%). Over
 10 the period 2000–2015, the CO₂ emissions in our study region more than doubled from 8790
 11 Tg yr⁻¹ to 19168 Tg yr⁻¹. Especially in East Asia and South Asia, they grew at very fast rates
 12 with increases of 127% and 125%, respectively. Despite the apparent policy breakthrough
 13 leading to the Paris Agreement in 2015, CO₂ emissions from fossil fuel and industry have
 14 continued to increase over the recent years. According to the latest estimates from the Global
 15 Carbon Project, the expected growth of global emissions in 2019 will be almost entirely due to
 16 China and India with expected annual growth rates of 2.6% and 1.8%, respectively (Peters et
 17 al., 2020).

18 The ocean is also a source and sink of greenhouse gases. Compared to the terrestrial sources,
 19 the ocean is just a minor contributor to the atmospheric CH₄, accounting for 1%–13% of the
 20 global atmospheric CH₄ budget (Saunois et al., 2016). The concentration of CH₄ in the Indian
 21 Ocean is characterized by a sharp decrease offshore (Naqvi et al., 2010a). Due to the large
 22 geographical changes in surface saturation and wind speed, the sea-to-air flux of CH₄ varies
 23 strongly in the northern Indian Ocean. Highest emissions were observed during the southwest

1 monsoon in the Arabian Sea ($\sim 64 \mu\text{mol m}^{-2} \text{d}^{-1}$), and the estimated overall CH_4 emission from
2 Arabian Sea amounts to $0.1\text{--}0.2 \text{ Tg yr}^{-1}$ (Naqvi et al., 2005), which is much smaller than the
3 total terrestrial emissions mentioned above ($\sim 182 \text{ Tg yr}^{-1}$ in 2015).

4 Unlike CH_4 , the ocean is a major source of N_2O , accounting for at least one third of global N_2O
5 emissions (Bange, 2006). Intense N_2O emissions are usually found in upwelling regions with
6 OMZs (Codispoti, 2010), such as in the Arabian Sea and Bay of Bengal (not shown). The South
7 Asian monsoon drives intense seasonal changes of upwelling in both OMZs, thus affecting the
8 regional N_2O productivity and emissions. The upwelling in the Arabian Sea is most intense
9 during the South Asian summer monsoon, leading to high oceanic N_2O production (Naqvi et
10 al., 2010a) and emissions of $0.34\text{--}0.99 \text{ Tg N}_2\text{O yr}^{-1}$ (Naqvi et al., 2010b), representing 2–31%
11 global oceanic N_2O emissions (Suntharalingam et al., 2019). However, the estimate by
12 Sudheesh et al. (2016) in the south-eastern Arabian Sea, based on the measurements from
13 Mangalore and Kochi, is almost four times lower than previous estimates. Raes et al. (2016)
14 proposed that the south-eastern Indian Ocean could be both a source and sink of N_2O ,
15 suggesting great uncertainty of the oceanic emission of N_2O in the Indian Ocean. The upwelling
16 driven by the summer monsoon also occurs in the Bay of Bengal, however, it is attenuated by
17 the intense precipitation and pronounced freshwater discharge from the Ganges, yielding lower
18 N_2O productivity (Singh and Ramesh, 2015) and much smaller emission ($\sim 0.03\text{--}0.11 \text{ Tg N}_2\text{O}$
19 yr^{-1} , Naqvi et al., 1994, 2010b). There is some indication that increased nitrogen deposition,
20 due to anthropogenic perturbation, already influences the air-sea flux of N_2O in the northern
21 Indian Ocean and will continue to do so into the future (Suntharalingam et al., 2019). Due to
22 sparse measurements, it is impossible to compare the oceanic N_2O emission of the Indian Ocean
23 with the terrestrial emissions directly. However, the emissions from the Arabian Sea alone are
24 about 9.6%–28% of the terrestrial emissions of the study region ($\sim 3.5 \text{ Tg yr}^{-1}$ in 2015),
25 suggesting the importance of the oceanic source in the Arabian Sea region. Enhanced N_2O sea-
26 to-air fluxes were also found in a zonal band between 5°S and 10°S as a result of wind-driven
27 upwelling during the OASIS research cruise in 2014 (Ma et al., 2018).
28
29

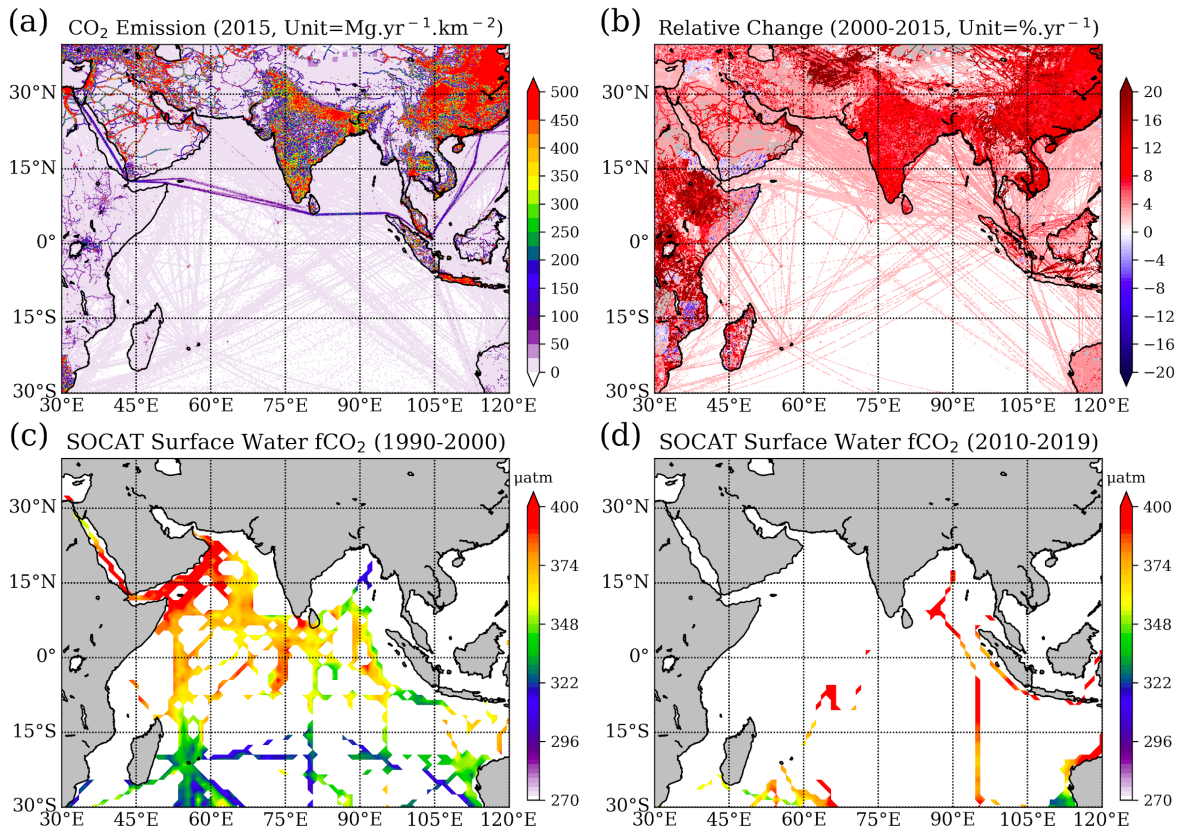


Figure 8. Annual mean CO₂ emissions for 2015 (a) and relative change with respect to 2000 (b) from EDGAR V5.0_GHG. Surface water fCO₂ observations (color shading, unit: μatm) over the Indian Ocean for 1990–2000 (c) and 2010–2019 (d) from SOCATv2019 (Bakker et al., 2016).

While the global oceans act as a net sink of CO₂, absorbing about 25% of the annual anthropogenic CO₂ emission (Le Quéré et al., 2018), the air-sea exchange of CO₂ varies at different spatial and temporal scales. The northern Indian Ocean is a net source of CO₂ to the atmosphere, while the southern Indian Ocean is a net sink (e.g., Sarma et al., 2013). Based on the inorganic carbon data collected in the Indian Ocean in 1995, for example, Bates et al. (2006) suggested that the BoB is a net oceanic source of atmospheric CO₂. Takahashi et al. (2009) constructed the climatological mean distribution for the sea surface water pCO₂ over the global oceans based on the observations from 1970 and 2007, and they suggested that the BoB is near equilibrium for CO₂. By examining numerical results produced by various ocean biogeochemical models and different atmospheric inversions, Sarma et al. (2013) argued that the BoB is a small annual net sink region for the atmospheric CO₂. Other studies report that on an annual scale, specific regions in the Bay of Bengal emits between ~ 1.61 and 2.45 ± 0.49 Mg CO₂ yr⁻¹ km⁻² (Dixit et al., 2019; Ye et al., 2019) with lowest emission of ~ 1.61 Mg CO₂ yr⁻¹ km⁻² found for 2014 in the western Bay of Bengal (Dixit et al., 2019). Significant impacts of tropical cyclones (Ye et al., 2019), biological productivity (Chakraborty et al., 2018), and freshwater discharge (Sarma et al., 2011) on the CO₂ air-sea exchange have been suggested for the Bay of Bengal. If compared to anthropogenic emissions of more than 500 Mg CO₂ yr⁻¹ km⁻² over large areas (Fig. 8a), the contribution of the northern Indian Ocean to the atmospheric CO₂ is relatively low. Analysing the Surface Ocean CO₂ Atlas (SOCATv2019; Bakker et al., 2016) demonstrates that in the Indian Ocean only a few CO₂ measurements are available for the last decade, especially when compared with the 1990s (Fig. 8c and d), making it impossible to assess the long-term changes of CO₂ air-sea exchange in this region. Northern Indian Ocean

1 [CO₂ flux variability may be influenced by ENSO events \(Valsala and Maksyutov, 2013\) and](#)
2 [hydrographic features \(i.e., eddies, Valsala and Murtugudde, 2015\).](#)

3 During the OASIS campaign in the western Indian Ocean (Zavarsky et al., 2018a), both positive
4 and negative CO₂ fluxes were observed based on the direct eddy covariance flux technique.
5 South of the equator, average values were 0.2 Mg day⁻¹ km⁻² and -0.28 Mg day⁻¹ km⁻²,
6 respectively, making this region a net sink of CO₂. These results are consistent with Chen et al.
7 (2011), who found significant spatial and temporal variability in the southern Indian Ocean
8 carbon sink. However, by comparing campaigns that occurred from 1999-2000 to those from
9 2004–2005, Chen et al. (2011) imply that the sink of the southern Indian Ocean is weakening.
10 A decadal variability analysis from 1991–2007 of dissolved CO₂ in surface seawater in the
11 southern Indian Ocean (20°S–55°S) suggests that it increased at a faster rate than atmospheric
12 CO₂ (Metzl, 2009), indicating that the ocean carbon sink weakened. The authors suggested that
13 the reduction was related to variability in the Southern Annular Mode. The weakening of Indian
14 Ocean carbon sink has also been found in a recent modelling study (DeVries et al. 2019). [The](#)
15 [southern Indian Ocean CO₂ fluxes are driven by both the solubility and biological pumps, with](#)
16 [indications that their variability is driving by ENSO forcing \(Valsala et al., 2013\).](#)

17 Carbonyl sulphide (COS) is another important long-lived trace gas that acts as a greenhouse
18 gas in the troposphere and as the main precursor of aerosols in the stratosphere (Brühl et al.
19 2012; Kremser et al. 2016). The ocean is the main source of COS to the atmosphere, previously
20 estimated at 441–542 Gg COS yr⁻¹, globally, but a revision of the vegetation sinks has led to
21 the hypothesis that the ocean source might be stronger than previously calculated. The missing
22 ocean source is hypothesised to be in the tropics (e.g., Suntharalingam et al., 2008; Glatthor et
23 al., 2015). Launois et al. (2015) modelled oceanic concentrations and emissions for this region
24 that are approximately an order of magnitude higher, but the values do not agree with the albeit
25 sparse COS measurements that exist in the Indian Ocean. A recent measurement and modelling
26 study on the OASIS campaign has shown that, in fact, the ocean source of COS is not higher
27 than previously determined (Lennartz et al., 2017). Daily integrated air-sea fluxes computed
28 for the southern Indian Ocean ranged between -0.045 and -0.000375 g COS km⁻², indicating
29 that the Indian Ocean may be a net sink for COS. In addition, COS is produced in the
30 atmosphere from DMS and carbon disulphide (CS₂) oxidation, both of which are emitted from
31 the ocean (Chin and Davis, 1993; Watts, 2000). These pathways increase the ocean source of
32 COS indirectly, but do not account for the full missing ocean source (Lennartz et al., 2017).
33 Campbell et al. (2015) and Lennartz et al. (2017) point to anthropogenic emissions of COS
34 from Asia to close the gap and, indeed, Lee and Brimblecombe (2016) find twice as much COS
35 in the atmosphere from anthropogenic emissions than previously thought. They report that
36 anthropogenic COS emissions account for approximately one third of global emissions and
37 originate from the paper industry and biofuel and coal combustion. Another study suggests that
38 COS emission from domestic use coal combustion only in China would be at least 57.2 ± 10.5
39 Gg COS yr⁻¹, an order of magnitude greater than recent estimates of COS emissions from the
40 total coal combustion in China (Du et al., 2016).

41 **4.3 [VOCs and S](#)hort-lived gases DMS, isoprene and bromoform**

42 [Volatile organic compounds \(VOCs\)](#)

43 [Volatile organic compounds \(VOCs\), such as alkanes, alkenes, and alkynes, are highly](#)
44 [reactive throughout the troposphere, influencing oxidants \(OH, O₃, NO₃\) \(Williams et](#)
45 [al. 2010\), peroxyacetyl nitrate \(PAN\), a reservoir for reactive nitrogen compounds, and](#)
46 [forming secondary organic aerosols \(Singh et al. 1995; Blando and Turpin 2000\).](#)

1 [Oxygenated VOCs play a special role in upper tropospheric OH production \(e.g., Singh](#)
2 [et al., 1995\).](#)2000

3 [The Middle East is a hotspot of VOC emissions, such as ethane and propane, from oil and gas](#)
4 [production. Interestingly, a recent study found that in addition deep water masses can be a large](#)
5 [source of VOCs that is comparable with total anthropogenic emissions from individual Middle](#)
6 [East countries \(Bourtsoukidis et al., 2020\). Other biogenic sources of VOCs include](#)
7 [surrounding forested areas \(Duflot et al., 2019\).](#)- [Formaldehyde \(HCHO\) is emitted via biomass](#)
8 [burning and fuel combustion. In addition, it has a secondary source via reactions between OH](#)
9 [and CH₄. Ship fuel combustion has recently been targeted a large source \(Gopikrishnan et al.](#)
10 [2021\). This was first postulated by Marbach et al. \(2009\) using satellite measurements of](#)
11 [HCHO and shown again by De Smedt et al. \(2021\).](#)

12 [In addition to the Bourtsoukidis et al. \(2020\) study cited above, the Indian Ocean has been](#)
13 [shown to be a main source of VOCs at other specific locations, such as at the Maïdo](#)
14 [Observatory \(Duflot et al., 2019\). Evidence of alkene emissions from the Indian Ocean and](#)
15 [specifically the Bay of Bengal was presented by Sahu et al. \(2010; 2011\) by demonstrating that](#)
16 [the ratios of ethene/propene are in line with fresh oceanic emissions \(2.3 ppt/ppt\). Alkene](#)
17 [emissions of seem to be controlled by dissolved organic carbon, wind speed, and sunlight. The](#)
18 [eastern Indian Ocean may be a source of biogenic VOCs, leading to the production of acids](#)
19 [\(diacids, oxocarboxylic acids, and \$\alpha\$ -dicarbonyls\) in the atmosphere \(Yang et al., 2020\). The](#)
20 [highly productive Arabian Sea OMZ area has been associated with enhanced production of](#)
21 [alkanes and alkenes related to– Trichodesmium and Thalassiosira phytoplankton species](#)
22 [\(Tripathi et al.,2020\).](#)

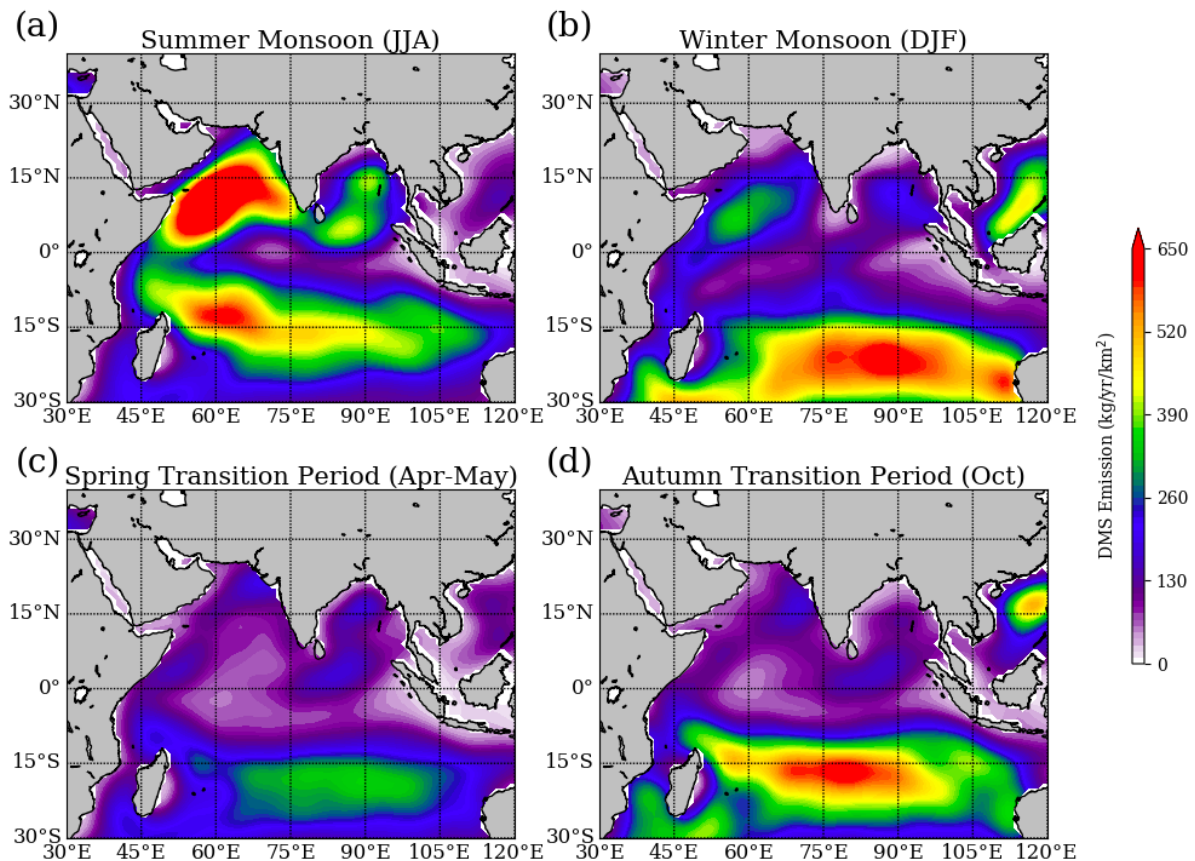
23 **Dimethylsulphide (DMS)**

24 [Marine DMS is ~~the~~ the largest source of biogenic sulphur to the atmosphere ~~is from marine DMS~~.](#)
25 DMS is produced from the algal derived precursor, dimethylsulphoniopropionate (DMSP),
26 which is cleaved by marine microbes to form DMS. Only a small fraction of this DMS is
27 released to the atmosphere. The seminal CLAW hypothesis proposed a feedback loop between
28 marine biogenic DMS production, emissions, and climate, via aerosol and cloud formation
29 (Charlson et al., 1987), triggering decades of research on DMS cycling in the ocean and
30 emission to the atmosphere. Lana et al. (2011) is the most comprehensive and up-to-date
31 monthly DMS concentration and flux climatology resulting from this large body of research.
32 Unfortunately, measurements in the Indian Ocean are sparse and most values in the climatology
33 are interpolated, with only 6271 non-uniformly spaced data points over 40 years available in
34 the Indian Ocean.

35 DMS emissions exhibit clear seasonality, with the highest fluxes, basin wide, evident during
36 the summer monsoon period. According to Lana et al. (2011), the summertime values in the
37 Indian Ocean are a global hotspot for DMS emissions. The largest values are found in the
38 Arabian Sea (Fig. 9). High biological productivity associated with the upwelling areas off north-
39 east Africa and the Arabian Sea are strongly correlated with the monsoon cycle (Yoder et al.,
40 1993). Combined with the strong, steady winds during the summer monsoon, fluxes of DMS
41 reach their peak. Lowest fluxes are computed during the spring transition period, likely
42 associated with low productivity and low wind speeds. Year round, there is a relatively large
43 flux area around 15°S, which migrates north and south according to the summer hemisphere
44 and is related to biogenic processes in the upwelling. Winds are always relatively high in this
45 region throughout the year, which also enhances the flux (Fig. 1). Maximum emissions of over
46 650 kg DMS k⁻² yr⁻¹ for the Arabian Sea (Lana et al., 2011) translate to slightly larger S flux to

1 the atmosphere from DMS than that from SO₂ ship emissions (approximately 335 kg S k⁻² yr⁻¹
2 from DMS and 250 kg S k⁻² yr⁻¹ from SO₂).

3 Gali et al. (2018) used satellite-based proxies to estimate the DMS concentration climatology
4 and reported that the Lana et al. (2011) climatology overestimates the DMS in the Indian Ocean
5 region by 25–50% in all the seasons. DMS direct flux measurements using the eddy covariance
6 technique and ocean concentration measurements were performed during the OASIS campaign
7 in order to compare directly with the Lana climatology in the western tropical Indian Ocean
8 (Zavarsky et al., 2018a). The oceanic DMS concentrations were found to be lower than those
9 in the climatology, but the difference was more pronounced south of 16°S where measured
10 values were a third of those in the climatology. North of 16°S, the measured ocean
11 concentrations were in better agreement with those in the climatology until the vicinity of the
12 Maldives, where they again were lower by a factor of three. The measured fluxes, subsequently,
13 were lower than the climatology for the region by approximately 60% on average. This was
14 attributed to lower measured oceanic concentrations, as well as lower measured wind speeds
15 than used in the climatology and a different gas transfer parameterisation. The directly derived
16 gas transfer parameterisation was linearly dependent on wind speed, while the climatology uses
17 a quadratic wind speed dependence. Nonetheless, the Indian Ocean appears to be a hotspot for
18 DMS emissions during the summer monsoon, but with more likely sulphur loading to the
19 atmosphere on the order of half of that from SO₂ ship emissions.

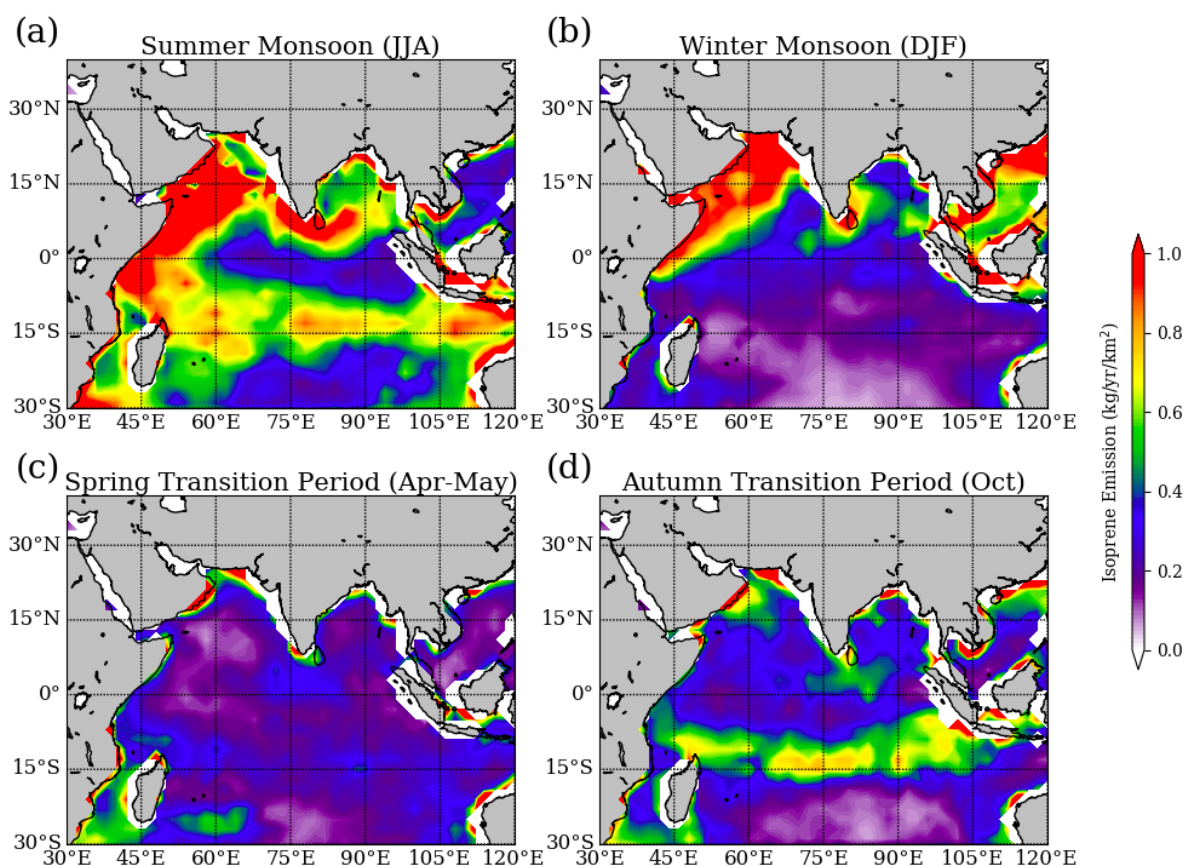


20
21 **Figure 9.** DMS emission for (a) summer monsoon (June – August), (b) winter monsoon (December –
22 February), (c) spring transition (April – May) and (d) autumn transition (October) periods from Lana
23 et al. (2011).

24
25 **Isoprene**

1 Isoprene (2-methyl-1,3-butadiene) is a biogenic ~~volatile organic compound (VOC)~~ and
2 accounts for half of the total global biogenic VOCs in the atmosphere (Guenther et al., 2012).
3 Most is emitted from terrestrial vegetation (400–600 TgC yr⁻¹, Guenther et al., 2006; Arneth et
4 al., 2008). The ocean source strength is much lower, and the magnitude is debated (Carlton et
5 al., 2009), with most estimates lower than 1 TgC yr⁻¹ (Palmer and Shaw, 2005; Arnold et al.,
6 2009; Gantt et al., 2009; Booge et al., 2016). It is known from laboratory studies that
7 phytoplankton produce isoprene (Exton et al., 2013 and references therein), but only a few
8 studies have performed direct measurements of marine isoprene concentrations worldwide.

9 Emitted isoprene affects the oxidative capacity of the atmosphere through ozone and OH
10 interactions and is a source for secondary organic aerosols (SOAs) (Carlton et al., 2009). Due
11 to the short atmospheric lifetime of minutes to a few hours, terrestrial isoprene does not reach
12 the atmosphere over much of the ocean and, thus, marine emissions of isoprene could play an
13 important role in SOA formation on regional and seasonal scales, especially in association with
14 increased production during phytoplankton blooms (Hu et al., 2013). Furthermore, isoprene
15 SOA yields increase under acid-catalysed particle phase reaction in low-NO_x conditions, which
16 dominate over open oceans regions (Surratt et al., 2010), and which are significantly higher
17 than that during neutral aerosol experiments (Henze and Seinfeld, 2006). [Here we provide data](#)
18 [from a published modelling study from the OASIS campaign with input variables from 2014 to](#)
19 [assess seasonal isoprene fluxes to the atmosphere from the Indian Ocean](#) ~~Here we use data from~~
20 ~~the OASIS campaign and a modelling study with input variables from 2014 to assess seasonal~~
21 ~~isoprene fluxes to the atmosphere from the Indian Ocean~~ (Booge et al., 2016, 2018).



22
23
24

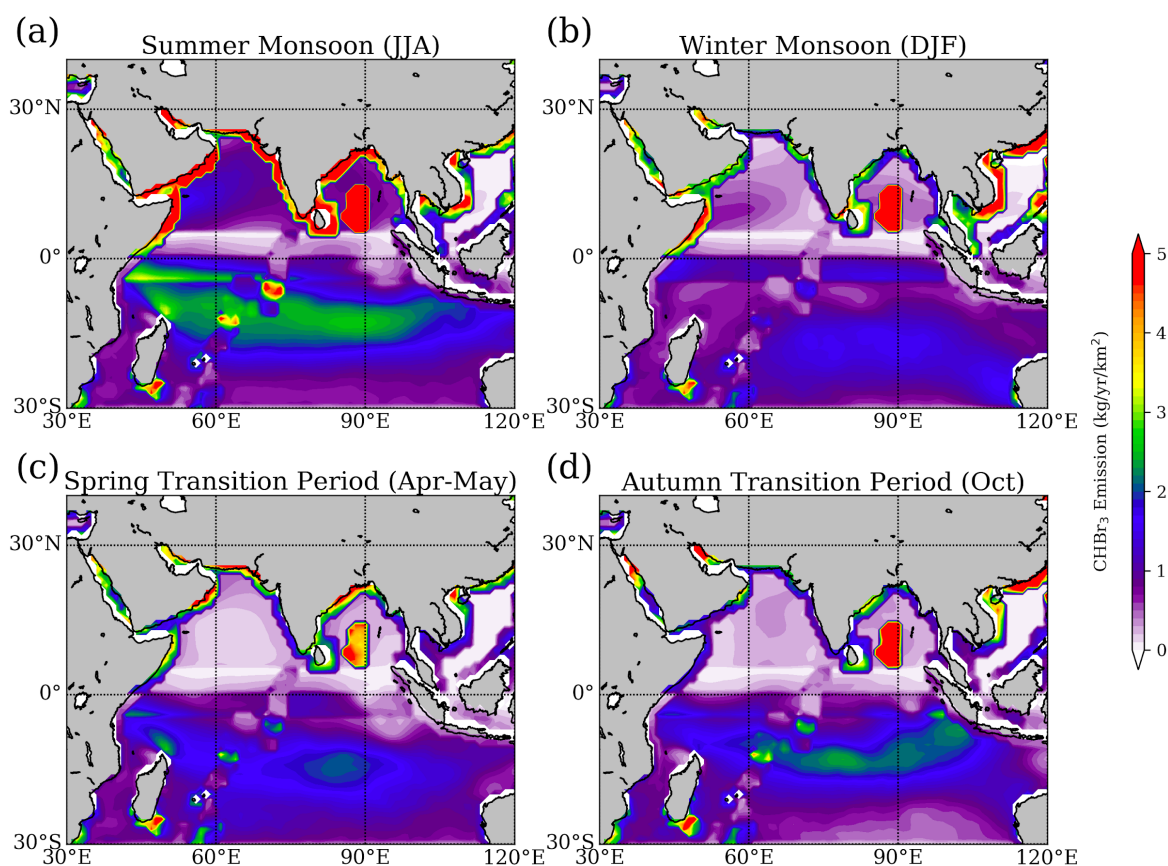
Figure 10. Same as Figure 9 but for isoprene from Booge et al. (2016).

1 Isoprene fluxes to the atmosphere change seasonally, with the highest values computed during
2 the summer monsoon over the entire Indian Ocean extent (Fig. 10). The summer values are the
3 second highest values, globally, during that season, following the Southern Ocean. Lowest
4 isoprene emissions in the Indian Ocean are found in the spring transition period. This seasonal
5 pattern is similar to the DMS emissions pattern. Computed fluxes during the winter monsoon
6 are high in the northern region of the Indian Ocean, especially in the Arabian Sea. A belt of
7 relatively high isoprene fluxes can be seen in the autumn transition period around 15°S, but the
8 values are lower than the highs seen during the summer (basin wide) and winter (Arabian Sea)
9 monsoon season. Unlike DMS, this is only visible in the summer and autumn seasons. Isoprene
10 production rates are phytoplankton functional type dependent and are driven further by light,
11 SST, salinity, and nutrients (Booge et al., 2018). High light and high SST favour higher
12 production, while high salinity and high nutrients lead to lower production. The combination
13 of the direct influence of wind speeds on fluxes and the interaction of the environmental factors
14 and isoprene production leads to the seasonal patterns.

15 **Halogens**

16 Halogenated very short-lived substances (VSLs, with lifetimes shorter than 6 months) from
17 the ocean, such as bromoform (CHBr_3), dibromomethane (CH_2Br_2) and methyl iodide (CH_3I),
18 contribute to atmospheric halogen loading and ozone depletion (Engel and Rigby et al., 2019).
19 The oceanic CHBr_3 surface concentrations are spatially and temporally highly variable. Natural
20 production of CHBr_3 involves marine organisms such as macroalgae and phytoplankton
21 (Gschwend et al., 1985), while CH_2Br_2 is formed in parallel and correlates with CHBr_3 in water
22 and air (Tokarczyk and Moore, 1994). A recent study suggests that heterotrophic processes in
23 the ocean can increase the flux of CH_2Br_2 from the sea to the atmosphere (Mehlmann et al.,
24 2020). Enhanced emissions of brominated VSLs coincide with biologically active equatorial
25 and coastal upwelling regions (Quack et al., 2007) and the distribution of macroalgae and
26 anthropogenic sources along the coasts (Carpenter and Liss, 2000; Maas et al., 2020). Iodinated
27 VSLs such as CH_3I , on the other hand, show elevated oceanic abundances in the subtropical
28 gyre regions in agreement with identified production by photochemical reactions (Richter and
29 Wallace, 2004).

30 Various CHBr_3 emission inventories have been derived from the extrapolation of measurement-
31 based data (Ziska et al., 2013; Fiehn et al., 2017), oceanic modelling (Stemmler et al., 2015),
32 top-down atmospheric modelling approaches (Liang et al., 2010) and a data-oriented machine-
33 learning algorithm (Wang et al., 2019). Overall, large differences between CHBr_3 emission
34 inventories exist with the observation-based, bottom-up emissions (Ziska et al., 2013) being
35 most consistent with atmospheric measurements in the tropics (Hossaini et al., 2013). All
36 inventories agree on the tropical Indian Ocean being a productive source region of CHBr_3 .



1
2 **Figure 11.** Bromoform (CHBr_3) emission for (a) summer monsoon (June – August), (b) winter
3 monsoon (December – February), (c) spring transition (April – May) and (d) autumn transition
4 (October) periods based on static surface concentrations and ERA-Interim meteorology for 2014 (Fiehn
5 et al., 2018).
6
7

8 Here we show the most recent bottom-up CHBr_3 emission inventory (Fiehn et al., 2018) based
9 on two campaigns in the marginal seas (Yamamoto et al., 2001; Roy et al., 2011), one campaign
10 in the open Indian Ocean (Fiehn et al., 2017) and extrapolations of measurements from other
11 oceans (Ziska et al., 2013) in Fig. 11. The emission inventory is based on static surface
12 concentration maps generated from atmospheric and oceanic surface ship-borne in-situ
13 measurements collected within the HalOcat (Halocarbons in the ocean and atmosphere)
14 database project (<https://halocat.geomar.de>, last access July 2020). While the concentration
15 maps do not provide any temporal variability, the emission parameterisation is based on
16 monthly mean meteorological ERA-Interim data allowing for relative emission peaks related
17 to maxima in the horizontal wind fields and sea surface temperature.

18 The CHBr_3 emissions peak along the Northern Hemisphere (NH) coastlines due to macroalgae
19 production and anthropogenic sources ($3.3\text{--}6.6\text{ kg yr}^{-1}\text{ km}^{-2}$), the central Bay of Bengal (up to
20 $11.1\text{ kg yr}^{-1}\text{ km}^{-2}$) and the southern tropical Indian Ocean ($2.2\text{ kg yr}^{-1}\text{ km}^{-2}$). The coastal
21 emissions in the Indian Ocean of the bottom-up inventory presented here agree well with other
22 emission estimates (Fiehn et al., 2018). High emissions along the coasts of Somalia and Oman
23 due to coastal upwelling detected in biogeochemical modelling studies (Stemmler et al., 2015)
24 are not captured here due to missing CHBr_3 measurements in this biogeochemical regime. The
25 emissions show a pronounced seasonal cycle with a peak during the summer monsoon period

1 (Fig. 11) due to higher wind speeds over the whole Indian Ocean during this time of year (Fig.
2 1).

3 Once destroyed in the atmosphere, brominated VSLS contribute to the family of inorganic
4 bromine (Br_y) consisting of bromine radicals such as bromine monoxide (BrO) and non-radical
5 reservoir species such as HBr and HOBr . Inorganic bromine has also other anthropogenic and
6 natural sources including methyl bromide, which is a product of biomass burning, leaded fuel
7 combustion, plant and marsh emissions, as well as soil fumigation (Mano and Andreae, 1994).
8 Inorganic bromine can also be released when sea salt is exposed to the atmosphere from young
9 sea-ice surfaces, frost flowers, snowpack, seawater and marine aerosols (Hay et al., 2007).

10 Similar to bromine, inorganic iodine such as iodine oxide (IO) is produced through the
11 degradation of its organic precursor CH_3I and other short-lived iodinated VSLS. The primary
12 source of iodine to the marine boundary layer, however, are believed to be inorganic iodine
13 emissions at the ocean surface from reactions of dissolved iodide with deposited gas-phase
14 ozone (Carpenter et al., 2013). Once in the atmosphere, inorganic iodine plays an important
15 role for the boundary layer chemistry by influencing the oxidising capacity through catalytically
16 removing O_3 and altering the HO_x and NO_x balance.
17

18 **5. Atmospheric composition**

19 During the South Asian summer monsoon, clean air dominates the atmospheric composition
20 over the Indian Ocean, leading to a completely different chemical regime than observed during
21 wintertime. As the ITCZ moves over the Indian subcontinent (Waliser and Gautier, 1993), air
22 mass transport via steady winds is directed from the ocean towards the land and anthropogenic
23 pollutants are confined to the continents. During this period, the intense summer monsoon
24 rainfalls also effectively remove many soluble species from the continental boundary layer.
25 During the winter monsoon and transitional months, the wind pattern is reversed with
26 continental air masses being transported towards and over the open ocean environment. This
27 leads to an increase in the anthropogenic origin trace gases and aerosol loading over the Indian
28 Ocean. Based on studies and campaigns that took place before 2010, Lawrence and Lelieveld
29 (2010) provided a comprehensive review of atmospheric composition over the Indian Ocean.
30 Here we summarize their most important findings and report on new datasets and results that
31 have emerged since then.

32 **5.1 Pollution and O_3**

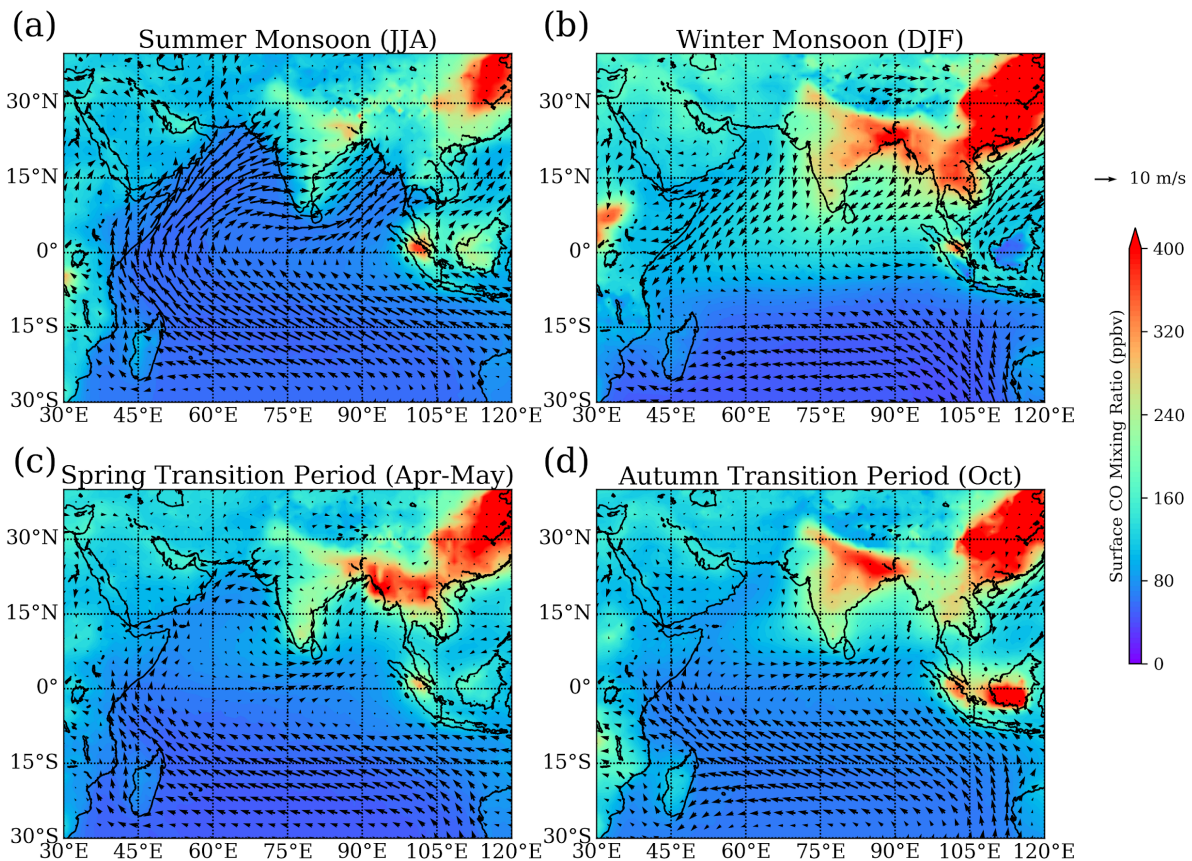
33 The surface distributions of anthropogenic pollutants and ozone levels are often highly
34 correlated as the majority of tropospheric ozone formation occurs when CO , NO_x , and other
35 ozone precursor gases react in the atmosphere in the presence of sunlight. Tropospheric ozone
36 is a greenhouse gas with a relatively short lifetime on the order of several weeks and is therefore
37 considered a near-term climate forcer. The direct radiative forcing of ozone is estimated to be
38 $0.40 \pm 0.20 \text{ W m}^{-2}$ (IPCC, 2013) and additional indirect radiative forcings can result from its
39 impact on vegetation, carbon uptake and methane lifetime (e.g., Lombardozzi et al., 2015; Fiore
40 et al., 2008). Ozone also acts as an environmental pollutant detrimental to human health, and
41 crop and ecosystem productivity (e.g., Monks et al., 2015). Changes of ozone precursor
42 emissions, low-frequency climate variability and long-term anthropogenic climate change all
43 impact the quantity and distribution of tropospheric ozone (e.g., Barnes et al., 2016).

44 The distribution and variations of pollutants and ozone over the Indian Ocean have been
45 investigated during individual campaigns (e.g., ICARB) and can be derived from continuous
46 in-situ (e.g., ozone profiling at Indian coastal stations) and satellite measurements (e.g., OMI

1 and MOPITT). The various data sets offer different advantages, allowing for a wide range of
 2 applications. While the in-situ measurements are characterised by higher resolution and lower
 3 uncertainties, they are usually limited in space (stations) or time (campaigns). The satellite
 4 measurements on the other hand, offer comprehensive spatial coverage and extend over longer
 5 time periods, but suffer from limited vertical resolution and higher uncertainties. Most available
 6 Indian Ocean campaigns and studies investigate O₃, CO and NO_x. As a result, the following
 7 sections focus on the distribution and variability of these three gases, while SO₂ and mercury
 8 are only discussed briefly.

9 **Carbon monoxide (CO) and nitrogen oxides (NO_x)**

10 The distribution of the major pollutant CO over the Indian Ocean is well known from MOPITT
 11 satellite measurements (e.g., Ghude et al., 2011; Srivastava et al., 2012a). Seasonal mean
 12 surface values for 2014/15–2018/19 show a clear gradient between CO over the Indian Ocean
 13 and over the landmass source regions (Fig. 12). Highest CO surface values over the Indian
 14 Ocean occur during the winter monsoon with multiannual mean mixing ratios of around 150
 15 ppb over the open ocean and 350–400 ppb over Bay of Bengal coastal waters (Fig. 12b). CO
 16 mixing ratios over marine regions of more than 150 ppb are considered as polluted continental
 17 air (Nowak et al., 2004), and during the winter monsoon most parts of the NH Indian ocean fall
 18 into this category. South of 5°S, mixing ratios drop below 100 ppb during winter and can be
 19 considered as part of the pristine oceanic regime.



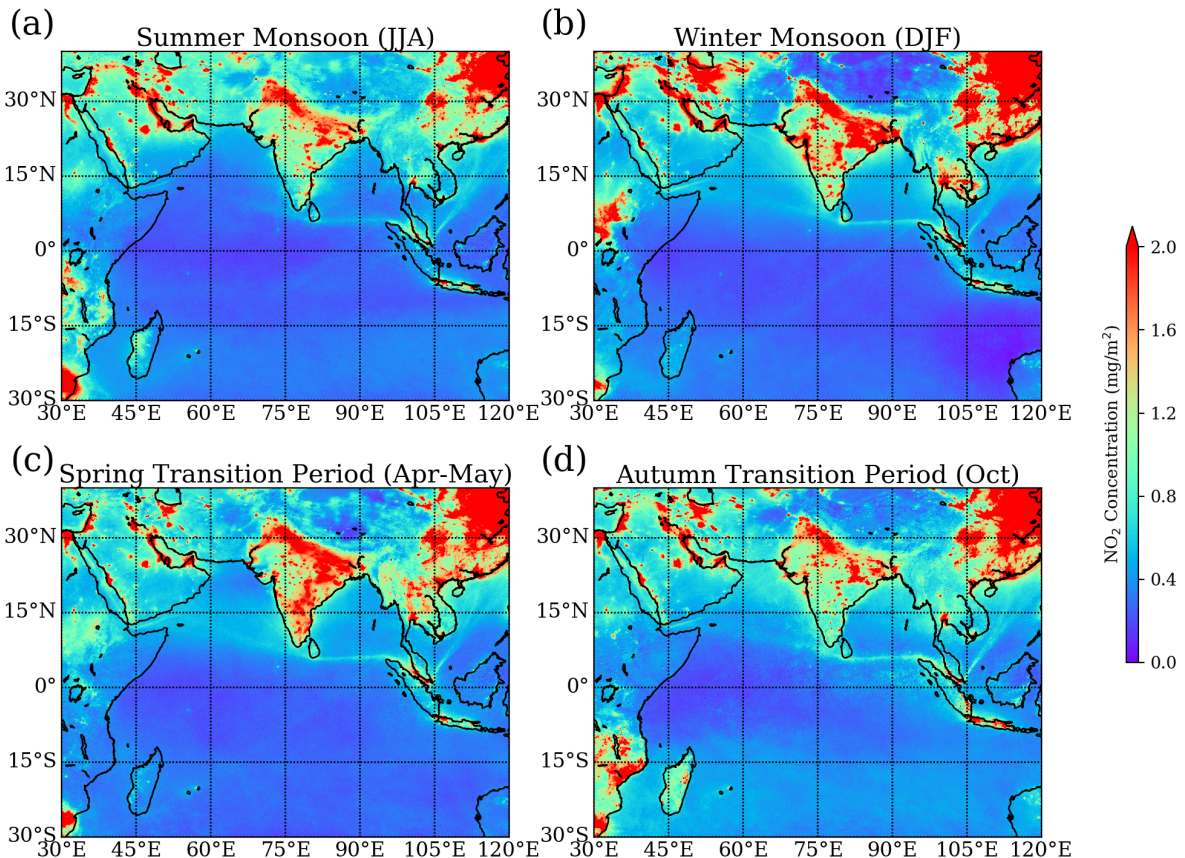
20
 21 **Figure 12.** Surface carbon monoxide (CO) mixing ratios from MOPITT (coloured shading) and surface
 22 wind from ERA-Interim (black arrows) for (a) summer monsoon 2014 – 2018 (June – August), (b)
 23 winter monsoon 2014/2015 – 2018/2019 (December – February), (c) spring transition 2014 – 2018
 24 (April – May) and (d) autumn transition 2014 – 2018 (October) periods.

25

1

2 The tropospheric distribution of NO_x is very relatively similar to that of CO, however with a
3 larger variability on small scales and steeper gradients between the continental source regions
4 and the Indian Ocean. Figure 13 shows the tropospheric NO_2 column from TROPOMI, which,
5 due to the fast photochemical cycling between NO and NO_2 , can be taken as a robust measure
6 for concentrations of nitrogen oxides. Seasonal mean values for 2018/19 show a clear gradient
7 of NO_2 , with maxima over the landmass source regions and minimum values over the equatorial
8 western Indian Ocean (Fig. 13). Coastal gradients are particularly pronounced around the Indian
9 coastline during the autumn transition period and winter monsoon. One clear difference in
10 comparison to the CO distribution is the appearance of enhanced NO_2 columns along the
11 shipping lanes, in particular along the major route at around 6°N over the Bay of Bengal from
12 the southern tip of India to Malaysia.

13 The INDOEX campaign showed that the winter monsoon season is characterized by strongly
14 enhanced CO abundances over the northern Indian Ocean, with values comparable to air
15 downwind of Europe and North America (Lawrence and Lelieveld, 2010). Based on
16 simultaneous measurements of methyl cyanide (CH_3CN) and model simulations, biomass
17 burning in South and Southeast Asia and subsequent transport of the polluted air towards the
18 Indian Ocean was identified as a major source of CO (Lelieveld et al., 2001). Over the open
19 Indian Ocean, southward transport along with chemical processing, dilution, and surface
20 deposition causes a strong north-south pollution gradient. In the boundary layer, the contrast
21 between polluted NH and pristine Southern Hemisphere (SH) air results in a sharp gradient
22 across the ITCZ (Lawrence et al., 2003), while the upper troposphere was identified as a region
23 for interhemispheric exchange of these air masses (Williams et al., 2002).



1 **Figure 13.** Tropospheric nitrogen dioxide (NO₂) column from TROPOMI for (a) summer monsoon
2 2019 (June – August), (b) winter monsoon 2018/2019 (December – February), (c) spring transition
3 2019 (April – May) and (d) autumn transition 2019 (October) periods.
4

5 Recent studies of atmospheric composition during the winter monsoon period have focused on
6 the Bay of Bengal where the ship-based measurements were conducted during the second part
7 of ICARB for December 2008–January 2009. Mixing ratios of NO₂ and CO show a distinct
8 spatial pattern with elevated values in the head and the south-east Bay of Bengal due to transport
9 from adjoining landmasses (Asatar and Nair, 2010; David et al., 2011). The in-situ
10 measurements reveal highest CO surface mixing ratios of 379±58 ppb over the south-east Bay
11 of Bengal, which exceed the MOPITT multiannual mean values (Fig. 12b). Similar to CO, the
12 NO₂ surface distribution exhibits prominent highs over the head and the south-east Bay of
13 Bengal, with lower values in the south (David et al., 2011). Analysis of back trajectories and
14 airflow patterns revealed that the high pollution over the head of the Bay of Bengal (15°N-
15 21°N) was advected from the Indo-Gangetic Plain, which is one of the major CO emission
16 centres (Fig. 3). The high pollution over the south-east Bay of Bengal, on the other hand, was
17 attributed to the effects of continental outflow from Southeast Asia, a transport pattern
18 discernible from the wind patterns in Fig. 12. Airborne measurements conducted during the
19 same campaign confirm the higher pollution over the northern and south-eastern part of the Bay
20 of Bengal (Srivastava et al., 2012b). Analyses of the acetylene/CO ratio suggested that air mass
21 samples taken over the northern Bay of Bengal were less chemically aged compared to samples
22 taken during the other flights.

23 Enhanced wintertime CO values of up to 365 ppbv were also found in the Arabian Sea near the
24 southwest coast of India, while lower levels of around 50 ppb prevailed over the equatorial
25 Indian Ocean during ICARB-2018 (Girach et al., 2020a). Consistent with previous campaign
26 results, the authors linked the enhanced surface values to the impact of South Asian outflow.
27 The study also highlighted the impact of convective outflow from Southeast Asia in the upper
28 troposphere on the pollution levels. Enhanced CO in the upper troposphere (300–200 hPa) over
29 the equatorial IO was suggested to result from anomalous westerlies associated with a disturbed
30 Walker cell and the influence of African forest fires.
31

32 Seasonal variations of NO_x at a surface station in Trivandrum, situated on the south-west coast
33 of India, also show highest values during the winter monsoon season due to land-based
34 emissions and transport patterns (David and Nair, 2011). While the strongest NO_x emissions
35 are located in East Asia, enhanced emissions also exist in southern India (Fig. 4) contributing
36 to the wintertime NO_x maxima over the Indian coastline (see also Fig. 13). Ship based
37 observations of NO₂ show a strong decreasing gradient in concentrations from the sub-continent
38 towards the open ocean. Observations made on the IIOE-2 expedition observed peak values of
39 854 ± 223 ppt close to Goa, but the values were below the detection limit of 120 ppt away from
40 the coast. A similar gradient is evident from the satellite retrieved tropospheric NO₂ with the
41 emissions of NO_x over the sub-continent leading to higher values close to the coast (Fig. 13;
42 Mahajan et al., 2019a).

43 The impact of anthropogenic emissions during the winter monsoon is evident over large parts
44 of the Indian ocean, as demonstrated by surface measurements from the island of Mahé in the
45 western Indian Ocean just south of the equator. Seasonal variations of CO values peak in
46 January–February as a result of the long-range transport of anthropogenic emissions from India
47 during this time of year (Wai et al., 2014). Reunion Island around 19°S, on the other hand, is
48 much less impacted by the winter monsoon due to the ITCZ functioning as a transport barrier.
49 Seasonal variations of CO measurements at two stations on Reunion Island peak in September–
50 November, primarily driven by the emissions from biomass burning in Africa and South

1 America (Zhou et al., 2018). The seasonal variations of the CO distribution given by the
2 MOPITT satellite observations (Fig. 12) are consistent with the findings of the in-situ
3 measurement studies discussed above.

4 During the summer monsoon, CO mixing ratios over the Arabian Sea, Bay of Bengal and the
5 Indian Ocean drop mostly below 80 ppb, except for over coastal waters in the Bay of Bengal
6 with values of up to 150 ppb (Fig 12). As the ITCZ moves north over the Indian subcontinent,
7 the large-scale air flow is directed from the Indian Ocean towards the land, preventing the
8 spread of pollution in the maritime environment. In addition, convective uplifting and mixing
9 also contribute to lower CO abundances over the Bay of Bengal (Girach and Nair, 2014a). The
10 coastal regions of Bangladesh and eastern India are exceptions, as they are impacted by strong
11 westerlies transporting polluted air from southern India and Sri Lanka resulting in elevated CO
12 mixing ratios larger than 150 ppb (Fig. 12a). In-situ measurements in 2018 conducted as part
13 of IIOE--2 confirmed elevated CO levels up to 164 ppb downwind of Chennai, a coastal
14 megacity in East India (Girach et al., 2020b). In addition, the impact of shipping emissions was
15 detected near 6°N with higher values of CO (up to 120 ppb) in the otherwise pristine airmasses
16 of the southern Bay of Bengal. The elevated pollution along the eastern India coastline is in
17 stark contrast to the western India coastline, with very low CO mixing ratios of well below 100
18 ppb. The overall prevalence of clean oceanic background air during the summer monsoon
19 season was confirmed by the low CO values detected over the equatorial Indian Ocean during
20 the OMO campaign in July/August 2015 (Tomsche et al., 2019). Vertical profiles of CO were
21 derived during flights over Gan (Maldives), which is situated close to the equator and, thus,
22 influenced by air from the southern Indian Ocean. The CO profiles over Gan with values of
23 ~60 ppb were found to be lower than the NH background and the Asian monsoon CO profiles
24 for all altitudes below 8 km (Fig. 2 in Tomsche et al., 2019). During the AQABA ship campaign
25 in summer 2017, low pollution levels over the Arabian Sea were confirmed by measurements
26 of relatively low NO_x mixing ratios (0.19 ppb, Tadic et al., 2019).

27 The transition periods during boreal spring and autumn are characterized by a large spatial and
28 temporal variability of the pollution distribution, which shifts between the clean summer regime
29 and the polluted winter regime. Mean CO mixing ratios in the Bay of Bengal and Arabian Sea
30 range between 100 and 200 ppb, while the equatorial and southern Indian Ocean are dominated
31 by clean oceanic air with CO values below 100 ppb (Fig 12c and d). ICARB measurements
32 during March--April 2006 show higher CO values in the Bay of Bengal compared to the
33 Arabian Sea and higher CO values towards the coast, as expected with continental pollution
34 being the main source of the observed values (Aneesh et al., 2008). Transport regimes start to
35 shift in March when the outflow from India into the Arabian Sea and from Southeast Asia into
36 the Bay of Bengal begins to weaken. This shift leads to slowly decreasing pollution, as observed
37 during ICARB where CO values over the northern Bay of Bengal were found to be around 234
38 ppb during March (Srivastava et al., 2012a), thus being lower than the above discussed winter
39 monsoon values. In April, offshore flow from the Indian subcontinent or Southeast Asia has
40 weakened further leading to very little pollution transport towards the ocean. The southern Bay
41 of Bengal is dominated by south-westerly winds (see also Fig 12c) carrying cleaner marine air,
42 as evident from CO mixing ratios of 88 ppb obtained during ICARB April measurements
43 (Srivastava et al., 2012a).

44 The boreal autumn transition period, also referred to as post-summer monsoon, marks the onset
45 of the polluted winter regime after the withdrawal of the monsoon winds. During this period, a
46 sudden increase of pollutant levels can be expected, in particular in coastal regions and over the
47 Bay of Bengal. During the SK-277 ship campaign, a large spatial heterogeneity of pollution
48 was observed over the Bay of Bengal (Mallik et al., 2013) reflecting the direct impact of air
49 masses being advected from different source regions in South Asia. Highest CO levels were
50 found in air masses originating in Southeast Asia with signatures of biomass and biofuel

1 burning. Continental pollution sources for NO_x were further enhanced by regional sources
2 possibly from ship emissions over the Bay of Bengal, which contains the international shipping
3 corridor connecting the southern tip of India and the Strait of Malaccaga.

4 **Sulfur dioxide (SO₂), mercury and ammonia**

5 In comparison to other pollutants, the SO₂ characterisation above the Indian Ocean is sparse.
6 Data available from the recent ICARB campaign in 2018, nonetheless, can be used to assess
7 the influence of anthropogenic SO₂ in the marine atmosphere over the Indian Ocean by using
8 non-sea salt sulfate aerosol (SO₄²⁺) as a proxy for SO₂. Aswini et al. (2020) show the presence
9 of ~~non-sea salt sulfate aerosol (SO₄²⁺)~~ in an intense pollution plume over the Arabian Sea and
10 the Indian Ocean during the winter monsoon. Meteorological conditions during this season are
11 favourable for SO₂ to SO₄²⁺ conversion. This is proposed to take place through photochemical
12 oxidation of SO₂ by the OH radical in the gas phase and through oxidation of SO₂ by H₂O₂ and
13 O₃ in the aqueous phase (Seinfeld and Pandis, 2006). About two-thirds of the total tropospheric
14 SO₄²⁺ formation is thought to occur through aqueous phase reactions (e.g., Warneck, 1999).

15 SO₂ has both anthropogenic and natural sources (i.e. oxidation of DMS), but comparison with
16 previous research cruise studies conducted nearly two decades ago shows a more than two-fold
17 increase in the concentration of nss-sulphate aerosols over the continental outflow region in the
18 Arabian Sea that appears to be due to anthropogenic SO₂ (Aswini et al., 2020). Despite
19 decreasing SO₂ emissions in East Asia since 2010, emissions are rapidly increasing in South
20 Asia, by about 10% per year with the Indo-Gangetic Plains being a major source region
21 (Lelieveld et al., 2019, Sec. 4). In order to further explore the contribution of anthropogenic
22 SO₂ to nss-sulphate aerosol formation, the ratio of methanesulphonic acid (MSA), due solely
23 to DMS oxidation, to SO₄²⁺ was computed. The average MSA/nss-SO₄²⁺ ratio during the
24 ICARB campaign was 3.1 x 10³. Over the more pristine sections of the cruise, the average ratio
25 was 4.7 x 10³. In remote marine regions, ratios of 0.065 have been found (Savoie and Prospero,
26 1989). The lower MSA/nss-SO₄²⁺ ratio implies that most of the nss-SO₄²⁺ is from anthropogenic
27 sources (Aswini et al., 2020).

28 Under the framework of the Global Mercury Observation System (GMOS) project, a mercury
29 monitoring station was set up on Amsterdam Island, a remote and small island located in the
30 southern Indian Ocean (Sprovieri et al., 2016). Observations of gaseous elemental mercury
31 (GEM), reactive gaseous mercury (RGM) and particle-bound mercury (PBM) from this station
32 over several years were reported by Angot et al. (2014). GEM concentrations were found to be
33 remarkably steady, with an average hourly mean concentration of 1.03 ± 0.08 ng m⁻³, and show
34 a small seasonal cycle. In comparison, the high altitude GMOS site in Kodaikanal located in
35 southern India shows significantly higher GEM concentrations of 1.54 ± 0.20 ng m⁻³ in 2013,
36 possibly related to different long-range transport patterns and closer proximity of anthropogenic
37 sources (Sprovieri et al., 2016).

38 RGM and PBM concentrations at Amsterdam Island were also very low (0.34 pgm⁻³ and 0.67
39 pgm⁻³, respectively), but displayed a strong seasonal variability (ranging between the detection
40 limit and 4.07 pgm⁻³ and 12.67 pgm⁻³, respectively). Analysis showed that, despite the
41 remoteness of the island, long-range transport from southern Africa contributed significantly to
42 the GEM and PBM budgets from July to September when biomass burning peaks in Africa
43 (Angot et al., 2014). During these periods, the higher GEM concentrations observed at
44 Amsterdam island were comparable to those recorded at other tropical stations distributed
45 around the globe. During periods of lower GEM concentrations, on the other hand, values of
46 less than 1 ng m⁻³ were found to be characteristic for air masses from the southern Indian
47 Ocean and Antarctic continent (Sprovieri et al., 2016).

1 Observations of ambient ammonia (NH₃) are rare in the Indian Ocean region. [Recent](#)
2 [measurements of NH₄ in aerosols over the Indian Ocean have been related to gaseous NH₃](#)
3 [emissions from land \(either anthropogenic or crustal sources, Aryasree et al., 2015; Aswini et](#)
4 [al., 2020\)](#). Earlier direct observations in 1980 by Ayers and Gras (1980) in the Southern Indian
5 Ocean showed a range between 2.2 and 4.4 nmol m⁻³. Later observations in the same region of
6 the ocean showed a lower range of 0.3 to 2.1 nmol m⁻³ (mean of 1.1 nmol m⁻³) (Norman and
7 Leck, 2005). In the north west Arabian Sea, observations of NH₃ were first carried out in 1999
8 reporting higher concentrations in the coastal environment 2.5 to 5.6 nmol m⁻³ (mean 3.8 nmol
9 m⁻³) as compared to the remote open ocean environment 0.4 to 1.8 nmol m⁻³ (mean 1 nmol m⁻³)
10 ³), showing the importance of continental fluxes to the ambient marine NH₃ loading (Gibb and
11 Mantouura, 1999a; 1999b). Similar to the Southern Indian Ocean, later observations by Norman
12 and Leck (2005) again reported a lower range between 0.05 and 0.2 nmol m⁻³ (0.1 nmol m⁻³).
13 The reason for this discrepancy between the two studies is not clear and was not discussed in
14 the study by Norman and Leck (2005).

15 Closer to the Indian coast, observations of NH₃ have been made in the Bay of Bengal over five
16 studies and show much higher concentrations as compared to the central or southern Indian
17 Ocean. Khemani et al. (1987) reported high concentrations of NH₃ in the coastal region in the
18 range between 117.6 and 211.8 nmol m⁻³ (mean 158.8 nmol m⁻³). Later, Carmichael et al. (2003)
19 also reported high NH₃ concentrations at two coastal sites (Bhubneswar: mean 288.2 nmol m⁻³
20 and Berhampur: mean 329.4 nmol m⁻³). These observations show a west-east positive gradient
21 close to the western coast of the Bay of Bengal, which is most likely driven by the local
22 transport of NH₃. Further to the northwest, Biswas et al. (2005) made observations of ambient
23 NH₃ close to the Sundarban mangrove forest which is one of the largest river deltas in the world.
24 They saw highly elevated levels, ranging from 105.2 to 675.0 nmol m⁻³ (mean 265.2 nmol m⁻³)
25 ³). The most recent reports in the literature were measurements done during the winter phase of
26 ICARB in the Bay of Bengal, which reported an average concentration of ranging between 11.7
27 and 441.2 nmol m⁻³ (mean 281.2 nmol m⁻³), with higher concentrations observed closer to the
28 coast and the lower concentrations observed in the open ocean environment (Sharma et al.,
29 2012). Unfortunately, no seasonal information is available due to the lack of continuous
30 observations through the entire year in the marine environment.

31 **Ozone**

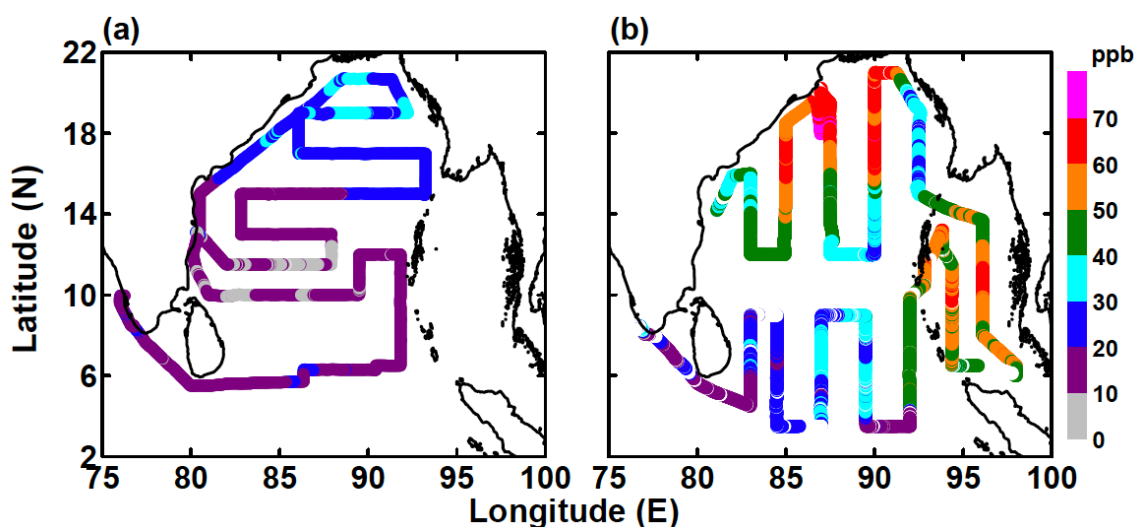
32 Ozone distribution over the Indian Ocean is largely determined by the abundance of precursor
33 gases, transport patterns and chemical processing. During the winter monsoon, the southern
34 Asian outflow brings ozone precursors such as CO, NO_x and VOCs from their source regions
35 in South and East Asia (Section 4) into the marine environment. Within the outflow, substantial
36 photochemical production of ozone occurs due to high pollution levels, [and](#) strong tropical solar
37 radiation, [and frequently which is particularly effective under](#) cloud-free conditions. As a result,
38 relatively high ozone mixing ratios of 60–70 nmol/mol have been observed off the coast of
39 India and over the Bay of Bengal up to a few hundred kilometres downwind (Lawrence and
40 Lelieveld, 2010 and references therein). [Similarly, high concentrations of up to 80 nmol/-mol](#)
41 [have also been reported off the western Indian coast in the Arabian Sea \(Lal and Lawrence,](#)
42 [2001\)](#). Once produced, ozone can be transported to the remote marine environment, where local
43 dominant sources of ozone precursor gases are absent. As a result, the marine boundary layer
44 is considered as an ideal place to study the processes that drive ozone photochemistry (e.g.,
45 Monks et al., 1998). Tropospheric ozone is also influenced by downward transport from the
46 stratosphere (e.g., Ganguly and Tzanis, 2011) and deposition to surfaces (Graedel and Crutzen,
47 1992). Photo-dissociation of ozone leads to increasing OH levels particularly within the highly
48 humid marine boundary layer affecting the chemistry of the tropical marine environment and
49 highlighting the importance of continental outflow over cleaner oceanic regions.

1 A continuous dataset of O₃ vertical profiles at Ahmedabad, a city in western India, shows a
2 clear annual cycle dominated by the wind patterns (Lal et al., 2014). The lowest ozone (~20
3 ppb) was observed near the surface during September, which is at the end of the summer
4 monsoon. Clean air from the ocean and removal of precursors due to monsoon rains drive this
5 reduction. Model simulations showed that the lower tropospheric (<3 km) O₃ during the
6 summer monsoon was transported from the Indian Ocean via the east coast of Africa and the
7 Arabian Sea. Observations of mid-tropospheric ozone are highest (70–75 ppb) during April–
8 June and lowest (40–50 ppb) during winter due to the impact of long-range transport from North
9 Africa, North America and the stratosphere. Balloon-borne O₃ measurements during 2011–
10 2014 at the southwest coast of India confirmed the highly dynamic nature of tropospheric O₃
11 profiles (Ajayakumar et al., 2019). The variations in their vertical structure and short-term
12 changes can be attributed to photochemistry as well as meteorological conditions in form of
13 synoptic scale systems, long range transport and stratospheric intrusions. Unfortunately, such
14 continuous measurements are not available at any site off the Indian subcontinent, but model
15 simulations suggest that a similar annual cycle can also be expected in the northern Indian
16 Ocean environment (Lal et al., 2014).

17 During the winter monsoon, measurements of ozone in the Bay of Bengal have been carried
18 out as a part of the ICARB campaign (David et al., 2011). The marine boundary layer showed
19 large variations in the mixing ratios of ozone and its precursor gases with similar spatial patterns
20 (Fig. 14a) pointing to the same source regions, but different relative contributions. In the head
21 and south-east of the Bay of Bengal, mixing ratios of ozone (61 ± 7 ppb and 53 ± 6 ppb) and
22 precursors (discussed earlier) were found to be very high. Air mass back trajectories originated
23 from the Indo-Gangetic Plain and Southeast Asian countries, respectively, both characterized
24 by high tropospheric ozone and NO₂ values. In the south/south-western part of the Bay of
25 Bengal, the ozone mixing ratios were low, and the back trajectories originated from coastal
26 regions. Here, the longer transit times over the marine environment could have resulted in the
27 OH-driven destruction of ozone and precursors as well as in changes of surface level mixing
28 ratios due to updrafts and downdrafts (David et al., 2011). ~~Three different ozone diurnal cycles~~
29 ~~were observed, with most patterns showing maximum mixing ratios in the morning followed~~
30 ~~by a decrease during the daytime and night-time increase.~~ Over this oceanic region,
31 photochemical production involving NO₂ did not play a major role for the ozone production,
32 while the high water vapour acted as a sink.

33 Post-winter observations during the spring transition season of near-surface ozone in the Bay
34 of Bengal were carried out as part of the first ICARB phase during March and April 2006 (Fig.
35 14b). Over the northern Bay of Bengal, higher ozone mixing ratios (~30 ppb, Nair et al., 2011)
36 were found to be well correlated with precursor gases indicating their co-located sources
37 (Srivastava et al., 2012a). Similar to the winter monsoon conditions, north-westerly winds
38 transported large amounts of anthropogenic pollutants from the Indo-Gangetic Plain to the
39 northern part of the Bay of Bengal causing the elevated pollution levels. The middle and
40 southern Bay of Bengal were more influenced by the open ocean environment and showed
41 lower ozone mixing ratios (~10–15 ppb, Nair et al., 2011). For both regions, the surface ozone
42 mixing ratios were anticorrelated with the boundary layer height. Ozone-sonde measurements
43 taken during the same campaign revealed an elevated plume between 1 and 3 km over the
44 northern Bay of Bengal with very high ozone mixing ratios of 60–90 ppb (Srivastava et al.,
45 2011). The plume was also characterised by higher temperature and lower specific humidity
46 compared to the background marine air over other regions. This elevated layer sandwiched
47 between the marine boundary layer and the free troposphere can be attributed to the advection
48 of land air mass as a consequence of land-sea breeze circulation near the coast or long-range
49 transport.

1 Observations over the Arabian sea during the ~~post-winter monsoon~~spring transition period
2 revealed a completely different picture. Ozone and pollutants showed significantly lower
3 mixing ratios when compared to the northern Bay of Bengal, suggesting the larger impact of
4 cleaner marine air (Srivastava et al., 2012a). This argument is further supported by the poor
5 inter-correlations of ozone and the various precursors. Based on simulations with the global
6 chemical transport model MOZART, the authors hypothesize that loss of ozone due to halogen
7 chemistry might be an additional reason for the relatively low ozone abundances over the
8 Arabian Sea. Latitudinal gradients of the gases were slightly negative most likely due to some
9 transport of polluted air from southern India over the southern Arabian Sea and continuous
10 dilution of pollution with time over this region. Such negative pollution gradients over the
11 Arabian sea during the transition periods were confirmed by the CO distribution obtained from
12 MOPITT (Srivastava et al., 2012a; Fig. 12c and d).
13



14
15 **Figure 14.** Surface ozone mixing ratios in the Bay of Bengal observed during a) boreal spring (March
16 ~~–~~April 2006, ICARB) and b) winter monsoon (December ~~–~~January 2009, ICARB). From David et
17 al., 2011, copyright 2011, reproduced with permission.

18 ~~Similarly, simultaneous measurements of O₃ and precursors were made over the Bay of Bengal~~
19 ~~during the post-summer monsoon season in October–November 2010. These measurements~~
20 ~~revealed large variability in O₃ (11 to 60 ppb) with maximum values found in the northern Bay~~
21 ~~of Bengal. Back trajectory analysis led to similar conclusion as the above mentioned ICARB~~
22 ~~study, revealing the influence of pollution plumes from the India–Bangladesh region and~~
23 ~~Southeast Asia in addition to long-range transport of pristine marine air from the Indian Ocean~~
24 ~~(Mallik et al., 2013).~~

25 During the summer monsoon period, unusually low levels of ozone (9 ppb) were reported for
26 the Arabian Sea during the ARMEX campaign in 2002 (Ali et al., 2009). Based on MOZART
27 model simulations, the authors attribute the low ozone abundances to chemical loss driven by
28 reactive halogens from sea salt, which can account for up to 30% of the total ozone loss (2.15
29 ppb day⁻¹). In addition, increased marine surface reactivity facilitated enhanced dry deposition
30 of ozone and thus also contributed to the observed low ozone levels (~0.12 ppb day⁻¹). Summer
31 monsoon ozone measurements in the Arabian Sea close to the Arabian Peninsula are available
32 from the AQABA ship campaign in 2017. Consistent with the low pollution levels detected in
33 this region, ozone mixing ratios were relatively low (22.5 ppb) representing remote MBL
34 conditions (Tadic et al., 2019). Net ozone production rates did not significantly deviate from

1 zero and indicate weak net ozone production of 5 ppb day⁻¹. In contrast, measurements during
2 the rest of the campaign in the Red Sea, Oman Gulf and Arabian Gulf revealed strongly
3 enhanced tropospheric ozone with larger ozone production rates of up to 28 ppb day⁻¹. The
4 sensitivity of ozone production to the prevailing conditions was assessed by defining ozone
5 production regimes in terms of the OH reactivities of VOCs and NO_x. Based on this analysis,
6 the relatively clean air of the Arabian Sea was found to be due to partially NO_x-limited ozone
7 production in this region (Pfannerstill et al., 2019).

8 Summer monsoon measurements in the Bay of Bengal report enhanced ozone and pollution
9 levels over the coastal regions, in particular, downwind of the tropical megacity Chennai. The
10 Copernicus Atmosphere Monitoring Service (CAMS) model simulations suggest that in the
11 Chennai plume, VOC-limited ozone production dominates in the morning and gradual shifts to
12 a NO_x-limited regime in the afternoon (Girach et al., 2020b).

13
14 During the autumn transition season, Similarly, simultaneous measurements of O₃ and
15 precursors were made over the Bay of Bengal ~~during the post-summer monsoon season~~ in
16 October ~~–~~–November 2010. These measurements revealed large variability in O₃ (11 ~~–~~–60
17 ppb) with maximum values found in the northern Bay of Bengal. Back trajectory analysis led
18 to similar conclusion as the above mentioned ICARB study, revealing the influence of pollution
19 plumes from the India-Bangladesh region and Southeast Asia in addition to long-range
20 transport of pristine marine air from the Indian Ocean (Mallik et al., 2013). Diurnal variations
21 found in surface ozone were also attributed to the interplay of these two processes.

22 In addition to the studies focusing on the Bay of Bengal and the Arabian Sea, observations of
23 O₃ were made along two ship tracks from the east and west of the Indian subcontinent and
24 heading towards the open oceans during December-March as a part of the ISOE 8 and IIOE-2
25 in 2014 and 2015. The ISOE 8 campaign started from Chennai on the east coast and headed
26 towards the Southern Ocean, while IIOE-2 started in Goa and went across the Arabian sea and
27 the north equatorial Indian Ocean towards Mauritius. Both of these campaigns show a strong
28 reduction in the ozone concentrations from ~50 ppb to ~5 ~~–~~–10 ppb within a few degrees off the
29 Indian coast (Mahajan et al. 2019a; 2019b), demonstrating that continental emissions are the
30 main drivers behind the high ozone concentrations close to the Indian subcontinent.

31 Diurnal variations of ozone in the marine boundary layer are driven by effects of large-scale
32 horizontal advection from source regions, entrainment of ozone rich air from higher altitudes,
33 photochemical production involving precursor gases, and loss mechanism involving OH
34 radicals. Over the last decade, significant progress has been made in understanding how the
35 different processes determine diurnal ozone variations based on in-situ observations
36 corroborated by chemistry simulations from box models, regional forecast models and chemical
37 reanalysis.

38 In polluted air masses, daytime photochemical production of ozone from anthropogenic
39 precursors such as NO_x has been observed (Nair et al., 2011; Mallik et al., 2013; Girach et al.,
40 2020b). Such photochemical production only occurs if a sufficient amount of precursor gases
41 is present and leads to peak ozone values around noon. Ozone daytime buildup has been
42 identified in the downwind of the shipping lane over the Bay of Bengal (Girach et al., 2020b)
43 and close to coastal cities (Nair et al., 2011). For the coastal region downwind of the tropical
44 megacity Chennai, the Copernicus Atmosphere Monitoring Service (CAMS) model simulations
45 suggest VOC limited ozone production in the morning which gradual shifts to a NO_x-limited
46 regime over in the afternoon (Girach et al., 2020b).

1 In pristine air masses over the Indian Ocean with low pollution levels and high water vapour,
 2 photochemical destruction of surface ozone occurs during daytime (Nair et al., 2011; Mallik et
 3 al., 2013; Girach et al., 2020b). Photolysis of ozone produces O(1D), which reacts with H₂O
 4 and produces OH radicals with the latter causing the destruction of ozone (Pitts and Pitts, 2000).
 5 Increase in the absolute water vapour content was found to coincide with the decrease in ozone
 6 and vice versa (Nair et al., 2011). During the night-time, ozone rich air can be entrained from
 7 free troposphere into the marine boundary layer allowing ozone recovery and leading to next
 8 day daytime destruction. Box model simulations have highlighted the importance of such
 9 entrainment processes given their high sensitivity to various background levels of ozone
 10 (Mallik et al., 2013).

11 In the remote marine regions, ozone is known to show ‘virtually no diurnal variation’ (Liu et
 12 al., 1983) due to the scarcity of precursor gases and the lack of exchange between the ozone-
 13 rich free troposphere and the ozone-poor boundary layer. The absence of in situ photochemical
 14 production of ozone has been observed during various Indian Ocean campaigns (e.g., Sahu et
 15 al., 2006; Lal et al., 2007; Girach et al., 2017; Girach et al., 2018). Such absence of daytime
 16 ozone build-up suggests that the observed spatio-temporal variations in surface ozone can be
 17 attributed to in situ photochemical build-up in air masses moving from coastal polluted regions
 18 towards the Indian Ocean (Ojha et al., 2012; Girach et al., 2018). Ozone simulations with the
 19 Weather Research and Forecasting model with Chemistry (WRF-Chem) along air mass
 20 trajectories suggest mean en-route ozone production in the outflow towards the Bay of Bengal
 21 (Girach et al., 2017).

22

23 **Table 4.** O₃ mean values [ppb] and latitudinal gradients reported for various campaigns in the Bay of
 24 Bengal, Arabian Sea and Indian Ocean. Ozone maximum values are given in the marine boundary layer
 25 (MBL) and in the elevated layer (EL), as available.

Season	Year and campaign	Region	O ₃ [ppb]	O ₃ maxima [ppb]	Latitudinal O ₃ gradient [ppb/°]	Reference
Winter monsoon	1999 INDOEX	Indian Ocean Arabian Sea 15°S–20°N	21.5 ± 3.5 43.9 ± 7.9	80 – 100 (EL)	1.5 – 2	Lelieveld et al. (2001) Lal et al. (2006)
	2001 BOBEX I	Bay of Bengal 13°N–20°N	42 ± 12	64 (MBL)	1.5	Lal et al. (2006)
	2008/2009 ICARB	Bay of Bengal 8°N–21°N	48 ± 8	65 (MBL)	2.1	David et al. (2011)
	2003 BOBEX II	Bay of Bengal 4°N–19°N	34 ± 6	50 (MBL)	1.4	Lal et al. (2007)
	2014 ISOE-8	Bay of Bengal Indian Ocean 11.5°N–55°S	range: 5 – 53	53 (MBL)		Mahajan et al. (2019 ^{ab})

	2015 HIOE-2	Arabian Sea Indian Ocean 11.5°N–20°S	range: 10 – 52	52 (MBL)		Mahajan et al. (2019 ba)
Post-winter monsoon <u>Spring transition</u>	2006 ICARB	Bay of Bengal 6°N–21°N	18	30 (MBL)	1.3 ± 0.1	Nair et al. (2011)
		Bay of Bengal 6°N–21°N	28.3 ± 14.4	55 (MBL) 80 (EL)	5.4 ± 0.9 (>12°N)	Srivastava et al. (2012a)
		Arabian Sea 9°N–22°N	19.8 ± 4.1	26 (MBL) 60 (EL)	-0.4 ± 0.2	Srivastava et al. (2012a)
Summer monsoon	<u>2002</u> <u>ARMEX</u>	<u>Arabian Sea</u> <u>10°N–17°N</u>	<u>9 ± 5</u>	<u>15 (MBL)</u>		<u>Ali et al. (2009)</u>
	2017 AQABA	Arabian Sea 12°N–23°N	22.5	35 (MBL)		Tadic et al., (2019)
	<u>2018</u> <u>HIOE-2</u>	<u>Bay of Bengal</u> <u>7°N–17°N</u>	<u>27.5 ± 6.3</u>	<u>45 (MBL)</u>		<u>Girach et al.</u> <u>(2020b)</u>
Summer <u>monsoon</u> and post- summer monsoon <u>autumn transition</u>	2002 BOBPS	Bay of Bengal 7°N–20°N	27 ± 6	43 (MBL)	1.3	Sahu et al. (2006)
Post-summer monsoon <u>Autumn transition</u>	<u>SK-277</u> 2010	Bay of Bengal 8°N–18°N	41 ± 9	60	3.95	Mallik et al. (2013)

1
2 Available ozone measurements from campaigns conducted in the Bay of Bengal, Arabian Sea
3 and Indian Ocean over the last decades have been summarized in Table 4. The measurements
4 reveal some clear spatial and seasonal patterns with highest ozone mixing ratios during the
5 winter monsoon, in particular in the Bay of Bengal and Arabian Sea. On average, ozone
6 abundances decrease during the ~~post-winter~~spring transition period and increase again after the
7 summer monsoon. Nearly all campaigns detected highest ozone values close to the northern
8 continental landmasses, reflecting direct impact of air masses originating from different
9 pollution source regions in South Asia and the Indo-Gangetic Plain. However, the situation can
10 also be reversed, with higher levels of ozone observed over the central Bay of Bengal, not near
11 the coastal regions (Lal et al., 2006), due to different types of wind patterns and possible
12 titration by fresh emissions of NO. Sharp latitudinal gradients ranging from 1.3 to 5.4 ppb O₃/°

1 with increasing ozone towards northern landmasses were identified during all campaigns except
2 for ICARB measurements in the Arabian Sea during the ~~post-winterspring~~ transition period.
3 The strength of the gradients depends on the season, with sharper gradients during the winter
4 and sometimes transition periods, and on the latitudinal extent, with sharper gradients closer to
5 the coastlines. Air-sea breeze triggered transport of polluted air masses in the elevated layer can
6 lead to substantially higher ozone values above the MBL, as demonstrated during the
7 campaigns where ozonesonde measurements were available. Direct comparisons of ozone
8 values in the Bay of Bengal and the Arabian Sea are in most cases not possible, except for the
9 ICARB ~~springpost-winter~~ campaign during which ozone peaked in the Bay of Bengal.

10 **5.2 Greenhouse gases**

11 Greenhouse gases are largely emitted from anthropogenic activities over the continents, as are
12 most of the atmospheric pollutants discussed above (Section 4). Therefore, both greenhouse
13 gases and pollution show a similar spatial distribution with higher values towards the coast and
14 lower values over the open ocean. However, greenhouse gases have in general longer lifetimes
15 resulting in overall smaller spatial gradients. In addition, they often have large sources from the
16 terrestrial biosphere of the NH midlatitudes, which can impact their seasonal cycle over coastal
17 and open ocean regions. In the following section, we discuss the distribution and variability of
18 the greenhouse gases CH₄, N₂O, CO₂ and COS.

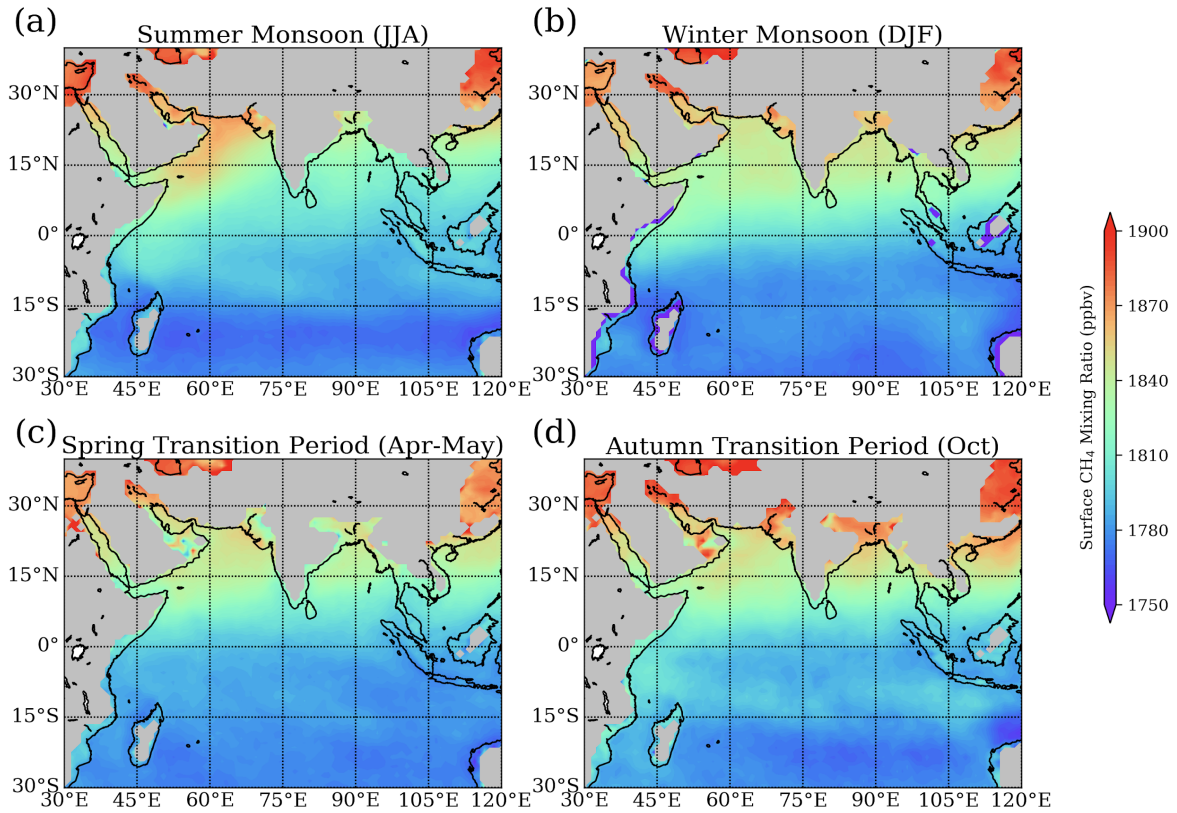
19 **Methane (CH₄)**

20 ~~The three-dimensional distribution of CH₄ over the Arabian Sea, Bay of Bengal and Indian
21 Ocean can be investigated based on AIRS satellite measurements (Fig. 15; Kavitha and Nair,
22 2019). In the boundary layer, CH₄ is higher towards the coast and lower over the open ocean
23 due to the proximity of the source rich land regions. In particular, the fossil fuel mining areas
24 in the Arab region are believed to contribute to enhanced CH₄ over the northern Arabian Sea
25 (Kavitha and Nair, 2019).~~

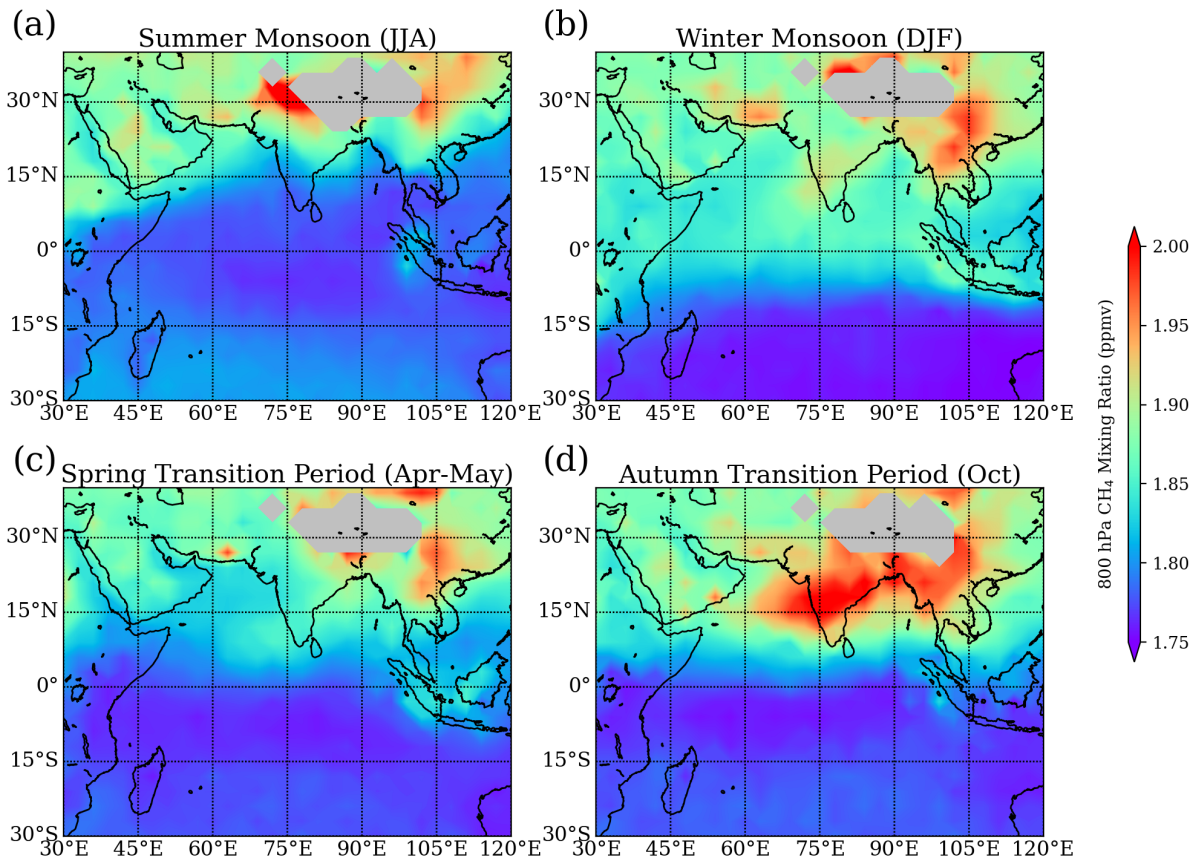
26 In-situ observations collected over the last two decades have significantly contributed to our
27 current understanding of the large-scale CH₄ distribution. revealed During the summer monsoon
28 season, near-surface CH₄ mixing ratios of 1830 ± 140 ppb were detected over the northern Bay
29 of Bengal during summer monsoon months in during the 2009 CTCZ campaign (Girach et al.,
30 2017) in agreement with the satellite observations (Fig. 15a). Back trajectory simulations linked
31 the enhanced values over the Bay of Bengal to emissions from central and northern India.
32 Overall, latitudinal CH₄ variations between 20°N and 30°S of up to 6% are much smaller than
33 latitudinal variations of CO over the same region of up to 150%. Ship data collected during the
34 winter monsoon shows decreasing CH₄ mixing ratios from the northern (1910 ppb) to southern
35 Bay of Bengal (1750 ppb) and slightly smaller abundances over the Arabian Sea (1700 to 1800
36 ppb) (Srivastava et al., 2012a). Station data for 1993–2002 from the west coast of India
37 revealed large seasonal variations with maximum values of up to 1980 ppb at the beginning of
38 the winter monsoon season (Bhattacharya et al., 2009) related to the interplay of seasonal
39 variations in emissions and transport. Maximum CH₄ mixing ratios of around 1870 ppb are
40 found over the northern and western Arabian Sea during the summer monsoon (Fig. 15a)
41 together with the strongest latitudinal gradients. Mixing ratios over this region are weaker
42 during the rest of the year resulting in a seasonal cycle quite different to the one observed over
43 other parts of the Indian Ocean. The elevated mixing ratios over the northern Arabian Sea
44 during the summer monsoon are somewhat surprising given that during this time of year south-
45 westerlies bring pristine oceanic air masses and transport from land regions is limited. One
46 possible explanation of this feature could be elevated oceanic CH₄ emissions from the coastal
47 upwelling. Such upwelling centres are found along the coast of the Arabian Peninsula and
48 Somalia during the summer monsoon (Section 2.2) and can trigger significant CH₄ release to

1 the atmosphere (Section 4.2; Bange et al., 1998). CH₄ over the eastern Arabian Sea and Bay of
2 Bengal shows a different seasonal cycle, with surface values peaking during the post-summer
3 and winter monsoon seasons. ~~CH₄ production from Asian rice cultivation maximises during the~~
4 ~~autumn transition season when the plants are fully grown (Section 4.2).~~ ~~During the post-summer~~
5 ~~autumn transition season, CH₄ production from Asian rice cultivation maximises as the plants~~
6 ~~are fully grown (Section 4.2).~~ At the same time, the onset of the winter regime starts to allow
7 for air mass transport from continental regions with significant anthropogenic influence. During
8 the winter monsoon, these transport patterns intensify bringing air masses with elevated CH₄
9 over the Indian Ocean.

10 The three-dimensional distribution of CH₄ above the boundary layer over the Arabian Sea, Bay
11 of Bengal and Indian Ocean can be investigated based on GOSAT satellite measurements (Fig.
12 15; CH₄ at 800 hPa). CH₄ is higher towards the coast and lower over the open ocean due to the
13 proximity of the source rich land regions. In particular, the fossil fuel mining areas in the Arab
14 region are believed to contribute to enhanced CH₄ over the northern Arabian Sea (Kavitha and
15 Nair, 2019). Overall, latitudinal CH₄ variations between 20°N and 30°S of up to 6% are much
16 smaller than latitudinal variations of CO over the same region of up to 150%. Consistent with
17 in-situ surface measurements, CH₄ at the top of the boundary layer of the eastern Arabian Sea
18 and Bay of Bengal maximises during the autumn transition and winter monsoon seasons. Peak
19 values of over 2000 ppb appear over the northern Bay of Bengal and along the Indian west coast.
20 The overall spatial distribution does not change much with height and at all altitudes between
21 850 ~~hPa~~ 200 hPa highest CH₄ values are found over the northern Arabian Sea and northern
22 Bay of Bengal (Kavitha and Nair, 2019). ~~However, the distinct seasonal cycle observed over~~
23 ~~the northern and western Arabian Sea changes with height to maximum mixing ratios during~~
24 ~~the post-monsoon season, further supporting the hypothesis that oceanic sources cause the~~
25 ~~surface CH₄ maxima during the summer. Similarly, the monthly variations of CH₄ mixing~~
26 ratios over all ~~other~~ oceanic regions remains more or less similar at all altitudes with a peak
27 during the ~~post-monsoon~~ autumn transition season.



1



2

1

2 **Figure 15.** ~~Surface~~ Methane (CH₄) mixing ratios at 800 hPa from ~~AIRS-GOSAT~~ for (a) summer
3 monsoon ~~2009+1 – 20145~~ (June – August), (b) winter monsoon ~~2009+1/2010+2 – 20145/20156~~
4 (December – February), (c) spring transition ~~2009+1 – 20145~~ (April – May) and (d) autumn transition
5 ~~2009+1 – 2004+5~~ (October) periods.

6

7 Over the equatorial Indian Ocean, CH₄ values at the top of boundary layer are relatively low
8 during all seasons with values mostly below 1800 ppb, except for the winter season during
9 which values can reach 1870 ppb (Fig. 15b). The OMO aircraft campaign in July/August 2015
10 confirmed ~~the~~ low CH₄ values detected by the satellite for the summer monsoon. Observations
11 over Gan (Maldives) show average CH₄ mixing ratios of 1778.3±19.5 ppb during the ~~monsoon~~
12 summer period being significantly lower than in the NH background or the Asian monsoon
13 profiles (Tomsche et al., 2019). CH₄ mixing ratios increase with height due to inter-hemispheric
14 transport mixing NH air masses into the SH at higher altitudes. As the NH air masses have
15 experienced convective uplift from the boundary layer, they advect higher CH₄ mixing ratios
16 into the SH (Bergamaschi et al., 2013).

17 The SH Indian Ocean has been found to be much less impacted by the winter monsoon
18 compared to the NH Indian Ocean due to the ITCZ functioning as a transport barrier. In situ
19 measurements from Reunion Island around 19°S, suggest the opposite seasonal cycle with
20 lowest CH₄ values in December–February and highest CH₄ values in August–September (Zhou
21 et al., 2018). Here, the CH₄ variability is not dominated by nearby land sources, but rather
22 seasonal variations of OH radicals drive the seasonal cycle of CH₄.

23 Nitrous oxide (N₂O)

24 Measurements of N₂O over the Indian Ocean are sparse. The distribution of N₂O derived during
25 a ship campaign in the Arabian Sea, equatorial Indian Ocean, and southwest part of the Bay of
26 Bengal during the ~~post-summer monsoon~~ autumn transition period (October–November 2004)
27 reveals clear latitudinal gradients (Mandal et al., 2006). Near the coast, N₂O values of 312 ppb
28 were found, and they increased towards the open ocean, with a maximum of 432 ppb at the
29 equator. In the equatorial SH, N₂O decreased sharply to 312 ppb and did not change
30 substantially during the rest of the cruise along the equator and in the southwest part of the Bay
31 of Bengal. Given the sparse data it is difficult to determine if the peak values around the equator
32 are caused by local oceanic emissions or are related to long-range transport from other sources.

33 Carbon dioxide (CO₂)

34 CO₂ satellite-based observations over the Indian Ocean reveal strong seasonal and latitudinal
35 gradients (Nalini et al., 2018; Nayak et al., 2011). During most seasons, larger CO₂ values over
36 the south and south-east Asian land masses are accompanied by pronounced latitudinal
37 gradients over the coastal regions and lower CO₂ values over the ocean. This distribution has
38 been confirmed by ship-based observations during the summer monsoon season (Kumar et al.,
39 2014) and during the ~~post-summer~~ autumn transition ~~monsoon~~ season (Mandal et al., 2006). The
40 measurements showed elevated CO₂ with large variability near the coastal region and relatively
41 low CO₂ with correspondingly lower variability over the open ocean.

42 CO₂ over the Bay of Bengal and Arabian Sea is characterized by a pronounced seasonal cycle,
43 with highest values in boreal spring and lowest values in autumn (Nalini et al., 2018). Satellite
44 observations show that during winter, a band of relatively low CO₂ mixing ratios (376–378
45 ppm) extends over the northern Indian Ocean between 0°–25°N in the west-east direction,
46 where the smallest values exist over the western Arabian Sea (Nayak et al., 2011). During boreal
47 spring, the CO₂ in this region increases, in particular over the Bay of Bengal. Seasonality over
48 the southern Indian Ocean shows a different pattern. Similarly, to the northern part, a belt of

1 low CO₂ is found during boreal winter between 10°S and 25°S. During boreal spring, however,
2 this band of relatively low CO₂ values remains prominent (Nayak et al., 2011), highlighting the
3 potential role of this region as an oceanic CO₂ sink (Section 4.2). [In addition, Valsala et al.](#)
4 [\(2020\) used 60 years of reanalysis data to identify that atmospheric mixing ratios over the](#)
5 [southeastern tropical region are driven by the Indian Ocean Dipole.](#)

6 Lagrangian transport simulations, carried out to analyse the seasonal cycle at two Indian coastal
7 stations, suggest that the seasonality of the CO₂ distribution over the Indian Ocean is driven by
8 atmospheric circulation changes combined with the seasonal cycle of CO₂ over land regions
9 (Nalini et al., 2018). While dominant marine contributions during the summer monsoon result
10 in slowly decaying values, the winter and spring monsoon season is characterized by sources
11 from the eastern continental land masses, leading to maximum values over the coastal stations
12 during spring. The equatorial Indian Ocean, on the other hand, shows only a weak seasonal
13 cycle when compared to Indian coastal locations, the Bay of Bengal, and the Arabian Sea. Here,
14 contributions from oceanic regions dominate during all seasons with smaller continental
15 contributions during the winter period. Overall, the anthropogenic emissions over the
16 continental land masses appear not to be a large source for CO₂ in the open Indian Ocean
17 environment.

18 **Carbonyl sulfide (COS)**

19 There are only three published datasets of ship or land-based observations of COS mixing ratios
20 over the Indian Ocean. The measurements were made over the course of a year at Amsterdam
21 Island (Mihalopoulos et al., 1991), on a research cruise in the eastern and southern Indian Ocean
22 in November (Inomata et al., 2006), and on the OASIS research cruise in the western tropical
23 Indian Ocean in July (Lennartz et al., 2017, see section 3). All measured COS values are either
24 at or below the global mean COS atmospheric mixing ratio of ~549 ppt and exhibit no clear
25 seasonal or latitudinal pattern (Lennartz et al., 2020). Satellite measurements and inverse
26 modelling studies show elevated values of the atmospheric COS mixing ratio over the Indian
27 Ocean, but the values are not as high as those over the Pacific Ocean and Maritime Continent
28 at similar latitudes (Glatthor et al., 2015; Kuai et al., 2015). The elevated values have led to the
29 hypothesis that the northern Indian Ocean is one of the missing source regions (Kuai et al.,
30 2015). Given the lack of compelling evidence from surface ocean measurements, however, it
31 does not appear that the Indian Ocean is the location of the missing source. Instead,
32 anthropogenic sources around Southeast Asia could be responsible, as discussed in section 4.

34 **5.3 [VOCs and S](#)hort-lived gases DMS, isoprene and halogens**

35 [VOCs](#)

36
37 [The VOC mixing ratios over the Bay of Bengal are higher during the winter monsoon than](#)
38 [during the summer monsoon for most VOCs, but with clear north-south gradients all year round](#)
39 [\(Sahu et al., 2011\). Alkenes show an opposite seasonality to the rest of the major VOCs, with](#)
40 [higher mixing ratios ~~in~~ during the summer monsoon and no clear latitudinal gradients.](#) [For the](#)
41 [other major VOCs, latitudinal gradients during the summer monsoon are caused by the transport](#)
42 [of pollutants from peninsular India to the northern Bay of Bengal and clean marine air over](#)
43 [southern Bay of Bengal. Latitudinal gradients during the winter monsoon are ascribed to](#)
44 [dilution and increased photochemical loss towards the southern Bay of Bengal. However,](#)
45 [measurements along the coasts during both seasons showed no clear latitudinal trend and were](#)
46 [influenced by photochemistry and stagnant air flow. Seasonal changes in the distribution of](#)
47 [VOCs in the surface layer over the Bay of Bengal resemble changes in wind speed \(Sahu et al.,](#)
48 [2010\). Diurnal variability of alkenes is evident in summer, but not winter, and there is evidence](#)

1 [that cyclones and convective activities in the summer season impact their mixing ratios. High](#)
2 [mixing ratios are also found over the Arabian Gulf \(Bourtsoukidis et al., 2020\). VOC](#)
3 [measurements at the Maïdo observatory in the southern Indian Ocean over two years reveal](#)
4 [VOCs in the surface layer from anthropogenic sources \(38%\), biomass burning \(33%\), and both](#)
5 [primary \(15%\) and secondary \(14%\) biogenic sources \(Verreyken et al., 2021\).](#)

6
7 [Regarding HCHO, Gopikrishnan et al. \(2021\) used satellite measurements for the period 2005–](#)
8 [2014 and found large amounts along the ship routes in the Indian Ocean. The values were](#)
9 [double the natural background without the presence of ships. The trend in HCHO](#)
10 [concentrations over the Indian Ocean shipping lanes is about \$0.008 \times 10^{15}\$ molec./cm²/year,](#)
11 [where the HCHO values and trends from the northern Indian Ocean routes are comparable to](#)
12 [those in the Panama Canal, Mediterranean Sea and Strait of Malacca.](#)

13 14 **DMS and isoprene**

15 DMS in the Arabian Sea is projected to act as a relatively large oceanic source of sulfur to the
16 atmosphere during the Asian summer monsoon season (Lana et al., 2011). These high emissions
17 have been confirmed by recent ship-based measurements during the AQABA campaign,
18 identifying elevated DMS values in the atmosphere ranging from 100 to 500 ppt (Edtbauer et
19 al., 2020). Given the low atmospheric background pollution and the elevated DMS mixing
20 ratios, the latter was found among the ten most important OH sinks with a reactivity of 0.02 s^{-1}
21 (Pfanterstill et al., 2019). During the OASIS campaign, similar atmospheric mixing ratios of
22 approximately 20–300 ppt were measured over the western tropical Indian Ocean. The
23 atmospheric distribution patterns in time and space during OASIS generally matched measured
24 fluxes (Zavarsky et al., 2018b). During this study, the directly measured DMS fluxes, as well
25 as calculated isoprene fluxes and sea spray fluxes, were correlated with satellite-derived aerosol
26 products over the region. Many of the correlations, which took into account the influence of
27 regional transport as computed FLEXPART trajectories, were statistically significant. The
28 aerosol product distribution more closely resembled the trace gas fluxes than the sea spray flux
29 distributions. Thus, sea spray appears to be more of a minor precursor than the trace gases. This
30 is supported by Quinn et al. (2017) who found a 30% contribution of sea spray to cloud
31 condensation nuclei in the tropics. These results illustrate the importance of the regional
32 coupling between marine-derived gaseous precursors and aerosol products in the remote MBL,
33 which can give rise to local feedback processes (Zavarsky et al., 2018b).

34 The longest continuous observations of atmospheric DMS in the Indian Ocean were obtained
35 at the Amsterdam Islands (37.8°S, 77.5°E) in the southern Indian Ocean (Scaire et al., 2000).
36 Measurements from 1990 to 1999 revealed atmospheric DMS ranging from 5 to 1900 ppt with
37 a clear seasonal cycle. Maximum DMS values in January were on average 20 times higher than
38 minimum values in July–August. These strong seasonal variations are not caused by
39 atmospheric transport patterns but are linked to a similar cycle in DMS concentration in
40 seawater induced by enhanced phytoplanktonic activity during the boreal summer. Model runs
41 using the Lana et al. (2011) climatology show a good match with these observations confirming
42 the dominant impact of oceanic processes on atmospheric DMS concentrations over the open
43 Indian Ocean (Mahajan et al., 2015b).

44 Atmospheric mixing ratios of isoprene were also measured during the OASIS campaign. The
45 mean measured mixing ratio was 2.5 ± 1.5 ppt (Booge et al., 2016), which is in agreement with
46 atmospheric measurements in other remote open ocean regions (Shaw et al., 2003). Booge et
47 al. (2016) used a top-down approach to calculate isoprene emissions in order to compare with
48 the bottom-up flux estimates using a box model, in which the only source of isoprene for the
49 air was assumed to be the sea-to-air flux (emission), the atmospheric lifetime was assumed to

1 be determined by reaction with OH (chemical loss, 1 h) and assuming air values to be zero at
2 the start. Computed atmospheric mixing ratios were 45 times lower than measured. In order to
3 calculate values consistent with measured mixing ratios, isoprene emissions must be more than
4 one order of magnitude greater than those computed using the bottom-up estimate based on
5 measured oceanic isoprene levels (section 4). This result agrees with isoprene emissions
6 computed with a numerical model by Luo and Yu (2010). One possible explanation could be
7 that production in the surface microlayer (SML) is not taken into account with the bottom-up
8 approach. Ciuraru et al. (2015) showed that isoprene can be produced photochemically by
9 surfactants in an organic monolayer directly at the air–sea interface. SML surfactant enrichment
10 has been observed (Wurl et al., 2011), which could result in about two orders of magnitude
11 larger isoprene fluxes than the highest fluxes calculated during the OASIS campaign. Further
12 field measurements targeting isoprene production in the SML could be a step forward in
13 reconciling the ocean source of isoprene to the atmosphere.

14 **Halogens**

15 The Indian Ocean is an important source region for halogenated VSLs such as CHBr_3 , CH_2Br_2
16 and CH_3I . During the OASIS ship campaign in summer 2014 in the west Indian Ocean, high
17 VSLs emissions with pronounced hotspots were detected (Fiehn et al., 2017). The prevailing
18 atmospheric mixing ratios, however, were generally low. The atmospheric mixing ratios of
19 CHBr_3 showed an overall mean of $1.51.20 \pm 0.35$ ppt. Elevated mixing ratios larger than 1.5
20 ppt were found in the equatorial region coinciding with lower wind speeds and maximum values
21 larger than 2 ppt were detected close to islands, where coastal sources appear to influence the
22 atmosphere. Atmospheric mixing ratios of CH_2Br_2 varied little around the mean value of 0.9
23 ppt and showed a similar pattern to the CHBr_3 mixing ratios. The CH_3I mixing ratios showed
24 relatively large variations with a mean of 0.8 ppt (Fiehn et al., 2017).

25 Reactive halogen species, such as iodine oxide (IO) and bromine oxide (BrO), that result from
26 VSLs and other sources (Section 4.3), were found to be below the detection limit or very low
27 over the Indian Ocean. In December 2000, measurements in the southern Indian Ocean were
28 carried out as preparative study for an intensive field campaign within the ELCID4 project with
29 ship track between Reunion Islands, Amsterdam Islands, Corzet Islands and Kerguelen Islands.
30 IO and BrO were both below the detection limit of the instrument, and hence upper limits of 4
31 ppt were reported for both species in the Indian Ocean (Hönninger, 2002). A field campaign in
32 the Maldives also reported upper limits for the BrO vertical columns (3×10^{14} molecules cm^{-2})
33 (Ladstätter-Weissenmayer et al., 2007). Observations on the ISOE and IIOE-2 cruises
34 reconfirmed that BrO was below the detection limit, with a lower upper limit of 2 ppt on cruises
35 starting from both the east and west of the Indian subcontinent (unpublished data). However,
36 ship-based observations have confirmed the presence of iodine oxide in the marine atmosphere,
37 although at low levels (<1 ppt). At these levels, the effect of halogen chemistry on ozone
38 destruction in the Indian Ocean MBL is significantly smaller than the Atlantic MBL, where
39 reactive halogen species can result in as much as 45% of the total ozone loss (Read et al., 2008).
40 Additionally, the outflow of NO_x from the Indian sub-continent can titrate iodine chemistry
41 through the formation of IONO_2 , which further reduces the impact of iodine on atmospheric
42 chemistry (Mahajan et al., 2019a, 2019b). Another land-based campaign observed between 2.4–
43 –3.1 ppt of IO at the Maldives (Oetjen, 2009). These results suggest that, although the reactive
44 species are low, they could contribute to local oxidative chemistry, considering that they are
45 higher than levels observed in the Atlantic MBL where they contribute towards significant
46 surface ozone loss (Mahajan et al., 2010).

47

48 **6 Synthesis and discussion**

1 Over the last decade, new knowledge of the atmospheric composition and related processes
2 over the Indian Ocean has been derived from intensive ship and aircraft campaigns, coastal
3 station measurements and satellite data. Here, we discuss how our understanding of the
4 atmospheric composition improved since 2010 and present new insights into long-term changes
5 and their impact on other Earth system components such as ocean biogeochemistry.

6 In Section 6.1, we provide a synthesis of the scientific progress made after 2010 taking into
7 account measurement data, updated emission inventories and insights from modelling studies
8 presented in Sections 3, 4 and 5. In section 6.2, we discuss how long-term changes of
9 atmospheric dynamics, oceanic processes and anthropogenic emissions impact the atmospheric
10 composition over the Indian Ocean. We highlight trends of air pollutants such as CO and NO₂
11 as well as greenhouse gases such as CH₄ estimated from satellite measurements. Quantifying
12 long-term changes of ozone or short-lived marine trace gases, however, is an ongoing
13 challenge given their high variability and the scarcity of long-term measurement stations, so
14 that currently reliable trend estimates are not available.

15 The changing atmospheric composition over the Indian Ocean influences radiative forcing, air
16 quality and weather on a regional scale and plays a role for remote regions like the stratosphere
17 via convective transport pathways (section 6.3). It can also interact with the ocean by impacting
18 biogeochemical cycles and marine ecosystems which can, in turn, feedback on the overlying
19 atmosphere. However, as discussed in section 6.4, the impacts of atmospheric pollution and
20 dust on the Indian Ocean's biogeochemistry, as well as potential climate feedbacks, are severely
21 understudied.

22

23 **6.1 Synthesis of scientific progress after 2010**

24 **Pollution and O₃**

25 Over the last decade, campaign and station measurements in the Bay of Bengal, Arabian Sea
26 and Indian Ocean have revealed new findings of the detailed distribution of pollution and ozone
27 with some clear spatial and seasonal patterns. Particular progress has been made in the Bay of
28 Bengal, where strongly elevated pollution and ozone abundances in the head and the south-
29 eastern part were detected during winter and attributed to advection from the Indo-Gangetic
30 Plain and continental outflow from Southeast Asia, respectively. Post-winter observations show
31 similar maxima in the head, but significantly lower values in middle and southern Bay of
32 Bengal due to open ocean influence. A completely different picture was found over the Arabian
33 sea, where during post-winter monsoon clean marine air results in significantly lower pollution
34 when compared to the northern Bay of Bengal. For the post-summer season, new findings
35 revealed a particularly large spatial heterogeneity of pollution and ozone. Enhanced NO_x in
36 Indian Ocean air masses in contrast to the typical latitudinal gradients was suggested to be
37 linked to emissions from international shipping lanes. During the summer monsoon period, zero
38 net ozone production was found in the Arabian Sea connected to low pollution levels.

39 Recent scientific progress has also been made in better understanding the large-scale
40 distribution of pollution and assessing long-term changes. Comparisons of current observations
41 and previous data obtained two decades earlier have demonstrated the growing influence of
42 anthropogenic SO₂ on the marine atmosphere over the Indian Ocean and Arabian Sea. This
43 pronounced increase has occurred despite the decreasing SO₂ emissions in East Asia and is
44 most likely related to rapidly increasing emissions in South Asia. Recent studies have also
45 revealed how far the impact of anthropogenic pollution can extend over the Indian Ocean.
46 Remote locations such as the island of Mahé just south of the equator show CO maxima during

1 winter that result from the long-range transport of anthropogenic emissions from India.
2 Pollution levels further south, on the other hand, such as over Reunion Island are driven by the
3 emissions from biomass burning in Africa and South America. In the case of NH_3 , trends have
4 yet to be identified due to the lack of continuous observations, with just a few campaigns
5 showing the difference between the coastal and open-ocean environments.

6 As discussed above, scientific studies conducted over the last 10 years have added many details
7 to our picture of the spatial distribution and sharp latitudinal gradients in pollution and,
8 particularly, in ozone. However, our understanding of seasonal, vertical and long-term changes
9 in ozone is still limited. A coastal ozone profile data set has revealed that the seasonal cycle of
10 ozone changes with altitude with surface maxima during September and mid-tropospheric
11 maxima during April–June, prompting the need for further continuous measurement stations at
12 different locations.

13 **Greenhouse gases**

14 By using the most recent EDGAR emissions database, we observe steady increases in emissions
15 over the last decade for CH_4 , N_2O , and CO_2 in the regions surrounding the Indian Ocean. This
16 is true not only for southern Asia, but also for East Asia, the Middle East, and East Africa, with
17 East Asia often being the largest emitter. This is especially significant for CO_2 emissions from
18 China despite the promises of the Paris Climate Accord. An important recent finding is that
19 especially high, and increasing, CH_4 emissions are observed from east African wetlands. As
20 these land-based emissions influence the atmosphere over the Indian Ocean, especially during
21 the winter monsoon season, it is necessary to periodically assess current levels and updated
22 long-term trends.

23 Another major advance in this review compared to previous work has been the explicit
24 inclusion of ocean sources and sinks of greenhouse gases in the region. The ocean is an
25 important source/sink, especially for N_2O (source), CO_2 (sink), and OCS (source), and its role
26 in regulating atmospheric budgets must be understood. Although CH_4 emissions from the ocean
27 are low compared to other sources, a recent remote sensing study reveals elevated mixing ratios
28 over the northern Arabian Sea during the summer monsoon that are somewhat unexpected and
29 may be due to elevated oceanic CH_4 emissions from coastal upwelling. In addition, the distinct
30 seasonal cycle over the northern and western Arabian Sea changes with altitude showing
31 maximum mixing ratios during the post-monsoon season, which supports the idea that surface
32 CH_4 maxima during the summer are due to oceanic sources. We also report a drastic decrease
33 in oceanic CO_2 observations over the last decades that must be rectified. Nonetheless, we report
34 an important finding that the CO_2 sink in the southern Indian Ocean appears to be weakening,
35 as observed by comparing data from campaigns that did occur from 1999–2000 to those from
36 2004–2005. This has been supported by a recent modelling study. Please note that all
37 information presented here for N_2O and OCS is primarily new, as it was either not included in
38 Lawrence and Lelieveld (2010) at all or only very sparsely.

39 Recent important progress has been made in understanding the interplay of greenhouse gases
40 and aerosols in driving physical trends in the region. As of the publishing of Lawrence and
41 Lelieveld (2010) it was thought that the suppression of summer precipitation may be a
42 combined consequence of aerosols and greenhouse gases, but the use of modeling tools to
43 understand anthropogenic drivers of trends in the monsoon and extreme weather was just
44 beginning. We now report that many studies have taken place since, focusing on monsoon
45 rainfall trends, extreme weather and forcing mechanisms. It is clear that the Indian Ocean
46 continues to warm due to greenhouse warming and this has serious consequences for both the
47 monsoon and extreme weather. This warming has been shown to be dampened by
48 anthropogenic aerosols. The recent hiatus period at the beginning of the 21st century

1 highlighted the importance of the Indian Ocean for the global heat budget. The warming is
2 expected to increase throughout the 21st century in response to continuing greenhouse gas
3 emissions, with the strongest warming in the Arabian Sea and western equatorial Indian Ocean
4 consistently projected in CMIP models.

6 **Short-lived gases DMS, isoprene and halogens**

7 Before 2010, short lived trace gases such as DMS, isoprene and halogens were some of the least
8 sampled compounds in the Indian Ocean. This review shows that over the last 10 years
9 significant improvements have been made in order to address the lack of data through multiple
10 campaigns by groups from all over the world. For DMS, the number of datapoints available in
11 the Indian Ocean in 2010 was 1313, since when the latest available dataset shows an increase
12 of ~40%. A similar increase is also observed in the Indian sector of the Southern Ocean, where
13 new campaigns have resulted in an increase of ~32% (NOAA-PMEL, 2020). These
14 observations are critical in improving the DMS emission estimates in the Indian Ocean region,
15 which were a major uncertainty in the currently available emission climatology (Lana et al.,
16 2011). Unfortunately, these observations are still not enough to identify a trend in DMS,
17 although new proxy-based estimations suggest an increase in oceanic DMS concentrations in
18 the global oceans, including the Indian Ocean (Galí et al., 2018).

19 In case of isoprene, there was also a lack of observations in the Indian Ocean until 2010, with
20 just a few campaigns reporting data. The OASIS campaign in 2014 (Booge et al., 2016, 2018)
21 along with other campaigns in the northern Indian Ocean and the Indian sector of the Southern
22 Ocean (Tripathi et al., 2020; Rodríguez-Ros et al., 2020) have increased our understanding of
23 isoprene emissions, highlighting important aspects such as the Arabian Sea isoprene emissions
24 peak in the oxygen minimum zone. An important correlation that has been reported over the
25 last few years is that the fluxes of DMS and isoprene show a significant positive correlation
26 with aerosol, suggesting a regional influence of marine emissions (Zavarsky et al., 2018b).

27 For the reactive halogen species, there has been a drastic improvement in the available dataset
28 in the Indian Ocean, with only one study showing the presence of reactive halogens in the Indian
29 Ocean pre-2010. New observations since 2014 have confirmed the ubiquitous presence of
30 reactive iodine and bromine species in the Indian Ocean, which interact with air pollutants from
31 the Indian subcontinent and need to be considered for regional air quality modelling. Iodine
32 chemistry by itself can be responsible for as much as 25% ozone destruction in the northern
33 Indian Ocean marine boundary layer. Thus, observations over the last 10 years have not only
34 increased the data available for the short-lived species, but also increased our understanding on
35 the importance of these species on the regional atmosphere.

36 **6.2 Long-term changes**

37 Long-term changes of atmospheric dynamics, oceanic processes and anthropogenic emissions
38 impact the atmospheric composition over the Indian Ocean with the growth of traffic and
39 industries being expected to lead to increasing air pollution. Available trend studies of pollution
40 and greenhouse gases make often use of long-term satellite measurements. Long-term changes
41 of atmospheric dynamics, oceanic processes and, in particular, anthropogenic emissions impact
42 the atmospheric composition over the Indian Ocean. The growth of traffic and industries can
43 be expected to lead directly to increasing air pollution, which can be detected by analysing
44 variations of the mean total columnar amount of tropospheric trace gases.

45 Despite the increasing emissions, CO abundances have been found to decrease in a number of
46 studies. Srivastava et al. (2012a), using monthly mean CO at 900 hPa obtained from MOPITT,
47 have observed lower offshore pollution during the transition periods than expected through

1 based on modelling studies using the with The Model for OZone And Related Tracers
2 (MOZART) model. They suggest that temporal dilution of pollutants is the main reason for this
3 mismatch. A study focusing on regions further south in the Indian Ocean indicates that CO was
4 decreasing (1.8% per year over Madagascar and 1.7% per year over Reunion Island) over the
5 years 2005 to 2009. The main drivers behind this decrease were identified as the La Niña
6 between 2006 and 2008 and the reduction in biomass burning emissions in southern Africa
7 (Toihir et al., 2015). Decreasing CO abundance in the lower troposphere was also found by
8 Girach and Nair (2014b) using MOPITT CO data for 2000–2014. The authors attributed the
9 negative trend of around 2% per year partly due to an increase in lower tropospheric water
10 vapour and ozone and partly to a strengthening of convective activity, uplifting CO to higher
11 altitudes. As a result of the latter, upper tropospheric CO was found to increase with a long-
12 term trend of up to 3.2% per year. A recent study conducted as part of ICARB observed lower
13 CO levels (200±43 ppbv) than those during the INDOEX campaign (229±40 ppbv) confirming
14 decreasing levels of CO over the IO (Girach et al, 2020). However, aAs demonstrated in section
15 4, CO emissions in most regions surrounding the Indian Ocean have increased, which highlights
16 the importance of the interplay of emission, dynamics, and chemistry for trace gas variability.
17 In particular, CO emissions along the Mekong River, north of the Persian Gulf, in Afghanistan
18 and East Africa have shown pronounced growth rates. Future studies of the CO trends over the
19 Indian Ocean over longer time periods are needed in order to understand how these changing
20 emissions, together with changing atmospheric dynamics and chemistry, impact the CO
21 concentrations in the marine atmosphere.

22 The variation of the mean total columnar amount of tropospheric NO₂ has been studied in detail
23 over the Indian subcontinent. Mahajan et al. (2015a) have reported an average increase of 2.20
24 ± 0.73 % yr⁻¹ using four different satellites across India. For OMI, this rate of increase from
25 2004–2013 was 2.79 ± 0.23 % yr⁻¹. This compares well to the rate of 2.9 ± 1.9 % yr⁻¹ reported
26 by Ghude et al. (2013), even though their study focused on urban locations. Studies focusing
27 on the atmosphere over the Indian Ocean are relatively scarce, but a study by Tournadre (2014)
28 reported a 50% increase along the Sri Lanka-Sumatra-China shipping lane. The OMI
29 tropospheric column data from 2003–2020 shows an increasing trend in the Arabian sea, close
30 to the Indian coast (0.83 ± 0.24 % yr⁻¹; t_B=3.41), but along the eastern coast in the Bay of Bengal
31 the trend is not significant (0.44 ± 0.29 % yr⁻¹; t_B=1.53). In the remote Indian ocean, OMI
32 observations show an increasing trend ranging between 0.76–1.87 % yr⁻¹, although the open
33 ocean trends might not be accurate considering the low columnar densities close to or below
34 the detection limit of the satellite instruments (unpublished data).

35 ~~Based on OMI satellite data, a positive long-term trend in annual mean ozone over the Arabian~~
36 ~~Sea and northern Bay of Bengal was detected for the ten-year period from 2000 to 2009 (David~~
37 ~~and Nair, 2013). The southern Bay of Bengal is an exception to this and shows a negative long-~~
38 ~~term change for annual mean ozone and the annual minimum with the latter representing~~
39 ~~background conditions.~~

40 Long-term changes of CH₄ have been estimated from AIRS satellite measurements over the
41 2003–2015 time period (Kavitha and Nair, 2019). Over the Arabian Sea and Bay of Bengal, a
42 consistent positive trend ranging from 2 ppb year⁻¹ to 6 ppb year⁻¹ was found at all pressure
43 levels comparable to trends over Indian land regions. Interestingly, the trend was larger at
44 higher altitudes (<500 hPa) and maximized at the 300 hPa–150 hPa level. The authors attributed
45 hypothesized that the changes of ~~the~~ growth rate with altitude are related to increased
46 convective activity uplifting CH₄, leading to a smaller growth rate at the lower levels and higher
47 growth at the upper levels.

48 Based on OMI satellite data, a positive long-term trend in annual mean ozone over the Arabian
49 Sea and northern Bay of Bengal was detected for the ten-year period from 2000 to 2009 (David

1 and Nair, 2013). The southern Bay of Bengal is an exception to this and shows a negative long-
2 term change for annual mean ozone and the annual minimum with the latter representing
3 background conditions. Overall, quantifying long-term changes of ozone is an ongoing
4 challenge given its high variability and the scarcity of long-term measurement stations, so that
5 currently no updated, reliable trend estimates are available.

6 Observations of reactive halogen species over the Indian Ocean do not display any significant
7 long-term trends, with BrO values below the stated upper limits of 2 ppt across observations
8 made over two decades. In the case of IO, annual observations since 2014 during the ISOE ship
9 campaigns have also not identified a significant difference, although the time period is less than
10 one decade and hence changes would not be expected beyond instrumental accuracy and natural
11 variation. Laboratory studies indicate a strong link between ozone concentrations in the MBL
12 and emissions of iodine species from the ocean surface (Carpenter et al., 2013, section 6.3).
13 Modelling studies suggest that ocean emissions of iodine species have increased on a global
14 scale over the last few decades driven by an increase in ozone concentrations due to
15 anthropogenic emissions (Saiz-Lopez et al., 2014, 2015). This increase has been observed
16 indirectly through an increase in the concentrations of iodine species in ice cores in the Alps
17 and in the Arctic (Cuevas et al., 2018; Legrand et al., 2018). However, in the absence of long-
18 term ozone observations or iodine fluxes in the Indian Ocean region, it is difficult to quantify
19 the change in iodine emissions.

20 The examples listed above make clear that not only the increasing anthropogenic emissions,
21 but also atmospheric dynamics, chemistry, and ocean-atmosphere interactions, are important
22 for the long-term changes of the atmospheric composition over the Indian Ocean. In particular,
23 changes of transport patterns and convective uplifting can amplify or dampen the emission-
24 driven changes of greenhouse gases and pollution. Furthermore, long-term changes of the
25 frequency of modes of interannual variability such as IOD or ENSO can mask long-term
26 changes of atmospheric composition if the analysed period is relatively short (e.g., Tohir et al.,
27 2015). Long-term changes of the frequency of such modes will likely also impact long-term
28 changes of the trace gas fields. In addition, physical, chemical, and biological processes in the
29 Indian Ocean, as well as dynamically driven changes of the air-sea gas exchange, can be
30 expected to impact the long-term trends of atmospheric composition.

31 32 7 Impact on the upper atmosphere and ocean

33 The changing atmospheric composition over the Indian Ocean can influence remote regions
34 like the stratosphere via convective transport pathways (Section 7.1). It can also interact with
35 the ocean by impacting biogeochemical cycles and marine ecosystems (Section 7.2), which can,
36 in turn, feedback on the overlying atmosphere. Here, we present new insights into how
37 atmospheric pollution over the Indian Ocean can impact other Earth system components.

38 39 **6.37.1 Impact on the stratosphere**

40 Marine trace gases emitted from the Indian Ocean can be transported into the stratosphere via
41 convection directly above the Indian Ocean or via the summer monsoon convection and
42 anticyclone. Recent studies have highlighted the role of the Indian Ocean as a source region for
43 stratospheric VSLs entrainment and similar mechanisms could also apply to other marine traces
44 gases.

45 Based on the OASIS campaign data and atmospheric modelling, Fiehn et al. (2017) have shown
46 that, from the west Indian Ocean boundary layer, VSLs can be transported into the tropical

1 tropopause layer and eventually into the stratosphere. The importance of the Indian Ocean
2 sources for the stratospheric halogen budget depends on the regional strength of emissions and
3 the transit time in preferred transport regimes. On very short timescales, convection above the
4 Indian Ocean lifts oceanic trace gases towards the tropopause. On longer timescales, the
5 summer monsoon circulation transports the oceanic VSLs towards India and the Bay of Bengal.
6 From there the VSLs are lifted with the monsoon convection and reach stratospheric levels in
7 the south-eastern part of the Asian monsoon anticyclone, which is generally the preferred
8 transport regime during the boreal summer. The stratospheric bromine injection from the
9 tropical Indian Ocean and west Pacific depends critically on the seasonality and spatial
10 distribution of the VSLs emissions (Fiehn et al., 2018). The main oceanic source regions for
11 the stratosphere include the Arabian Sea and Bay of Bengal in boreal summer and the tropical
12 west Pacific Ocean in boreal winter. For the OASIS case study in the western tropical Indian
13 Ocean, the projected CH₂Br₂ entrainment was very high due to high surface emissions, while
14 the entrainment of CHBr₃ and CH₃I was found to be relatively small compared to case studies
15 in the tropical west Pacific Ocean (Fiehn et al., 2017; Tegtmeier et al., 2012). Overall, the Indian
16 Ocean is a strong source of VSLs for the stratosphere and modelled CHBr₃ shows a global
17 maximum over India, the Bay of Bengal, and the Arabian Sea (Tegtmeier et al., 2020)

18 Besides contributing to stratospheric halocarbons, during the summer monsoon, the Indian
19 Ocean and surrounding areas are potentially important source regions for stratospheric
20 entrainment of other naturally produced gases such as N₂O and COS (Ma et al., 2018; Lennartz
21 et al., 2017). The open Indian Ocean is in general a rather weak, but likely perennial and far-
22 reaching (in terms of atmospheric transport) source of several trace gases to the atmosphere.
23 However, it is unclear to what extent the atmospheric mixing ratios at a given location in the
24 north Indian Ocean might ~~actually~~ correspond to air masses transported from the southwest
25 Indian Ocean, where they have been enriched in oceanic trace gases (Ma et al., 2018). Such
26 knowledge is necessary for quantifying the total contribution of the Indian Ocean emissions to
27 the stratosphere and should be addressed in future studies. Potentially important feedback may
28 occur if, for example, more N₂O is emitted to the atmosphere as a result of over fertilization
29 (see section 6.3) and subsequently makes its way to the stratosphere. As N₂O contributes to
30 stratospheric ozone depletion, resulting radiation changes at the ocean surface could feed back
31 on biological and chemical processes.

32 **6.4 — Impact on the ocean**

33 ~~Changes of the atmospheric composition over the Indian Ocean, together with changing~~
34 ~~transport patterns and river inputs, affect oceanic production and biogeochemical trace gas~~
35 ~~cycling, which in turn feedback on the overlying atmosphere. Satellite derived time series~~
36 ~~measurements indicate that the gaseous atmospheric pollution and annual aerosol load,~~
37 ~~including ship emissions, are increasing over the northern Indian Ocean and especially over the~~
38 ~~Bay of Bengal (Hsu et al., 2012, Tournadre, 2014). River inputs lead to low salinities in the~~
39 ~~surface mixed layer, resulting in strong stratification that dampens coastal upwelling and traps~~
40 ~~nutrients in the subsurface (Prasanna Kumar et al., 2002, Rixen et al., 2006). Another concern~~
41 ~~is how potentially changing monsoon intensity will affect air mass trajectories (Goes et al.,~~
42 ~~2005), which influence deposition to the sea surface over the Indian Ocean.~~

43 ~~While it is clear that the changing atmosphere and river input lead to an additional supply of~~
44 ~~nutrients, trace metals, and potentially toxic substances, it is not known how this additional~~
45 ~~supply will impact ocean biogeochemistry and in particular the OMZs. The impact of~~
46 ~~atmospheric deposition on biota has been reported for many different types of oceanic areas~~
47 ~~(Guieu et al., 2014). In both field and laboratory experiments, it has been shown that the~~
48 ~~deposited material can have both favourable (nutrifying, e.g., Rahav et al., 2018) and non-~~
49 ~~favourable effects (toxic, e.g., Paytan et al., 2009, Jordi et al., 2012, Wang et al., 2015) on~~

1 biological processes. Further, it has been shown that mixing natural and anthropogenic sources
2 of gases and aerosols may alter the properties and subsequent functionality of deposited
3 materials (increased bioavailability, e.g., Herut et al., 2016, Krom et al., 2016, Jickells et al.,
4 2017, Mahowald et al., 2018). There is evidence that atmospheric deposition alters the DOM
5 concentrations and characteristics in the surface ocean, with differing effects from natural vs.
6 anthropogenic or mixed sources (Sánchez-Pérez et al., 2016). The impacts of atmospheric
7 deposition include changing biomass standing stocks, primary and bacterial production, and N₂
8 fixation. However, predicting the impacts of atmospheric deposition to marine ecosystems is
9 restricted by limited knowledge of the specific sources, constituents, and transport pathways of
10 the atmospheric material delivered to oceanic regions, as well as the effect of steady vs. episodic
11 deposition. Any changes to biological processes have the potential to alter trace gas cycling in
12 the surface ocean. For example, when species such as *Trichodesmium* (e.g., Guieu et al., 2019)
13 or *Emiliania huxleyi* (coccolithophorid, e.g. Guerreiro et al., 2017) are affected, isoprene and
14 DMS, respectively, can be impacted. In addition, biogeochemical changes due to atmospheric
15 deposition in the SML could be important for trace gas cycling and air-sea exchange, for
16 example through reactions with deposited ozone (Zhou et al. 2014, Chiu et al. 2017, Mungall
17 et al. 2017, see below) or changes to the heterotrophic community (Astrahan et al. 2016).

18 To date, evidence of the influence of anthropogenic input, especially atmospheric deposition,
19 on the Indian Ocean appears to be mixed. There is an indication that the anthropogenically-
20 derived nitrogen input to the northern Indian Ocean, supplied by both atmospheric deposition
21 and riverine fluxes (Jickells et al., 2017), has significantly increased in recent decades. This
22 external nutrient source has the potential to affect the vulnerable biogeochemical systems of the
23 Arabian Sea and Bay of Bengal. The overfertilization of the surface waters increases primary
24 productivity and therewith remineralization in the water column, which contributes to enhanced
25 ocean deoxygenation and thus N₂O production via denitrification and nitrification cycles. As a
26 consequence, the air-sea flux of N₂O increases and can be expected to continue to do so in the
27 future via this feedback cycle (Suntharalingam et al., 2019). Furthermore, some modelling
28 studies show that atmospheric deposition will lead to less CO₂ uptake and less ocean
29 acidification (GESAMP 2012). Guieu et al. (2019), on the other hand, modelled that iron
30 deposition doubles primary production and is most important for non-N₂-fixing microbes.
31 Future changes in wind, temperature, and dust sources could influence primary productivity in
32 the region (GESAMP 2012). The increase of atmospheric CO₂ and its uptake by the ocean
33 enhances ocean acidification, which in turn can impact oceanic biogeochemical cycles and trace
34 gas emission to the atmosphere in multiple ways. One example is the oceanic sulfur cycle which
35 is linked to marine emissions of DMS. The DMS air-sea flux increased in short-term
36 experiments (96 h) with a concurrent decline of the oceanic precursor (Hopkins and Archer,
37 2014) and decreased in longer-term experiments (5 weeks) in response to a shift in the
38 phytoplankton community (Hopkins et al., 2010). Overall, the data suggest an increase in
39 biological stress-induced processes and shows that a marine trace-gas system can change in
40 response to anthropogenic perturbation.

41 As mentioned above, another example for the complex interaction between natural and
42 anthropogenic processes in marine surface water and atmosphere is the deposition of
43 tropospheric ozone, an important secondary pollutant from anthropogenic precursor gases, on
44 the ocean. Its deposition and reaction with marine iodide, which is linked to biological
45 productivity, increases the input of inorganic iodine to the atmosphere (Carpenter et al., 2013).
46 This major source of reactive iodine species in the marine atmosphere, in turn, forms a
47 significant sink for atmospheric ozone through catalytic destruction. In polluted regions,
48 however, anthropogenic NO_x inactivates the reactive species to reservoir species (Mahajan,
49 2019b). As highest ozone values are generally detected closer to the northern continental
50 landmasses with sharp gradients at the coastlines and towards lower latitudes, these processes

1 may increase the gradients. The atmospheric deposition of ozone on marine surface water and
2 subsequent reaction with dissolved organic matter can also form volatile organoiodine
3 compounds (Martino et al., 2009) or organobromine compounds (Kornmüller, 2007).
4 Especially in polluted coastal regions, their formation from this process is expected in addition
5 to the release of organohalogens formed during industrial disinfection processes (Maas et al.,
6 2020). Measurement based modelling showed that an unexpected formation of ozone from
7 reactive bromine and iodine species can occur in the marine boundary layer near coastlines and
8 ship plumes under VOC limited conditions associated with high nitrogen oxide concentrations
9 (Shechner and Tas, 2017). Similar to the mechanism above, this could lead to higher ozone
10 gradients from the polluted coast towards the pristine ocean illustrating the complex
11 interactions of the chemical ocean-atmosphere interactions.

12 Evidence is mounting that anthropogenically influenced ocean-atmosphere interactions impact
13 higher trophic levels. The bioaccumulation of persistent organic pollutants and mercury in fish
14 are of prevailing concern for fish stocks and human health (Brooks et al., 2019). In turn, marine-
15 derived volatile forms of iodine, sulfur, and selenium are essential to recycle the elements onto
16 the land and can be important for human health (Rayman, 2000; Fuge and Johnson, 2015).

17 18 **7.2 6.4 Impact on the ocean**

19 Changes of the atmospheric composition over the Indian Ocean, together with changing
20 transport patterns and river inputs, affect oceanic production and biogeochemical trace gas
21 cycling, which in turn feedback on the overlying atmosphere (e.g., Rixen et al, 2020 this issue).
22 Satellite-derived time-series measurements indicate that the atmospheric pollution of some
23 gases and annual aerosol load, including ship emissions, are increasing over the northern Indian
24 Ocean and especially over the Bay of Bengal (Hsu et al., 2012, Tournadre, 2014). River inputs
25 lead to low salinities in the surface mixed layer, resulting in strong stratification that dampens
26 coastal upwelling and traps nutrients in the subsurface (Prasanna Kumar et al., 2002, Rixen et
27 al., 2006). Other concerns include how potentially changing monsoon intensity will affect air
28 mass trajectories (Goes et al., 2005), which influence deposition to the sea surface over the
29 Indian Ocean and that Indian Ocean warming exacerbates ocean acidification (e.g., in the
30 Arabaian Sea, Sreesh et al., 2019).

31
32 It has been shown that atmospheric deposition can have both favourable (nutrifying, e.g., Rahav
33 et al., 2018) and unfavourable effects (toxic, e.g., Paytan et al., 2009, Jordi et al., 2012, Wang
34 et al., 2015) on biological processes. Further, it has been shown that mixing natural and
35 anthropogenic sources of gases and aerosols may alter the properties and subsequent
36 functionality of the deposited materials (increased bioavailability, e.g., Herut et al., 2016, Krom
37 et al., 2016, Jickells et al., 2017, Mahowald et al., 2018). Biogeochemical changes due to
38 atmospheric deposition in the SML can be important for trace gas cycling and air-sea exchange,
39 for example through reactions with deposited ozone (Zhou et al. 2014, Chiu et al. 2017, Mungall
40 et al. 2017, see below) or changes to the heterotrophic community (Astrahan et al. 2016). Some
41 modelling studies show that atmospheric deposition will lead to less CO₂ uptake and less ocean
42 acidification (GESAMP 2012), while iron deposition doubles primary production (Guieu et al.,
43 2019). The bioaccumulation of persistent organic pollutants and mercury in fish are of
44 prevailing concern for fish stocks and human health (Brooks et al., 2019). In turn, marine-
45 derived volatile forms of iodine, sulfur, and selenium are essential to recycle the elements onto
46 the land and can be important for human health (Rayman, 2000; Fuge and Johnson, 2015).

47
48 To date, the anthropogenically-derived nitrogen input to the northern Indian Ocean, supplied
49 by both atmospheric deposition and riverine fluxes (Jickells et al., 2017), has significantly
50 increased in recent decades. This external nutrient source has the potential to affect the

1 [vulnerable biogeochemistry, by increasing overfertilization of the surface waters.](#)
2 [Overfertilization can increase primary productivity, remineralization in the water column,](#)
3 [enhanced ocean deoxygenation and thus N₂O production via denitrification and nitrification](#)
4 [cycles. As a consequence, the air-sea flux of N₂O increases \(Suntharalingam et al., 2019\), which](#)
5 [can be expected to continue in the future.](#)

6
7 [Another example for the complex interaction between natural and anthropogenic processes in](#)
8 [marine surface water and the atmosphere is the deposition of tropospheric ozone, and its](#)
9 [reaction with marine iodide, which is linked to biological productivity and increases the input](#)
10 [of inorganic iodine to the atmosphere \(Carpenter et al., 2013\). This major source of reactive](#)
11 [iodine species in the marine atmosphere, in turn, forms a significant sink for atmospheric ozone](#)
12 [through catalytic destruction. In polluted regions, however, the anthropogenic NO_x inactivates](#)
13 [the reactive species to reservoir species \(Mahajan, 2019b\), thus volatile organoiodine](#)
14 [compounds \(Martino et al., 2009\) or organobromine compounds \(Kornmüller, 2007-\) are](#)
15 [formed by ozone deposition. Especially in the polluted coastal regions of the northern](#)
16 [landmasses, their formation adds to the release of organohalogens formed during industrial](#)
17 [disinfection processes \(Maas et al., 2020; 2021\). Unexpected formation of ozone from reactive](#)
18 [bromine and iodine species can occur in the marine boundary layer under, near coastlines and](#)
19 [ship plumes, under VOC-limited conditions associated with high nitrogen oxide concentrations](#)
20 [\(Shechner and Tas, 2017\).](#)

23 **87 Summary and current knowledge gaps**

24
25 The atmospheric composition over the Indian Ocean is determined by a complex array of
26 atmospheric transport patterns, [chemistry](#), anthropogenic emissions, and atmosphere-ocean
27 interactions. Emissions of pollutants and greenhouse gases in the regions surrounding the Indian
28 Ocean generally correspond to population densities and economic activities with emission
29 centres in the Indo-Gangetic Plain, northern China, and Java. The distribution of all major
30 pollutants and greenhouse gases [showshows](#) pronounced differences between the landmass
31 source regions and the Indian Ocean, with strong gradients over the coastal areas. During the
32 winter monsoon, the north-south pollution gradients continue over the open Indian Ocean
33 driven by southward transport along with chemical processing, dilution, and surface deposition.
34 In the boundary layer, the contrast between polluted NH and pristine SH air results in a sharp
35 gradient across the ITCZ, where interhemispheric exchange of these air masses occurs in the
36 upper troposphere. During the summer monsoon, clean air dominates the atmospheric
37 composition over the [northern](#) Indian Ocean, leading to a different chemical regime with low
38 atmospheric pollutant levels. [Over the last decade, new knowledge of the atmospheric](#)
39 [composition and related processes over the Indian Ocean has been derived from intensive ship](#)
40 [and aircraft campaigns, coastal station measurements and satellite data. Here, we provide a](#)
41 [synthesis of the scientific progress made after 2010 taking into account the measurement data,](#)
42 [updated emission inventories and modelling studies presented in Sections 3 to 7.](#)

43 **8.1 Pollution and O₃**

44 [Over the last decade, campaign and station measurements have revealed new findings of the](#)
45 [distribution of pollution and ozone with some clear spatial and seasonal patterns. Over the Bay](#)
46 [of Bengal strongly elevated pollution and ozone were detected in the head and the south-eastern](#)
47 [part during winter and attributed to advection from the Indo-Gangetic Plain and continental](#)
48 [outflow from Southeast Asia, respectively. Post-winter observations show similar maxima in](#)
49 [the head, but significantly lower values in middle and southern Bay of Bengal due to open](#)

1 ocean influence. A completely different picture was found over the Arabian sea, where during
2 spring transition period clean marine air results in significantly lower pollution when compared
3 to the northern Bay of Bengal. Recent studies have also revealed that the impact of
4 anthropogenic pollution can extend far over the Indian Ocean. Remote locations such as the
5 island of Mahé just south of the equator show CO maxima during winter that result from the
6 long-range transport of anthropogenic emissions from India. Pollution levels further south such
7 as over Reunion Island are driven by the emissions from biomass burning in Africa and South
8 America. In addition to continental pollution source, ship emissions are known to impact the
9 Indian Ocean air masses leading to enhanced NO_x abundances. Black carbon aerosols also show
10 enhancements over Bay of Bengal shipping lanes, and thus similar signatures for CO could be
11 expected. However, no studies have so far reported enhanced CO abundances in close proximity
12 to Indian Ocean shipping lanes prompting the need for further investigations.

13 Given the strongly increasing pollutant emissions from the surrounding continents, similar
14 trends might be expected in pollutants over the Indian Ocean. Comparisons of current
15 observations and previous data obtained two decades earlier have demonstrated the growing
16 influence of anthropogenic SO₂ on the marine atmosphere over the Indian Ocean. This
17 pronounced increase has occurred despite the decreasing SO₂ emissions in East Asia and is
18 most likely related to rapidly increasing emissions in South Asia. For tropospheric NO₂ column
19 data an increasing trend was detected to be significant in the Arabian sea, close to the Indian
20 coast. Lower tropospheric CO, on the other hand, was found to decrease, due to increasing
21 water vapour and ozone as well as a strengthening of convective activity, uplifting CO to higher
22 altitudes.

23 Scientific studies conducted over the last 10 years have added many details to our picture of the
24 spatial distribution in ozone. Latitudinal gradients with increasing ozone towards northern
25 landmasses were found to depend on the season, with sharper gradients during the winter and
26 transition periods, and on the latitudinal extent, with sharper gradients closer to the coastlines.
27 It has been noted that local wind patterns can lead to changes of the ozone seasonal cycle and
28 pronounced deviations of the ozone distribution causing complex temporal and spatial
29 variations. Diurnal variations of boundary layer ozone were found to follow different regimes
30 with daytime photochemical production from anthropogenic precursors occurring only in
31 polluted air masses. In pristine air masses, the absence of in situ photochemical production
32 leads to either no diurnal ozone variation or photochemical destruction during daytime and
33 entrainment of ozone rich from the free troposphere during nighttime. Despite the notable
34 progress, a complete picture of the seasonal, latitudinal, and vertical ozone variations as well
35 as reliable and updated trend estimates are momentarily not available.

36 Satellite measurements of CO and NO₂ have revealed highest surface pollution during the
37 winter monsoon over the Bay of Bengal and the Arabian Sea coastal waters. During this time,
38 most parts of the NH Indian Ocean fall into the category of polluted continental air. Based on
39 recent ship campaign data, pollution maxima over the head and the south-east Bay of Bengal
40 driven by air mass advection from the Indo-Gangetic Plain and Southeast Asia have been
41 identified. One clear difference in the CO and NO₂ distribution is the appearance of enhanced
42 NO₂ columns along the major shipping lanes. The region south of 5°S can be considered as part
43 of the pristine oceanic regime all year around with minimum values of pollution over the
44 equatorial western Indian Ocean. Long term changes of pollution in the Indian Ocean MBL
45 and in particular how they are driven by changing emissions and transport patterns require
46 further investigation in the future.

47 Ozone measurements from multiple ship campaigns revealed spatial and seasonal patterns very
48 similar to the pollution fields. Nearly all campaigns detected highest ozone values close to the
49 northern continental landmasses reflecting direct impact of pollution source regions. The sharp

1 latitudinal ozone gradients maximise close to the coastlines during the transition periods due to
2 changing transport regimes. Vertical profiles can show substantially higher ozone values above
3 the MBL due to air-sea breeze triggered transport of polluted air masses in the elevated layer.
4 It has been noted that unusual types of wind patterns can lead to pronounced deviations of the
5 ozone distribution shifting maxima to different regions. A complete picture of the seasonal,
6 latitudinal and vertical ozone variations is not available from current measurements and, thus,
7 the chemical production and loss processes driving ozone distributions are not well known.

8 **8.2 Greenhouse gases**

9 Emissions of CH₄, N₂O, and CO₂ in the regions surrounding the Indian Ocean have increased
10 steadily over the last decade with East Asia often being the largest emitter. Important recent
11 findings in this area have revealed high, and increasing, CH₄ emissions from east African
12 wetlands. The ocean also acts as an important source/sink, especially for N₂O (source), CO₂
13 (sink), and OCS (source), and its role in regulating atmospheric budgets must be understood.
14 Campaign data collected in 1999–2000 and 2004–2005 suggests that the CO₂ sink in the
15 southern Indian Ocean is weakening, a conclusion further supported by a recent modelling
16 study. Despite such alarming findings, we report here a drastic decrease in oceanic CO₂
17 observations over the last decades that must be rectified.

18 The distribution of greenhouse gases over the Indian Ocean shows many similarities when
19 compared to the pollution fields, presenting higher values towards the coast due to the proximity
20 of the source rich land regions. However, longer atmospheric lifetimes and active air-sea
21 exchange also lead to some clear differences, such as the latitudinal variations of greenhouse
22 gases being much smaller than the latitudinal variations of the shorter-lived pollutants. In
23 addition, greenhouse gas emissions are characterized by pronounced seasonal variations as a
24 result of their biogenic and agricultural sources. Over the northern Indian Ocean, CH₄
25 maximises during the autumn transition and winter monsoon following the seasonal cycle of
26 rice cultivation, while CO₂ is characterized by highest values in boreal spring due to biogenic
27 sources from the eastern continental land masses. Seasonality over the southern Indian Ocean
28 shows different patterns with seasonal variations of OH radicals leading to CH₄ maxima during
29 summer and air-sea exchange leading to relatively constant CO₂ levels. Long-term changes of
30 CH₄ show positive trends that maximized in the upper troposphere potentially driven by
31 increased convective activity.

32 Over the last decade, important progress has been made in understanding the interplay of
33 greenhouse gases and aerosols in driving physical trends in the region. It is clear now that the
34 Indian Ocean continues to warm due to greenhouse warming partially dampened by
35 anthropogenic aerosols. This warming has been shown to have serious consequences for the
36 monsoon and extreme weather in this region as well as for the global heat budget, as highlighted
37 by the recent hiatus period at the beginning of the 21st century. The warming is expected to
38 increase throughout the 21st century in response to continuing greenhouse gas emissions, with
39 the strongest warming in the Arabian Sea and western equatorial Indian Ocean consistently
40 projected in CMIP models.

42 **8.3 Short-lived gases DMS, isoprene and halogens**

43 For marine short-lived gases such as DMS, isoprene and halogenated VSLs, the Indian Ocean
44 is a hotspot emission region. Before 2010, short lived gases were some of the least sampled
45 compounds in the Indian Ocean. This review shows that over the last 10 years significant
46 improvements have been made in addressing the lack of data through multiple campaigns by
47 groups from all over the world.

1 For DMS, the number of datapoints available in the Indian Ocean has increased by 30–40%
2 since 2010. These new measurements can provide critical input for improving DMS emission
3 estimates, which are a major uncertainty in the currently available emission climatology. While
4 the total data are still too sparse to identify a long-term trend in DMS, proxy-based estimations
5 suggest an increase in global oceanic DMS concentrations, including the Indian Ocean. New
6 ship campaign data showed that oceanic sulfur fluxes in the form of DMS emissions are the
7 major precursor of aerosols in the summer monsoon remote MBL, with the possibility to
8 significantly contribute to cloud condensation nuclei in the tropical Indian Ocean.

9 In the case of isoprene, new campaigns conducted over the last 10 years have increased our
10 understanding of isoprene emissions, highlighting aspects such as the Arabian Sea isoprene
11 emissions peak in the oxygen minimum zone. An important new finding revealed that fluxes of
12 DMS and isoprene show a significant positive correlation with aerosol, suggesting a regional
13 influence of marine emissions.

14 New observations since 2014 have confirmed the ubiquitous presence of reactive iodine and
15 bromine species in the Indian Ocean, which interact with air pollutants from the Indian
16 subcontinent and need to be considered for regional air quality modelling. While the levels of
17 reactive halogen species were overall low, iodine chemistry was found to be responsible for up
18 to 25% ozone destruction in the northern Indian Ocean marine boundary layer. The improved
19 availability of reactive halogen dataset in the Indian Ocean demonstrates how important regular
20 in-situ observations are for our understanding of the regional atmospheric chemistry and
21 composition.

24 **8.4 Knowledge gaps**

25 Long-term changes of the atmospheric composition over the Indian Ocean are driven by
26 increasing anthropogenic emissions, but also by atmospheric dynamics such as changes of
27 transport patterns and convection. Furthermore, physical, chemical, and biological processes in
28 the Indian Ocean can be expected to play a role for the long-term trends of atmospheric
29 composition. Possible changes in stratification, mixing, microbial speciation, and primary
30 productivity will influence trace gases in the atmosphere via modified oceanic emissions.
31 Similarly, ocean acidification can impact biogenic trace gas production and exchange. In
32 addition to changes of oceanic trace gas production, most of the observed and predicted
33 atmospheric long-term changes can influence air-sea gas exchange. For example, more rainfall
34 and intensified cyclone activities could lead to more turbulence at the sea surface and higher
35 fluxes of gases. In most cases, the direction and magnitude of such changes are currently unclear
36 and future studies are required in order to link oceanic changes to observed changes of
37 atmospheric composition.

38 Our current understanding of the Indian Ocean is mostly based on sporadic ship campaigns and
39 remote sensing data. Details of the large-scale features such as the seasonal cycles over the
40 individual ocean basins, variations of the latitudinal gradients, the vertical distributions and
41 long-term changes for several trace gases are not well known, and nor are all the processes well
42 understood. Large uncertainties remain in the current emission inventories that are used in
43 models and data for validation of model simulations is sparse. Dedicated long-term
44 measurement stations, such as they exist in the Atlantic (e.g., Cape Verde Atmospheric
45 Observatory), Pacific (e.g., Mauna Loa Observatory) or the Southern Ocean (e.g., Pointe
46 Bénédicte station), are required in order to link the distribution of trace gases over the Indian
47 Ocean to transport patterns and chemical regimes and to investigate feedback and forcing
48 mechanisms. In addition to long term stations, it is imperative to maintain a repository of the
49 past and future observations made in the Indian Ocean. Identifying long term trends, which are

1 crucial to understanding the processes and impacts of climate change, are hindered by the lack
2 of a consolidated database.

3 Interactions between the Indian Ocean and the atmosphere are bidirectional, and it has become
4 clear that the changing atmospheric composition can impact many oceanic processes, leading
5 to feedback mechanisms. Severe atmospheric pollution, known as the ‘South Asian Brown
6 Cloud’ transports high levels of gaseous pollutants and aerosols (including dust) containing
7 various nutrients and toxic substances to the Indian Ocean. This review only covers gas-phase
8 composition over the Indian Ocean, however, the complex interactions between anthropogenic
9 and marine trace gases and aerosols are also highly important for atmosphere-ocean feedback
10 mechanisms and climate impacts. Interactions between aerosols and trace gases can form new
11 particles, thus contributing to cloud formation, and wet deposition in the clear marine
12 atmosphere, as well as influence storm patterns and tropical cyclones. Such dynamical effects
13 together with the additional supply of pollution and aerosols will impact biogeochemical and
14 biological processes in the Indian Ocean. The connection between ocean biogeochemistry and
15 atmospheric deposition involves several issues of importance for society, including global and
16 regional pollution, the health of the ocean, fisheries, ocean fertilization, and carbon
17 sequestration, all related to the UN Sustainable Development Goals. However, the impacts of
18 atmospheric pollution and dust on the Indian Ocean’s biogeochemistry, trace gas cycling, and
19 potential climate feedbacks, are severely understudied. Further research is needed to understand
20 how sources, transport, reactivity, and the atmosphere-ocean feedback mechanisms interact.
21 Such understanding is required in order to predict future changes, to assess if such changes can
22 have harmful effects on the environment and to find pathways which strengthen atmosphere,
23 ocean and community resilience in the Indian ocean region and globally.

24

25 **Appendix A: Major abbreviations and terms**

26

27	AQABA	Air Quality and climate change in the Arabian Basin
28	AIRS	Atmospheric Infrared Sounder
29	<u>ARMEX</u>	<u>Arabian Sea Monsoon Experiment</u>
30	BOB	Bay of Bengal
31	BOBEX	Bay of Bengal Experiment
32	BOBPS	Bay of Bengal Processes Studies
33	CMIP	Coupled Model Intercomparison Project
34	<u>CTCZ</u>	<u>Continental Tropical Convergence Zone experiment</u>
35	EACC	East African Coastal Current
36	EDGAR	Emissions Database for Global Atmospheric Research
37	EMC	East Madagascar Current
38	ENSO	El Niño–Southern Oscillation
39	GMOS	Global Mercury Observation System
40	GOME	Global Ozone Monitoring Experiment
41	GOSAT	Greenhouse Gases Observing Satellite
42	ICARB	Integrated Campaign for Aerosols, gases and Radiation Budget
43	IGP	Indo-Gangetic Plains
44	IIOE-2	2nd International Indian Ocean Expedition program
45	INDOEX	Indian Ocean Experiment
46	IO	Indian Ocean
47	IOD	Indian Ocean Dipole
48	ISOE	Indian Southern Ocean Expedition
49	ITF	Indonesian Throughflow
50	ITZC	Intertropical Convergence Zone

1	MBL	Marine Boundary Layer
2	MJO	Madden-Julian Oscillation
3	MSLP	Mean surface level pressure
4	MOPITT	Measurements of Pollution in the Troposphere
5	NH	Northern Hemisphere
6	NMHC	Non-Methane Hydrocarbon
7	NMVOG	Non-Methane Volatile Organic Compound
8	OASIS	Organic VSLS and their air sea exchange from the Indian Ocean to the
9		Stratosphere
10	OMI	Ozone Monitoring Instrument
11	OMO	Oxidation Mechanism Observations
12	OMZ	Oxygen Minimum Zone
13	OVOC	Oxidized Volatile Organic Compound
14	PESO	Pilot Expedition to the Southern Ocean
15	SCIAMACHY	Scanning Imaging Absorption Spectrometer for Atmospheric Chartography
16	SEC	South Equatorial Current
17	SECC	South Equatorial Countercurrent
18	SH	Southern Hemisphere
19	SICC	South Indian Countercurrent
20	SML	Surface Microlayer
21	SOA	Secondary Organic Aerosols
22	SST	Sea Surface Temperature
23	TROPOMI	TROPOspheric Monitoring Instrument
24	VOC	Volatile Organic Compound
25	VSLs	Very Short-Lived Substances

26
27

28 **Data availability.**

29 EDGAR pollutant and greenhouse gas emission data are available from
30 <https://edgar.jrc.ec.europa.eu>, SOCAT CO₂ data are available from
31 <https://www.socat.info/index.php/data-access/>, MOPITT V8 Level 3 CO data are available
32 from <https://www2.acom.ucar.edu/mopitt>, GOSAT CH₄ profiles are available
33 at <http://www.gosat.nies.go.jp/en/>, AIRS version 6 level 3 CH₄ data are available from
34 https://aedise.gesdisc.eosdis.nasa.gov/data/Aqua_AIRS_Level3/AIRX3STM.006/, and
35 TROPOMI Level 2 NO₂ data are available from <https://scihub.copernicus.eu/>.

36

37 **Author contributions.**

38 The authors wrote the article together. ST coordinated the writing processes. The paper was
39 written jointly by all co-authors with ST and CM designing the review and contributing to all
40 sections. YJ contributed to sections 3 and 5; BQ contributed to sections 2, 7 and 8; AM
41 contributed to sections 5 and 6.

42

43 **Competing interests.**

44 The authors declare that they have no conflict of interest.

45

46 **Special issue statement.**

47 This article is part of the special issue “Understanding the Indian Ocean system: past, present
48 and future (BG/ACP/OS/SE inter-journal SI)”. It is not associated with a conference.

49

50 **Acknowledgments**

1 [We thank Jonathan Williams, Liji M. David, Imran A. Girach, Vinu Valsala, Hermann Bange,](#)
2 [Sinikka Lennartz, and Damian Arevalo for helpful discussions of the manuscript and Debora](#)
3 [Griffin for assisting with the TROPOMI data. We thank Jonathan Williams, Hermann Bange,](#)
4 [Liji M. David, Sinikka Lennartz, and Damian Arevalo for helpful discussions of the manuscript](#)
5 [and Debora Griffin for assisting with the TROPOMI data.](#) The Surface Ocean CO₂ Atlas
6 (SOCAT) is an international effort, endorsed by the International Ocean Carbon Coordination
7 Project (IOCCP), the Surface Ocean Lower Atmosphere Study (SOLAS) and the Integrated
8 Marine Biosphere Research (IMBeR) program, to deliver a uniformly quality-controlled
9 surface ocean CO₂ database. The many researchers and funding agencies responsible for the
10 collection of data and quality control are thanked for their contributions to SOCAT. IITM is
11 funded by the Ministry of Earth Sciences, Government of India.

12 **References**

13
14
15 [Ajayakumar, R. S., Nair, P. R., Girach, I. A., Sunilkumar, S. V., Muhsin, M., and Chandran, P.](#)
16 [R. S.: Dynamical nature of tropospheric ozone over a tropical location in Peninsular India: Role](#)
17 [of transport and water vapor. Atmospheric Environment, 218, 117018, 2019.](#)

18
19 [Ali, K., Beig, G., Chate, D. M., Momin, G. A., Sahu, S. K., and Safai, P. D.: Sink mechanism](#)
20 [for significantly low level of ozone over the Arabian Sea during monsoon, J. Geophys. Res.,](#)
21 [114, D17306, doi:10.1029/2008JD011256, 2009.](#)

22
23 Alory, G., and Meyers, G.: Warming of the upper equatorial Indian Ocean and changes in the
24 heat budget (1960–99). J. Climate, 22 (1), 93–113. doi:10.1175/2008jcli2330.1, 2009.

25
26 Aneesh, V.R., Mohankumar, G. and Sampath, S.: Spatial distribution of atmospheric carbon
27 monoxide over Bay of Bengal and Arabian Sea: Measurements during pre-monsoon period of
28 2006. J Earth Syst Sci 117, 449–455, <https://doi.org/10.1007/s12040-008-0044-8>, 2008.

29
30 Angot, H., Barret, M., Magand, O., Ramonet, M., and Dommergue, A.: A 2-year record of
31 atmospheric mercury species at a background Southern Hemisphere station on Amsterdam
32 Island. Atmos. Chem. Phys., 14(20), 11461–11473. [https://doi.org/10.5194/acp-14-11461-](https://doi.org/10.5194/acp-14-11461-2014)
33 2014, 2014.

34
35 Annamalai, H., Taguchi, B., McCreary J.P., Nagura, M., and Miyama T.: Systematic errors in
36 south Asian monsoon simulation: importance of Equatorial Indian Ocean processes. J. Climate,
37 30, 8159–817, 2017.

38
39 Arneth, A., Monson, R. K., Schurgers, G., Niinemets, Ü., and Palmer, P. I.: Why are estimates
40 of global terrestrial isoprene emissions so similar (and why is this not so for monoterpenes)?,
41 Atmos. Chem. Phys., 8, 4605-4620, [10.5194/acp-8-4605-2008](https://doi.org/10.5194/acp-8-4605-2008), 2008.

42
43 Arnold, S. R., Spracklen, D. V., Williams, J., Yassaa, N., Sciare, J., Bonsang, B., Gros, V.,
44 Peeken, I., Lewis, A. C., Alvain, S., and Moulin, C.: Evaluation of the global oceanic isoprene
45 source and its impacts on marine organic carbon aerosol, Atmos. Chem. Phys., 9, 1253-1262,
46 [10.5194/acp-9-1253-2009](https://doi.org/10.5194/acp-9-1253-2009), 2009.

47
48 [Aryasree, S., Nair, P.R., Girach, I.A. et al. Winter time chemical characteristics of aerosols over](#)
49 [the Bay of Bengal: continental influence. Environ Sci Pollut Res 22, 14901–14918.](#)
50 <https://doi.org/10.1007/s11356-015-4700-7>, 2015.

51

1 Asatar, G. I. and Nair., P. R.: Spatial distribution of near-surface CO over Bay of Bengal during
2 winter: role of transport, *J. Atmos. Sol.-Terr. Phy.*, 72, 1241–1250,
3 doi:10.1016/j.jastp.2010.07.025, 2010.
4
5 Asharaf, S., and Ahrens, B.: Indian summer monsoon rainfall processes in climate change
6 scenarios. *J. Climate*, 28(13), 5414–5429, 2015.
7
8 Astrahan P., Herut B., Paytan A., and Rahav E.: The Impact of Dry Atmospheric Deposition
9 on the Sea-Surface Microlayer in the SE Mediterranean Sea: An Experimental Approach,
10 *Frontiers in Marine Science*, 3, 222, doi=10.3389/fmars.2016.00222, 2016.
11
12 Aswini, A. R., Hegde, P., Aryasree, S., Girach, I. A., and Nair, P. R.: Continental outflow of
13 anthropogenic aerosols over Arabian Sea and Indian Ocean during wintertime: ICARB-2018
14 campaign, *Sci. Total Environ.*, 712, 135214, <https://doi.org/10.1016/j.scitotenv.2019.135214>,
15 2020.
16
17 Ayers, G. P. and Gras, J. L.: Ammonia gas concentration over the Southern Ocean, *Nature*, 284,
18 539–540, 1980.
19
20 Bakker, D. C. et al.: A multi-decade record of high quality fCO₂ data in version 3 of the Surface
21 Ocean CO₂ Atlas (SOCAT). *Earth Syst. Sci. Data*, 8: 383-413. doi:10.5194/essd8-383-2016,
22 2016.
23
24 Bange, H. W., Ramesh, R., Rapsomanikis, S., and Andreae, M.: Methane in surface waters of
25 the Arabian Sea, *Geophys. Res. Lett.*, 25, 3547–3550, 1998.
26
27 Bange, H. W.: New Directions: The importance of the oceanic nitrous oxide emissions, *Atmos.*
28 *Environ.*, 40, 198–199, 2006.
29
30 Barnes, E. A., Fiore, A. M. and Horowitz, L. W.: Detection of trends in surface ozone in the
31 presence of climate variability. *J. Geophys. Res.*, 121: 6112–6129. DOI:
32 10.1002/2015JD024397, 2016.
33
34 Bauer, S. E., Tsigaridis, K., and Miller, R.: Significant atmospheric aerosol pollution caused by
35 world food cultivation, *Geophys. Res. Lett.*, 43, 5394-5400,
36 <https://doi.org/10.1002/2016GL068354>, 2016.
37
38 Behrenfeld, M. J., O'Malley, R. T., Siegel, D. A., McClain, C. R., Sarmiento, J. L., Feldman,
39 G. C., Milligan, A. J., Falkowski, P. G., Letelier, R. M., and Boss, E. S.: Climate-driven trends
40 in contemporary ocean productivity. *Nature*, 444(7120):752–755, 2006.
41
42 [Belikov, D.A., Saitoh, N., Patra, P.K., Chandra, N.: GOSAT CH₄ Vertical Profiles over the](#)
43 [Indian Subcontinent: Effect of a Priori and Averaging Kernels for Climate Applications.](#)
44 [Remote Sens. 13, 1677. <https://doi.org/10.3390/rs13091677>, 2021.](#)
45
46 Bengtsson, L.: The global atmospheric water cycle, *Environ. Res. Lett.*, 5, 025002.
47 <http://dx.doi.org/10.1088/1748-9326/5/2/025002>, 2010.
48
49 Bergamaschi, P., S. Houweling, A. Segers, M. Krol, C. Frankenberg, R. A. Scheepmaker, E.
50 Dlugokencky, S. C. Wofsy, E. A. Kort, C. Sweeney, T. Schuck, C. Brenninkmeijer, H. Chen,
51 V. Beck, C. Gerbig: Atmospheric CH₄ in the first decade of the 21st century: Inverse modeling

1 analysis using SCIAMACHY satellite retrievals and NOAA surface measurements, *J. Geophys.*
2 *Res.*, 118, 7350– 7369, doi:10.1002/jgrd.50480, 2013.

3

4 [Bhattacharya, S. K., Borole, D. V., Francy, R. J., Allison, C. E., Steele, L. P., Krummel, P.,](#)
5 [Langenfelds, R., Masarie, K. A., Tiwari, Y. K., and Patra, P. K.: Trace gases and CO₂ isotope](#)
6 [records from Cabo de Rama, India. *Current Science*, 97\(9\), 1336–1344,](#)
7 <http://www.jstor.org/stable/24109728>, 2009.

8

9 Biswas, H., Chatterjee, A., Mukhopadhyaya, S. K., De, T. K., Sen, S., and Jana, T. K.: Estimation
10 of ammonia exchange at the land-ocean boundary condition of Sundarban mangrove northeast
11 coast of Bay of Bengal, India, *Atmos. Environ.*, 39, 4489– 4499, 2005.

12

13 [Blando, J.D., Turpin, B.J.: Secondary organic aerosol formation in cloud and fog droplets:](#)
14 [a literature evaluation of plausibility, *Atmos. Environ.*, 34, 1623–1632, 2000.](#)

15

16 Blunden, J. and D. S. Arndt, Eds.: State of the Climate in 2019~~8~~. *Bull. Amer. Meteor. Soc.*, ~~100~~
17 ~~(9),~~ ~~Si S305101(8),~~ ~~S1-S429,~~ doi:10.1175/2019BAMSStateoftheClimate.1
18 ~~10.1175/2020BAMSStateoftheClimate.1~~, 2020~~19~~.

19

20 Boersma, K. F., Eskes, H. J., Richter, A., De Smedt, I., Lorente, A., Beirle, S., van Geffen, J.
21 H. G. M., Zara, M., Peters, E., Van Roozendael, M., Wagner, T., Maasakkers, J. D., van der A,
22 R. J., Nightingale, J., De Rudder, A., Irie, H., Pinardi, G., Lambert, J.-C., and Compernolle, S.
23 C.: Improving algorithms and uncertainty estimates for satellite NO₂ retrievals: results from the
24 quality assurance for the essential climate variables (QA4ECV) project, *Atmos. Meas. Tech.*,
25 11, 6651–6678, <https://doi.org/10.5194/amt-11-6651-2018>, 2018.

26

27 [Bollasina, M. A., Ming, Y. and Ramaswamy, V., Anthropogenic Aerosols and the Weakening](#)
28 [of the South Asian Summer Monsoon, *Science*, 334, 6055, 502-505, 2011.](#)

29

30 Booge, D., Marandino, C. A., Schlundt, C., Palmer, P. I., Schlundt, M., Atlas, E. L., Bracher,
31 A., Saltzman, E. S., and Wallace, D. W. R.: Can simple models predict large-scale surface
32 ocean isoprene concentrations?, *Atmos. Chem. Phys.*, 16, 11807-11821, 10.5194/acp-16-
33 11807-2016, 2016.

34

35 Booge, D., Schlundt, C., Bracher, A., Endres, S., Zäncker, B., and Marandino, C. A.: Marine
36 isoprene production and consumption in the mixed layer of the surface ocean – a field study
37 over two oceanic regions, *Biogeosciences*, 15, 649-667, 10.5194/bg-15-649-2018, 2018.

38

39 Bourtsoukidis, E., Ernle, L., Crowley, J. N., Lelieveld, J., Paris, J. D., Pozzer, A., Walter, D.,
40 and Williams, J.: Non-methane hydrocarbon (C₂–C₈) sources and sinks around the Arabian
41 Peninsula, *Atmos. Chem. Phys.*, 19, 7209-7232, 10.5194/acp-19-7209-2019, 2019.

42

43 [Bovensmann, H., Burrows, J. P., Buchwitz, M., Frerick, J., Noël, S., Rozanov, V. V., Chance,](#)
44 [K. V., and Goede, A. P. H.: SCIAMACHY: Mission Objectives and Measurement Modes, *J.*](#)
45 [Atmos. Sci., 56, 127–150, 10.1175/1520-0469\(1999\)056<0127:Smoomm>2.0.Co;2, 1999.](#)

46

47 [Bollasina, M. A., Ming, Y. and Ramaswamy, V., Anthropogenic Aerosols and the Weakening](#)
48 [of the South Asian Summer Monsoon, *Science*, 334, 6055, 502–505, 2011.](#)

49

50 [Bourtsoukidis, E., Pozzer, A., Sattler, T. Matthaios, V.N., Ernle, L. Edtbauer, A., Fischer, H.,](#)
51 [Könemann, T., Osipov, S., Paris, J.-D., Pfannerstill, E. Y., Stöner, C., Tadic, I., Walter, D.,](#)

1 [Wang, N., Lelieveld, J., Williams, J.: The Red Sea Deep Water is a potent source of atmospheric](#)
2 [ethane and propane. Nat. Commun., -, 447, <https://doi.org/10.1038/s41467-020-14375-0>, 2020.](#)
3
4 [Bovensmann, H., Burrows, J. P., Buchwitz, M., Frerick, J., Noël, S., Rozanov, V. V., Chance,](#)
5 [K. V., and Goede, A. P. H.: SCIAMACHY: Mission Objectives and Measurement Modes, J.](#)
6 [Atmos. Sci., 56, 127-150, \[10.1175/1520-0469\\(1999\\)056<0127:Smoomm>2.0.Co;2\]\(https://doi.org/10.1175/1520-0469\(1999\)056<0127:Smoomm>2.0.Co;2\), 1999.](#)
7
8 Brooks, S. D., T. D. Jickells, P. S. Liss, D. C. O. Thornton, and R. Zhang: Biogeochemical
9 Coupling between Ocean and Atmosphere—A Tribute to the Lifetime Contribution of Robert
10 A. Duce. *J. Atmos. Sci.*, 76, 3289–3298, <https://doi.org/10.1175/JAS-D-18-0305.1>, 2019.
11
12 Brühl, C., Lelieveld, J., Crutzen, P. J., and Tost, H.: The role of carbonyl sulphide as a source
13 of stratospheric sulphate aerosol and its impact on climate, *Atmos. Chem. Phys.*, 12, 1239-
14 1253, [10.5194/acp-12-1239-2012](https://doi.org/10.5194/acp-12-1239-2012), 2012.
15
16 Butler, A.H., J.S. Daniel, R.W. Portmann, A.R. Ravishankara, P.J. Young, D.W. Fahey, and
17 K.H. Rosenlof: Diverse policy implications for future ozone and surface UV in a changing
18 climate. *Environ. Res. Lett.*, 11: 064017, 2016.
19
20 Burrows, J. P., Weber, M., Buchwitz, M., Rozanov, V., Ladstätter-Weißmayer, A., Richter,
21 A., DeBeek, R., Hoogen, R., Bramstedt, K., Eichmann, K.-U., Eisinger, M., and Perner, D.:
22 The Global Ozone Monitoring Experiment (GOME): Mission Concept and First Scientific
23 Results, *J. Atmos. Sci.*, 56, 151-175, [10.1175/1520-0469\(1999\)056<0151:Tgomeg>2.0.Co;2](https://doi.org/10.1175/1520-0469(1999)056<0151:Tgomeg>2.0.Co;2),
24 1999.
25
26 Cai, W. et al.: Increased frequency of extreme Indian Ocean Dipole events due to greenhouse
27 warming. *Nature* 510, 254–258, 2014.
28
29 Cai, W., A. Sullivan, and T. Cowan: Climate change contributes to more frequent consecutive
30 positive Indian Ocean Dipole events. *Geophys. Res. Lett.*, 36, L19783,
31 [doi:10.1029/2009GL040163](https://doi.org/10.1029/2009GL040163), 2009.
32
33 Campbell, J. E., Whelan, M. E., Seibt, U., Smith, S. J., Berry, J. A., and Hilton, T. W.:
34 Atmospheric carbonyl sulfide sources from anthropogenic activity: Implications for carbon
35 cycle constraints, *Geophys. Res. Lett.*, 42, 3004-3010, [10.1002/2015gl063445](https://doi.org/10.1002/2015gl063445), 2015.
36
37 Carlton, A. G., Wiedinmyer, C., and Kroll, J. H.: A review of Secondary Organic Aerosol
38 (SOA) formation from isoprene, *Atmos. Chem. Phys.*, 9, 4987-5005, [10.5194/acp-9-4987-](https://doi.org/10.5194/acp-9-4987-2009)
39 [2009](https://doi.org/10.5194/acp-9-4987-2009), 2009.
40
41 Carmichael, G. R., Ferm, M., Thongboonchoo, N., Woo, J. H., Chan, L. Y., Murano, K., Viet,
42 P. H., Mossberg, C., Bala, R., Boonjawat, J., Upatum, P., Mohan, M., Adhikary, S. P., Shrestha,
43 A. B., Pinaar, J. J., Brunke, E. B., Chen, T., Jie, T., Guoan, D., Peng, L. C., Dhiharto, S.,
44 Harjanto, H., Jose, A. M., Kimani, W., Kirouane, A., Lacaus, J.-P., Richard, S., Barturen, O.,
45 Cerda, J. C., Athayde, A., Tavares, T., Cotrina, J. S., and Bilici, E.: Measurements of sulfur
46 dioxide, ozone and ammonia concentration in Asia, Africa and South America using passive
47 samplers, *Atmos. Environ.*, 37, 1293–1308, 2003.
48
49 Carpenter, L. J., and Liss, P. S.: On temperate sources of bromoform and other reactive organic
50 bromine gases, *J. Geophys. Res.*, 105(D16), 20539– 20547, [doi:10.1029/2000JD900242](https://doi.org/10.1029/2000JD900242), 2000.
51

1 Carpenter, L. J., MacDonald, S. M., Shaw, M. D., Kumar, R., Saunders, R. W., Parthipan, R.,
2 Wilson, J. and Plane, J. M. C.: Atmospheric iodine levels influenced by sea surface emissions
3 of inorganic iodine, *Nat. Geosci.*, 6(2), 108–111, doi:10.1038/ngeo1687, 2013.
4
5 [Chakraborty, K., V. Valsala, G. V. M. Gupta and V. V. S. S. Sarma, \(2018\): Dominant](#)
6 [biological control over upwelling on pCO₂ in sea east of Sri Lanka, *J. Geophysical Res.*,](#)
7 [doi.org/10.1029/2018JG004446.](#)
8
9 Chang, J.-H.: The Indian Summer Monsoon, *Geogr. Rev.*, vol. 57, no. 3, 373–396, 1967.
10
11 Charlson, R., Lovelock, J., Andreae, M., and Warren, S. G.: Oceanic phytoplankton,
12 atmospheric sulphur, cloud albedo and climate. *Nature* 326, 655–661.
13 <https://doi.org/10.1038/326655a0>, 1987.
14
15 Chen, L., Xu, S., Gao, Z., Chen, H., Zhang, Y., Zhan, J., and Li, W.: Estimation of monthly air-
16 sea CO₂ flux in the southern Atlantic and Indian Ocean using in-situ and remotely sensed data,
17 *Remote Sens. Environ.*, 115, 1935-1941, <https://doi.org/10.1016/j.rse.2011.03.016>, 2011.
18
19 Chen, J., and Bordoni, S.: Early summer response of the East Asian summer monsoon to
20 atmospheric CO₂ forcing and subsequent sea surface warming, *J. Climate*. 295431–46, 2016.
21
22 ~~Cheng, L., F. Zheng, and J. Zhu: Distinctive ocean interior changes during the recent warming~~
23 ~~slowdown. *Sci. Rep.*, 5, 14346, <https://doi.org/10.1038/srep14346>, 2015.~~
24
25 Chin, M. and Davis, D. D.: Global sources and sinks of OCS and CS₂ and their distributions,
26 *Global Biogeochem. Cy.*, 7, 321–337, 1993.
27
28 Chiu, R., Tinel, L., Gonzalez, L., Ciuraru, R., Bernard, F., George, C., and Volkamer, R.: UV
29 photochemistry of carboxylic acids at the air-sea boundary: A relevant source of glyoxal and
30 other oxygenated VOC in the marine atmosphere, *Geophys. Res. Lett.*, 44, 1079– 1087,
31 doi:10.1002/2016GL071240, 2017.
32
33 Ciais, P., Dolman, A. J., Bombelli, A., Duren, R., Pregon, A., Rayner, P. J., Miller, C., Gobron,
34 N., Kinderman, G., Marland, G., Gruber, N., Chevallier, F., Andres, R. J., Balsamo, G., Bopp,
35 L., Bréon, F. M., Broquet, G., Dargaville, R., Battin, T. J., Borges, A., Bovensmann, H.,
36 Buchwitz, M., Butler, J., Canadell, J. G., Cook, R. B., DeFries, R., Engelen, R., Gurney, K. R.,
37 Heinze, C., Heimann, M., Held, A., Henry, M., Law, B., Luysaert, S., Miller, J., Moriyama,
38 T., Moulin, C., Myneni, R. B., Nussli, C., Obersteiner, M., Ojima, D., Pan, Y., Paris, J. D., Piao,
39 S. L., Poulter, B., Plummer, S., Quegan, S., Raymond, P., Reichstein, M., Rivier, L., Sabine,
40 C., Schimel, D., Tarasova, O., Valentini, R., Wang, R., van der Werf, G., Wickland, D.,
41 Williams, M., and Zehner, C.: Current systematic carbon-cycle observations and the need for
42 implementing a policy-relevant carbon observing system, *Biogeosciences*, 11, 3547-3602,
43 10.5194/bg-11-3547-2014, 2014.
44
45 Ciuraru, R., Fine, L., Pinxteren, M. V., D’Anna, B., Herrmann, H., and George, C.: Unravelling
46 New Processes at Interfaces: Photochemical Isoprene Production at the Sea Surface, *Environ.*
47 *Sci. Technol.*, 49, 13199–13205, doi:10.1021/acs.est.5b02388, 2015.
48
49 Codispoti, L. A.: Interesting times for marine N₂O. *Science*, 327(5971), 1339–1340.
50 <https://doi.org/10.1126/science.1184945>, 2010.
51

1 Conte, L., Szopa, S., Séférian, R., and Bopp, L.: The oceanic cycle of carbon monoxide and its
2 emissions to the atmosphere, *Biogeosciences*, 16, 881–902, [https://doi.org/10.5194/bg-16-881-](https://doi.org/10.5194/bg-16-881-2019)
3 2019, 2019.
4
5 Crippa, M., Oreggioni, G., Guizzardi, D., Muntean, M., Schaaf, E., Lo Vullo, E., Solazzo, E.,
6 Monforti-Ferrario, F., Olivier, J.G.J., Vignati, E.: Fossil CO₂ and GHG emissions of all world
7 countries - 2019 Report, EUR 29849 EN, Publications Office of the European Union,
8 Luxembourg, ISBN 978-92-76-11100-9, doi:10.2760/687800, JRC117610, 2019.
9
10 Crippa, M., Solazzo, E., Huang, G., Guizzardi, D., Koffi, E., Muntean, M., Schieberle, C.,
11 Friedrich, R., and Janssens-Maenhout, G.: High resolution temporal profiles in the Emissions
12 Database for Global Atmospheric Research, *Sci. Data*, 7, 121, 10.1038/s41597-020-0462-2,
13 2020.
14
15 Cuevas, C. A., Maffezzoli, N., Corella, J. P., Spolaor, A., Vallelonga, P., Kjær, H. A.,
16 Simonsen, M., Winstrup, M., Vinther, B., Horvat, C., Fernandez, R. P., Kinnison, D.,
17 Lamarque, J.-F., Barbante, C. and Saiz-Lopez, A.: Rapid increase in atmospheric iodine levels
18 in the North Atlantic since the mid-20th century, *Nat. Commun.*, 9(1), 1452,
19 doi:10.1038/s41467-018-03756-1, 2018.
20
21 Da-Allada, C.Y., Gaillard, F. and Kolodziejczyk, N.: Mixed-layer salinity budget in the tropical
22 Indian Ocean: seasonal cycle based only on observations. *Ocean Dynam.*, 65, 845–857,
23 <https://doi.org/10.1007/s10236-015-0837-7>, 2015.
24
25 Daniel, J. S., and Solomon, S.: On the climate forcing of carbon monoxide, *J. Geophys. Res.*,
26 103(D11), 13249– 13260, doi:10.1029/98JD00822, 1998.
27
28 David, L. M., Girach, I. A., and Nair, P. R.: Distribution of ozone and its precursors over Bay
29 of Bengal during winter 2009: role of meteorology, *Ann. Geophys.*, 29, 1613–1627,
30 <https://doi.org/10.5194/angeo-29-1613-2011>, 2011.
31
32 David, L. M., and Nair, P. R.: Diurnal and seasonal variability of surface ozone and NO_x at a
33 tropical coastal site: Association with mesoscale and synoptic meteorological conditions, *J.*
34 *Geophys. Res.*, 116, D10303, doi:10.1029/2010JD015076, 2011.
35
36 David, L. M. and Nair, P. R.: Tropospheric column O₃ and NO₂ over the Indian region observed
37 by Ozone Monitoring Instrument (OMI): Seasonal changes and long-term trends, *Atmos.*
38 *Environ.*, 65, 25–39, <https://doi.org/10.1016/j.atmosenv.2012.09.033>, 2013.
39
40 Davidson, E. A.: The contribution of manure and fertilizer nitrogen to atmospheric nitrous
41 oxide since 1860. *Nat. Geosci.*, 2:659–662. <https://doi.org/10.1038/NGEO608>, 2009.
42
43 Deeter, M. N., Edwards, D. P., Francis, G. L., Gille, J. C., Mao, D., Martínez-Alonso, S.,
44 Worden, H. M., Ziskin, D., and Andreae, M. O.: Radiance-based retrieval bias mitigation for
45 the MOPITT instrument: the version 8 product, *Atmos. Meas. Tech.*, 12, 4561-4580,
46 10.5194/amt-12-4561-2019, 2019.
47
48 [De Smedt, I., Pinardi, G., Vigouroux, C., Compernelle, S., Bais, A., Benavent, N., Boersma,](#)
49 [F., Chan, K.-L., Donner, S., Eichmann, K.-U., Hedelt, P., Hendrick, F., Irie, H., Kumar, V.,](#)
50 [Lambert, J.-C., Langerock, B., Lerot, C., Liu, C., Loyola, D., PETERS, A., Richter, A., Rivera](#)
51 [Cárdenas, C., Romahn, F., Ryan, R. G., Sinha, V., Theys, N., Vlietinck, J., Wagner, T., Wang,](#)

1 [T., Yu, H., and Van Roozendaal, M.: Comparative assessment of TROPOMI and OMI](#)
2 [formaldehyde observations and validation against MAX-DOAS network column](#)
3 [measurements, Atmos. Chem. Phys., 21, 12561–12593, \[https://doi.org/10.5194/acp-21-12561-\]\(https://doi.org/10.5194/acp-21-12561-2021\)](#)
4 [2021, 2021.](#)

5

6 DeVries, T., Le Quéré, C., Andrews, O., Berthet, S., Hauck, J., Ilyina, T., Landschützer, P.,
7 Lenton, A., Lima, I. D., Nowicki, M., Schwinger, J., and Séférian, R.: Decadal trends in the
8 ocean carbon sink, Proc. Natl. Acad. Sci. USA, 116, 11646–11651, 10.1073/pnas.1900371116,
9 2019.

10

11 Dixit, A., L, K., Bharti, R., and Mahanta, C.: Net Sea–Air CO₂ Fluxes and Modeled Partial
12 Pressure of CO₂ in Open Ocean of Bay of Bengal, IEEE J. Sel. Top. Appl., 12, 2462–2469,
13 10.1109/JSTARS.2019.2902253, 2019.

14

15 Dong L, Zhou T and B. Wu: Indian Ocean warming during 1958–2004 simulated by a climate
16 system model and its mechanism. Clim. Dynam., 42, 203–217, doi.org/10.1007/s00382-013-
17 1722-z (2014), 2014.

18

19 Dong, L. and T. Zhou: The Indian Ocean sea surface temperature warming simulated by CMIP5
20 models during the twentieth century: Competing forcing roles of GHGs and anthropogenic
21 aerosols. J. Clim. 27, 3348–3362, 2014.

22

23 Du, Y. and S. P. Xie: Role of atmospheric adjustments in the tropical Indian Ocean warming
24 during the 20th century in climate models. Geophys. Res. Lett., 35, L08712, 2008.

25

26 Du, Y., Zhang, Y., Feng, M., Wang, T., Zhang, N., and S.E. Wijffels: Decadal trends of the
27 upper ocean salinity in the tropical Indo–Pacific since mid-1990s. Sci. Rep., 5:16050.
28 doi.org/10.1038/srep16050, 2015.

29

30 Du, Q., Zhang, C., Mu, Y., Cheng, Y., Zhang, Y., Liu, C., Song, M., Tian, D., Liu, P., Liu, J.,
31 Xue, C., and Ye, C.: An important missing source of atmospheric carbonyl sulfide: Domestic
32 coal combustion, Geophys. Res. Lett., 43, 8720–8727, 10.1002/2016gl070075, 2016.

33

34 [Dufлот, V., Tulet, P., Flores, O., Barthe, C., Colomb, A., Deguillaume, L., Vařtilingom, M.,](#)
35 [Perring, A., Huffman, A., Hernandez, M. T., Sellegri, K., Robinson, E., O'Connor, D. J.,](#)
36 [Gomez, O. M., Burnet, F., Bourrienne, T., Strasberg, D., Rocco, M., Bertram, A. K., Chazette,](#)
37 [P., Totems, J., Fournel, J., Stamenoff, P., Metzger, J.-M., Chabasset, M., Rousseau, C.,](#)
38 [Bourrienne, E., Sancelme, M., Delort, A.-M., Wegener, R. E., Chou, C., and Elizondo, P.:](#)
39 [Preliminary results from the FARCE 2015 campaign: multidisciplinary study of the forest–gas–](#)
40 [aerosol–cloud system on the tropical island of La Réunion, Atmos. Chem. Phys., 19, 10591–](#)
41 [10618, <https://doi.org/10.5194/acp-19-10591-2019>, 2019.](#)

42

43 Edtbauer, A., Stönnner, C., Pfannerstill, E. Y., Berasategui, M., Walter, D., Crowley, J. N.,
44 Lelieveld, J., and Williams, J.: A new marine biogenic emission: methane sulfonamide
45 (MSAM), DMS and DMSO₂ measured in air over the Arabian Sea, Atmos. Chem. Phys.
46 Discuss., <https://doi.org/10.5194/acp-2019-1021>, in review, 2020.

47

48 [Endresen, Ø., Sørgård, E., Sundet, J.K., Dalsøren, S.B., Isaksen, I.S.A., Berglen, T.F., and](#)
49 [Gravir, G.: Emission from international sea transportation and environmental impact, Journal](#)
50 [of Geophysical Research, 108, 4560. doi:10.1029/2002JD002898, 2003.](#)

51

1 Engel, A., Rigby, M., Burkholder, J. B., Fernandez, R. P. Froidevaux, L., Hall, B. D., Hossaini,
2 R., Saito, T., Vollmer, M. K., Yao, B.: Update on ozone-depleting substances (ODSs) and other
3 gases of interest to the Montreal Protocol. In Scientific assessment of ozone depletion: 2018,
4 Doherty, S. J., Means, T., Stewart, B. C., McCarrick, A., Dailey-Fisher, D., Reiser, A. M., Eds.;
5 Global ozone research and monitoring project, Vol. 58; WMO (World Meteorological
6 Organization): Geneva; pp 1.1-1.87, 2019.
7
8 Ethe', C., Basdevant, C., Sadourny, R., Appu, K. S., Harenduprakash, L., Sarode, P. R., and
9 Viswanathan, G.: Air mass motion, temperature, and humidity over the Arabian Sea and
10 western Indian Ocean during the INDOEX intensive phase, as obtained from a set of
11 superpressure drifting balloons, *J. Geophys. Res.*, 107, 8023, doi:10.1029/2001JD001120,
12 2002.
13
14 Exton, D. A., Suggett, D. J., McGenity, T. J., and Steinke, M.: Chlorophyll-normalized isoprene
15 production in laboratory cultures of marine microalgae and implications for global models,
16 *Limnol. Oceanogr.*, 58, 1301-1311, 10.4319/lo.2013.58.4.1301, 2013.
17
18 Fadnavis, S., Semeniuk, K., Schultz, M. G., Mahajan, A. S., Pozzoli, L., Sonbawane, S., and
19 Kiefer, M.: Transport pathways of peroxyacetyl nitrate in the upper troposphere and lower
20 stratosphere from different monsoon systems during the summer monsoon season. *Atmos.*
21 *Chem. Phys.*, 15(14), 11477–11499. <https://doi.org/10.5194/acp-15-11477-2015>, 2015.
22
23 Fiehn, A., Quack, B., Hepach, H., Fuhlbrügge, S., Tegtmeier, S., Toohey, M., et al.: Delivery
24 of halogenated very short-lived substances from the west Indian Ocean to the stratosphere
25 during the Asian summer monsoon. *Atmos. Chem. Phys.*, 17(11), 6723–6741.
26 <https://doi.org/10.5194/acp-17-6723-2017>, 2017.
27
28 Fiehn, A., Quack, B., Stemmler, I., Ziska, F., and Krüger, K.: Importance of seasonally resolved
29 oceanic emissions for bromoform delivery from the tropical Indian Ocean and west Pacific to
30 the stratosphere. *Atmos. Chem. Phys.*, 18(16), 11,973–11,990. [https://doi.org/10.5194/acp-18-](https://doi.org/10.5194/acp-18-11973-2018)
31 [11973-2018](https://doi.org/10.5194/acp-18-11973-2018), 2018.
32
33 Fiore, A.M., West, J.J., Horowitz, L.W., Naik, V. and Schwarzkopf, M.D.: Characterizing the
34 tropospheric ozone response to methane emission controls and the benefits to climate and air
35 quality. *J. Geophys. Res.*, 113(D08): 307. DOI: 10.1029/2007JD009162, 2008.
36
37 Franke, K., Richter, A., Bovensmann, H., Eyring, V., Jöckel, P., Hoor, P., and Burrows, J. P.:
38 Ship emitted NO₂ in the Indian Ocean: comparison of model results with satellite data, *Atmos.*
39 *Chem. Phys.*, 9, 7289–7301, <https://doi.org/10.5194/acp-9-7289-2009>, 2009.
40
41 Fuge, R., and C. C. Johnson: Iodine and human health, the role of environmental geochemistry
42 and diet, a review. *Appl. Geochem.*, 63, 282–302, 2015.
43
44 Galí, M., Levasseur, M., Devred, E., Simó, R., and Babin, M.: Sea-surface dimethylsulfide
45 (DMS) concentration from satellite data at global and regional scales. *Biogeosciences*, 15(11),
46 3497–3519. <https://doi.org/10.5194/bg-15-3497-2018>, 2018.
47
48 Ganguly, N.D. and Tzanis, C.: Study of Stratosphere-troposphere exchange events of ozone in
49 India and Greece using ozonesonde ascents. *Met. Apps*, 18: 467-474. doi:10.1002/met.241,
50 2011.
51

1 Gantt, B., Meskhidze, N., and Kamykowski, D.: A new physically-based quantification of
2 marine isoprene and primary organic aerosol emissions, *Atmos. Chem. Phys.*, 9, 4915-4927,
3 10.5194/acp-9-4915-2009, 2009.

4

5 GESAMP: Rep. Stud. GESAMP 84: 69, 2012.

6

7 Ghude, S. D., Beig, G., Kulkarni, P. S., Kanawade, V. P., Fadnavis, S., Remedios, J. J., and
8 Kulkarni, S. H.: Regional CO pollution over the Indian-subcontinent and various transport
9 pathways as observed by MOPITT, *Int. J. Remote Sens.*, 32, 6133–6148, 2011.

10

11 Ghude, S.D., Kulkarni, S.H., Jena, C., Pfister, G.G., Beig, G., Fadnavis, S., van der A, R.J.:
12 Application of satellite observations for identifying regions of dominant sources of nitrogen
13 oxides over the Indian Subcontinent. *J. Geophys. Res.*, 118, 1075e1089.
14 <http://dx.doi.org/10.1029/2012JD017811>, 2013.

15

16 Gibb, S. W. and Mantoura, R. F. C.: Ocean-atmosphere exchange and atmospheric speciation
17 of ammonia and methylamines in the region of the NW Arabian Sea, *Global Biogeochem.*
18 *Cycles*, 13, 161–178, 1999a.

19

20 Gibb, S. W., Mantouura, R. F. C., and Liss, P. S.: Ocean-atmosphere exchange and speciation
21 of ammonia and methylamines in the region of the NW Arabian Sea, *Global Biogeochem.*
22 *Cycles*, 13, 161–178, 1999b.

23

24 [Girach, I. A. and Nair, P. R.: On the vertical distribution of carbon monoxide over Bay of](#)
25 [Bengal during winter: role of water vapour and vertical updrafts, *J. Atmos. Sol. Terr. Phys.*,](#)
26 [117, 31– 47, doi:10.1016/j.jastp.2014.05.003, 2014a.](#)

27

28 [Girach, I. A. and Nair, P. R.: Carbon monoxide over Indian region as observed by MOPITT,](#)
29 [Atmos. Environ., 99, 599–609, <https://doi.org/10.1016/j.atmosenv.2014.10.019>, 2014b.](#)

30

31 Girach, I. A., Ojha, N., Nair, P. R., Pozzer, A., Tiwari, Y. K., Kumar, K. R., and Lelieveld, J.:
32 Variations in O₃, CO, and CH₄ over the Bay of Bengal during the summer monsoon season:
33 shipborne measurements and model simulations, *Atmos. Chem. Phys.*, 17, 257–275,
34 <https://doi.org/10.5194/acp-17-257-2017>, 2017.

35

36 [Girach, I. A., Ojha, N., Nair, P. R., Tiwari, Y. K., and Kumar, K. R., Variations of trace gases](#)
37 [over the Bay of Bengal during the summer monsoon. *Journal of Earth System Science*, doi:](#)
38 [10.1007/s12040-017-0915-y, 2018.](#)

39

40 [Girach, I. A., Nair, P. R., Ojha, N., and Sahu, S. K.: Tropospheric carbon monoxide over the](#)
41 [northern Indian Ocean during winter: Influence of inter-continental transport, *Climate*](#)
42 [Dynamics, 54, 5049–5064. <https://doi.org/10.1007/s00382-020-05269-4>, 2020a.](#)

43

44 [Girach, L. A., N. Tripathi, P.R. Nair, L.K. Sahu, N. Ojha: O₃ and CO in the South Asian outflow](#)
45 [over the Bay of Bengal: impact of monsoonal dynamics and chemistry, *Atm. Environ*, 233, p.](#)
46 [117610, 10.1016/j.atmosenv.2020.117610, 2020b.](#)

47

48 Glatthor, N., Höpfner, M., Baker, I. T., Berry, J., Campbell, J. E., Kawa, S. R., Krysztofiak, G.,
49 Leyser, A., Sinnhuber, B.-M., Stiller, G. P., Stinecipher, J., von Clarmann, T.: Tropical sources
50 and sinks of carbonyl sulfide observed from space, *Geophys. Res. Lett.*, 42, 10,082–10,090,
51 doi:10.1002/2015GL066293, 2015.

1
2 Goes, J.I., P.G. Thoppil, H. Gomes, and J.T. Fasullo: Warming of the Eurasian landmass is
3 making the Arabian Sea more productive, *Science*, 308 (5721), 545-547,
4 10.1126/science.1106610, 2005.
5
6 Gopika, S., Izumo, T., Vialard, J., Lengaigne, M., Suresh, I. and M. R. R. Kumar: Aliasing of
7 the Indian Ocean externally-forced warming spatial pattern by internal climate variability,
8 *Clim. Dynam.*, 54, 1-2, 1093-1111, 2020.
9
10 [Gopikrishnan, G. S., and Kuttippurath, J.: A decade of satellite observations reveal significant](#)
11 [increase in atmospheric formaldehyde from shipping in Indian Ocean, *Atmos. Environ.*, 246,](#)
12 [118095, <https://doi.org/10.1016/j.atmosenv.2020.118095>, 2021](#)
13
14 Graedel, T. E. and Crutzen, P. J.: *Atmospheric Change: an Earth System Perspective*, W. H.
15 Freeman, New York, 1992.
16
17 Gregg, W. W., and Rousseaux, C. S.: Global ocean primary production trends in the modern
18 ocean color satellite record (1998–2015). *Environ. Res. Lett.* 2019;14:1–9, 2019.
19
20 Gschwend, P. M., MacFarlane, J. K. and Newman, K. A.: Volatile halogenated organic
21 compounds released to seawater from temperate marine macroalgae, *Science* 227, 1033–1035,
22 1985.
23
24 Guenther, A., Karl, T., Harley, P., Wiedinmyer, C., Palmer, P. I., and Geron, C.: Estimates of
25 global terrestrial isoprene emissions using MEGAN (Model of Emissions of Gases and
26 Aerosols from Nature), *Atmos. Chem. Phys.*, 6, 3181-3210, 10.5194/acp-6-3181-2006, 2006.
27
28 Guenther, A. B., Jiang, X., Heald, C. L., Sakulyanontvittaya, T., Duhl, T., Emmons, L. K., and
29 Wang, X.: The Model of Emissions of Gases and Aerosols from Nature version 2.1
30 (MEGAN2.1): an extended and updated framework for modeling biogenic emissions, *Geosci.*
31 *Model Dev.*, 5, 1471-1492, 10.5194/gmd-5-1471-2012, 2012.
32
33 Guerreiro, C. V., Baumann, K.-H., Brummer, G.-J. A., Fischer, G., Korte, L. F., Merkel, U.,
34 Sá, C., de Stigter, H., and Stuut, J.-B. W.: Coccolithophore fluxes in the open tropical North
35 Atlantic: influence of thermocline depth, Amazon water, and Saharan dust, *Biogeosciences*, 14,
36 4577–4599, <https://doi.org/10.5194/bg-14-4577-2017>, 2017.
37
38 Guieu, C., O. Aumont, A. Paytan, L. Bopp, C. S. Law, N. Mahowald, E. P. Achterberg, E.
39 Marañón, B. Salihoglu, A. Crise, T. Wagener, B. Herut, K. Desboeufs, M. Kanakidou, N.
40 Olgun, F. Peters, E. Pulido-Villena, A. Tovar-Sanchez and C. Völker: The significance of the
41 episodic nature of atmospheric deposition to Low Nutrient Low Chlorophyll regions, *Global*
42 *Biogeochem. Cy.*, 28, 1179– 1198, doi:10.1002/2014GB004852, 2014.
43
44 Guieu, C., A., Azhar, M., Aumont, O., Mahowald, N., Levy, M., Ethé, C., and Lachkar, Z.:
45 Major impact of dust deposition on the productivity of the Arabian Sea. *Geophys. Res. Lett.*,
46 46, 6736– 6744. <https://doi.org/10.1029/2019GL082770>, 2019.
47
48 Han, W., and J. P. McCreary: Modelling salinity distributions in the Indian Ocean, *J. Geophys.*
49 *Res.*, 106, 859 – 877, 2001.
50

1 Han, W. et al.: Indian Ocean decadal variability: a review. *Bull. Am. Meteorol. Soc.* 95, 1679–
2 1703, 2014.

3

4 Han, Z., Su, T., Zhang, Q., Wen, Q., and G. Feng: Thermodynamic and dynamic effects
5 of increased moisture sources over the Tropical Indian Ocean in recent decades, *Clim. Dynam.*,
6 53:7081–7096, 2019.

7

8 Hastenrath, S. and Polzin, D., Dynamics of the surface wind field over the equatorial Indian
9 Ocean. *Q.J.R. Meteorol. Soc.*, 130: 503-517. doi:10.1256/qj.03.79, 2004.

10

11 Hastenrath, S., Zonal Circulations over the Equatorial Indian Ocean. *J. Climate*, 13, 2746–2756,
12 [https://doi.org/10.1175/1520-0442\(2000\)013<2746:ZCOTEI>2.0.CO;2](https://doi.org/10.1175/1520-0442(2000)013<2746:ZCOTEI>2.0.CO;2), 2000.

13

14 Hay, T., Kreher, K. and Riedel, K.: Bromine explosions and Antarctic ozone. *Water and*
15 *Atmosphere*, 15, pp. 12–13, 2007.

16

17 Henze, D. K., and Seinfeld, J. H.: Global secondary organic aerosol from isoprene oxidation,
18 *Geophys. Res. Lett.*, 33, 10.1029/2006gl025976, 2006.

19

20 ~~Hermes, J. C., Masumoto, Y., Beal, L. M., Roxy, M. K., Vialard, J., Andres, M., Annamalai,~~
21 ~~H., Behera, S., D'Adamo, N., Doi, T., Feng, M., Han, W., Hardman Mountford, N., Hendon,~~
22 ~~H., Hood, R., Kido, S., Lee, C., Lee, T., Lengaigne, M., Li, J., Lumpkin, R., Navaneeth, K. N.,~~
23 ~~Milligan, B., McPhaden, M. J., Ravichandran, M., Shinoda, T., Singh, A., Sloyan, B., Strutton,~~
24 ~~P. G., Subramanian, A. C., Thurston, S., Tozuka, T., Ummenhofer, C. C., Unnikrishnan, A. S.,~~
25 ~~Venkatesan, R., Wang, D., Wiggert, J., Yu, L., and Yu, W.: A Sustained Ocean Observing~~
26 ~~System in the Indian Ocean for Climate Related Scientific Knowledge and Societal Needs,~~
27 ~~*Frontiers in Marine Science*, 6, 10.3389/fmars.2019.00355, 2019.~~

28

29 Herut B., Rahav E., Tsagaraki T. M., Giannakourou A., Tsiola A., Psarra S., Lagaria A.,
30 Papageorgiou N., Mihalopoulos N., Theodosi C. N., Violaki K., Stathopoulou E., Scoullou M.,
31 Krom M. D., Stockdale A., Shi Z., Berman-Frank I., Meador T. B., Tanaka T., and Paraskevi
32 P.: The Potential Impact of Saharan Dust and Polluted Aerosols on Microbial Populations in
33 the East Mediterranean Sea, an Overview of a Mesocosm Experimental Approach, *Frontiers in*
34 *Marine Science*, 3, 226, doi=10.3389/fmars.2016.00226, 2016.

35

36 Hönninger, G.: Halogen Oxide Studies in the Boundary Layer by Multi Axis Differential
37 Optical Absorption Spectroscopy and Active Longpath-DOAS. University of Heidelberg, 2002.

38

39 Hood, R. R., Urban, E. R., McPhaden, M. J., Su, D., and Raes, E.: The 2nd International Indian
40 Ocean Expedition (IIOE-2): Motivating New Exploration in a Poorly Understood Basin,
41 *Limnol. Oceanogr. Bulletin*, 25, 117-124, 10.1002/lob.10149, 2016.

42

43 Hood R. R., Beckley, L. E. and Wiggert, J. D.: Biogeochemical and ecological impacts of
44 boundary currents in the Indian Ocean. *Prog. Oceanogr.*, 156: 290–325, 2017.

45

46 Hopkins, F. E. and Archer, S. D.: Consistent increase in dimethyl sulfide (DMS) in response to
47 high CO₂ in five shipboard bio assays from contrasting NW European waters, *Biogeosciences*,
48 11, 4925–4940, <https://doi.org/10.5194/bg-11-4925-2014>, 2014.

49

1 Hopkins, F. E., Turner, S. M., Nightingale, P. D., Steinke, M., Bakker, D., and Liss, P. S.:
2 Ocean acidification and marine trace gas emissions, *P. Natl. Acad. Sci. USA*, 107, 760–765,
3 2010.
4
5 Hossaini, R., Mantle, H., Chipperfield, M. P., Montzka, S. A., Hamer, P., Ziska, F., Quack, B.,
6 Krüger, K., Tegtmeier, S., Atlas, E., Sala, S., Engel, A., Bönisch, H., Keber, T., Oram, D.,
7 Mills, G., Ordóñez, C., Saiz-Lopez, A., Warwick, N., Liang, Q., Feng, W., Moore, F., Miller,
8 B. R., Marécal, V., Richards, N. A. D., Dorf, M., and Pfeilsticker, K.: Evaluating global
9 emission inventories of biogenic bromocarbons, *Atmos. Chem. Phys.*, 13, 11819–11838,
10 10.5194/acp-13-11819-2013, 2013.
11
12 Hsu, N. C., Gautam, R., Sayer, A. M., Bettenhausen, C., Li, C., Jeong, M. J., Tsay, S.-C., and
13 Holben, B. N.: Global and regional trends of aerosol optical depth over land and ocean using
14 SeaWiFS measurements from 1997 to 2010, *Atmos. Chem. Phys.*, 12, 8037–8053,
15 <https://doi.org/10.5194/acp-12-8037-2012>, 2012.
16
17 Hu, Q. H., Xie, Z. Q., Wang, X. M., Kang, H., He, Q. F., and Zhang, P.: Secondary organic
18 aerosols over oceans via oxidation of isoprene and monoterpenes from Arctic to Antarctic, *Sci*
19 *Rep*, 3, 2280, 10.1038/srep02280, 2013.
20
21 Hu, S., and Sprintall, J.: Observed strengthening of interbasin exchange via the Indonesian seas
22 due to rainfall intensification. *Geophys. Res. Lett.* 44, 1448–1456. doi:
23 10.1002/2016GL072494, 2017.
24
25 Inamdar, S., Tinel, L., Chance, R., Carpenter, L. J., Sabu, P., Chacko, R., Tripathy, S. C.,
26 Kerkar, A. U., Sinha, A. K., Bhaskar, P. V., Sarkar, A., Roy, R., Sherwen, T., Cuevas, C., Saiz-
27 Lopez, A., Ram, K., and Mahajan, A. S.: Estimation of Reactive Inorganic Iodine Fluxes in the
28 Indian and Southern Ocean Marine Boundary Layer, *Atmos. Chem. Phys. Discuss.*, 2020, 1-
29 57, 10.5194/acp-2019-1052, 2020.
30
31 Inomata, Y., Hayashi, M., Osada, K., and Iwasaka, Y.: Spatial distributions of volatile sulfur
32 compounds in surface seawater and overlying atmosphere in the northwestern Pacific Ocean,
33 Eastern Indian Ocean, and Southern Ocean, *Global Biogeochem. Cy.*, 20, GB2022,
34 <https://doi.org/10.1029/2005gb002518>, 2006.
35
36 IPCC. Climate Change 2013: The Physical Science Basis. In: Stocker, TF, Qin, D, Plattner, G-
37 K, Tignor, M, Allen, SK, Boschung, J, Nauels, A, Xia, Y, Bex, V and Midgley, PM (eds.),
38 Contribution of Working Group I to the Fifth Assessment Report of the Intergovernmental
39 Panel on Climate Change, 1535. Cambridge University Press, Cambridge, United Kingdom and
40 New York, NY, USA, 2013.
41
42 Ito, A., Nishina, K., Ishijima, K. et al. Emissions of nitrous oxide (N₂O) from soil surfaces and
43 their historical changes in East Asia: a model-based assessment. *Prog Earth Planet Sci* 5, 55,
44 <https://doi.org/10.1186/s40645-018-0215-4>, 2018.
45
46 Iyengar, G. R., V. S. Prasad, and K. J. Ramesh, Circulation characteristic associated with Inter
47 Tropical Convergence Zone during northern winter, *Curr. Sci.*, 76, 903–906, 1999.
48
49 Jensen, T. G.: Cross-equatorial pathways of salt and tracers from the northern Indian Ocean:
50 Modelling results, *Deep Sea Res., Part II*, 50, 2111 – 2128, 2003.
51

1 Jickells, T. D., E. Buitenhuis, K. Altieri, A. R. Baker, D. Capone, R. A. Duce, F. Dentener, K.
2 Fennel, M. Kanakidou, J. LaRoche, K. Lee, P. Liss, J. J. Middelburg, J. K. Moore, G. Okin, A.
3 Oschlies, M. Sarin, S. Seitzinger, J. Sharples, A. Singh, P. Suntharalingam, M. Uematsu, L. M.
4 Zamora: A reevaluation of the magnitude and impacts of anthropogenic atmospheric nitrogen
5 inputs on the ocean. *Global Biogeochem. Cy.*, 31, 289–305, [https://](https://doi.org/10.1002/2016GB005586)
6 doi.org/10.1002/2016GB005586, 2017.
7
8 Jordi, A., G. Basterretxea, A. Tovar-Sánchez, A. Alastuey, and X. Querol: Copper aerosols
9 inhibit phytoplankton growth, *Proc. Natl. Acad. Sci. USA*, 109 (52) 21246-21249; DOI:
10 10.1073/pnas.1207567110, 2012.
11
12 Kavitha, M. and P. R. Nair: Satellite-retrieved vertical profiles of methane over the Indian
13 region: impact of synoptic-scale meteorology, *Int. J. Remote Sens.*, 40:14, 5585-5616, DOI:
14 10.1080/01431161.2019.1580791, 2019.
15
16 Khemani, L. T., Momin, G. A., and Singh, G.: Variation in trace gases concentrations in
17 different environments in India, *PA- GEOPH.*, 125, 151–158, 1987.
18
19 Kitoh, A., Endo, H., Krishna Kumar, K., Cavalcanti, IFA, Goswami, P. and Zhou, T.: Monsoons
20 in a changing world: A regional perspective in a global context. *J. Geophys. Res.*, 118(8):3053–
21 3065, 2013.
22
23 Kim, P. S., Jacob, D. J., Liu, X., Warner, J. X., Yang, K., Chance, K., Thouret, V., and Nedelec,
24 P.: Global ozone–CO correlations from OMI and AIRS: constraints on tropospheric ozone
25 sources, *Atmos. Chem. Phys.*, 13, 9321–9335, <https://doi.org/10.5194/acp-13-9321-2013>,
26 2013.
27
28 Kornmüller, A.: Review of fundamentals and specific aspects of oxidation technologies in
29 marine waters. *Water Sci Technol*, 55 (12): 1–6. doi: <https://doi.org/10.2166/wst.2007.379>,
30 2007.
31
32 Kremser, S., Thomason, L. W., von Hobe, M., Hermann, M., Deshler, T., Timmreck, C.,
33 Toohey, M., Stenke, A., Schwarz, J. P., Weigel, R., Fueglistaler, S., Prata, F. J., Vernier, J.-P.,
34 Schlager, H., Barnes, J. E., Antuña-Marrero, J.-C., Fairlie, D., Palm, M., Mahieu, E., Notholt,
35 J., Rex, M., Bingen, C., Vanhellemont, F., Bourassa, A., Plane, J. M. C., Klocke, D., Carn, S.
36 A., Clarisse, L., Trickl, T., Neely, R., James, A. D., Rieger, L., Wilson, J. C., and Meland, B.:
37 Stratospheric aerosol—Observations, processes, and impact on climate, *Rev. Geophys.*, 54,
38 278-335, [10.1002/2015rg000511](https://doi.org/10.1002/2015rg000511), 2016.
39
40 Krishnamurti, T. N., Jha, B., Rasch, P. J., and Ramanathan, V.: A high resolution global
41 reanalysis highlighting the winter monsoon, Part I, Reanalysis fields, *Met. Atmos. Phys.*, 64,
42 123–150, 1997a.
43
44 Krishnamurti, T. N., Jha, B., Rasch, P. J., and Ramanathan, V.: A high resolution global
45 reanalysis highlighting the winter monsoon, Part II, transients and passive tracer transports,
46 *Met. At- mos. Phys.*, 64, 151–171, 1997b.
47
48 Krishnan, R. et al.: *Assessment of Climate Change over the Indian Region*, Springer Singapore,
49 DOI [10.1007/978-981-15-4327-2](https://doi.org/10.1007/978-981-15-4327-2), 2020.
50

1 Krom M. D., Shi Z., Stockdale A., Berman-Frank I., Giannakourou A., Herut B., Lagaria A.,
2 Papageorgiou N., Pitta P., Psarra S., Rahav E., Scoullou M., Stathopoulou E., Tsiola A., and
3 Tsagaraki T. M.: Response of the Eastern Mediterranean Microbial Ecosystem to Dust and Dust
4 Affected by Acid Processing in the Atmosphere, *Frontiers in Marine Science*, 3, 133
5 doi=10.3389/fmars.2016.00133, 2016.
6
7 Krotkov, N. A., McLinden, C. A., Li, C., Lamsal, L. N., Celarier, E. A., Marchenko, S. V.,
8 Swartz, W. H., Bucsela, E. J., Joiner, J., Duncan, B. N., Boersma, K. F., Veefkind, J. P., Levelt,
9 P. F., Fioletov, V. E., Dickerson, R. R., He, H., Lu, Z., and Streets, D. G.: Aura OMI
10 observations of regional SO₂ and NO₂ pollution changes from 2005 to 2015, *Atmos. Chem.*
11 *Phys.*, 16, 4605-4629, 10.5194/acp-16-4605-2016, 2016.
12
13 Kuai, L., Worden, J. R., Campbell, J. E., Kulawik, S. S., Li, K.-F., Lee, M., Weidner, R. J.,
14 Montzka, S. A., Moore, F. L., Berry, J. A., Baker, I., Denning, A. S., Bian, H., Bowman, K.
15 W., Liu, J., and Yung, Y. L.: Estimate of carbonyl sulfide tropical oceanic surface fluxes using
16 Aura Tropospheric Emission Spectrometer observations, *J. Geophys. Res.*, 120, 11012–11023,
17 <https://doi.org/10.1002/2015JD023493>, 2015.
18
19 Kumar, K.R., Tiwari, Y.K., Valsala, V., and R. Murtugudde: On understanding the land–ocean
20 CO₂ contrast over the Bay of Bengal: A case study during 2009 summer monsoon. *Environ Sci*
21 *Pollut Res* 21, 5066–5075, <https://doi.org/10.1007/s11356-013-2386-2>, 2014.
22
23 Kunhikrishnan, T., Lawrence, M. G., von Kuhlmann, R., Richter, A., Ladstaetter, A., and
24 Burrows, J. P.: Analysis of tropospheric NO_x over Asia using the Model of Atmospheric
25 Transport and Chemistry (MATCH-MPIC) and GOME-satellite observations, *Atmos.*
26 *Environ.*, 38, 581–596, 2004.
27
28 [Kurokawa, J., Ohara, T., Morikawa, T., Hanayama, S., Janssens-Maenhout, G., Fukui, T.,](#)
29 [Kawashima, K., and Akimoto, H.: Emissions of air pollutants and greenhouse gases over Asian](#)
30 [re-gions during 2000–2008: Regional Emission inventory in ASia\(REAS\) version 2, *Atmos.*](#)
31 [*Chem. Phys.*, 13, 11019–11058, doi:10.5194/acp-13-11019-2013, 2013.](#)
32
33 Lachkar, Z., Levy, M. and Smith, S.: Intensification and deepening of the Arabian Sea oxygen
34 minimum zone in response to increase in Indian monsoon wind intensity. *Biogeosciences* 15,
35 159–186, 2018.
36
37 Ladstätter-Weissenmayer, A., Altmeyer, H., Bruns, M., Richter, A., Rozanov, A., Rozanov, V.,
38 Wittrock, F., and Burrows, J. P.: Measurements of O₃, NO₂ and BrO during the INDOEX
39 campaign using ground based DOAS and GOME satellite data, *Atmos. Chem. Phys.*, 7, 283-
40 291, 2007.
41
42 Lago, V., Wjiffels, S.E., Durack, P.J., Church, J.A., Bindoff, N.L., and Marsland, S.J.:
43 Simulating the role of surface forcing on observed multidecadal upper-ocean salinity changes.
44 *J. Clim.*, 29:5575–5588. <https://doi.org/10.1175/JCLI-D-15-0519.1>, 2016.
45
46 Lal, S., Chand, D., Sahu, L. K., Venkataramani, S., Brasseur, G., and Schultz, M. G.: High
47 levels of ozone and related gases over the Bay of Bengal during winter and early spring of 2001,
48 *Atmos. Environ.*, 40, 1633–1644, 2006.
49
50 [Lal, S. and Lawrence, M. G.: Elevated mixing ratios of surface ozone over the Arabian Sea,](#)
51 [*Geophys. Res. Lett.*, 28, 1487–1490, 2001.](#)

1
2 Lal, S., Sahu, L. K., and Venkataramani, S.: Impact of transport from the surrounding
3 continental regions on the distributions of ozone and related trace gases over the Bay of Bengal
4 during February 2003, *J. Geophys. Res.*, 112, D14302, doi:10.1029/2006JD008023, 2007.
5
6 Lal, S., Venkataramani, S., Chandra, N., Cooper, O. R., Brioude, J., and Naja, M.: Transport
7 effects on the vertical distribution of tropospheric ozone over western India, *J. Geophys. Res.*,
8 119, 10012-10026, 10.1002/2014jd021854, 2014.
9
10 Lamb, P. J., and Hastenrath, S., *Climatic Atlas of the Indian Ocean: Surface Climate and*
11 *Atmospheric Circulation*. Madison: The University of Wisconsin Press, 1979.
12
13 Lana, A., Bell, T. G., Simó, R., Vallina, S. M., Ballabrera-Poy, J., Kettle, A. J., Dachs, J., Bopp,
14 L., Saltzman, E. S., Stefels, J., Johnson, J. E., and Liss, P. S.: An updated climatology of surface
15 dimethylsulfide concentrations and emission fluxes in the global ocean, *Global Biogeochem.*
16 *Cy.*, 25, 10.1029/2010gb003850, 2011.
17
18 Latif, M. and T.P. Barnett: Interactions of the Tropical Oceans. *J. Climate*, 8, 952–964,
19 [https://doi.org/10.1175/1520-0442\(1995\)008<0952:IOTTO>2.0.CO;2](https://doi.org/10.1175/1520-0442(1995)008<0952:IOTTO>2.0.CO;2), 1995.
20
21 Launois, T., Belviso, S., Bopp, L., Fichot, C. G., and Peylin, P.: A new model for the global
22 biogeochemical cycle of carbonyl sulfide; Part 1: Assessment of direct marine emissions with
23 an oceanic general circulation and biogeochemistry model, *Atmos. Chem. Phys.*, 15, 2295-
24 2312, 10.5194/acp-15-2295-2015, 2015.
25
26 Lawrence, M. G., Rasch, P. J., von Kuhlmann, R., Williams, J., Fischer, H., de Reus, M.,
27 Lelieveld, J., Crutzen, P. J., Schultz, M., Stier, P., Huntrieser, H., Heland, J., Stohl, A., Forster,
28 C., Elbern, H., Jakobs, H., and Dickerson, R. R.: Global chemical weather forecasts for field
29 campaign planning: predictions and observations of large-scale features during MINOS,
30 CONTRACE, and INDOEX, *Atmos. Chem. Phys.*, 3, 267–289, doi:10.5194/acp-3- 267-2003,
31 2003.
32
33 Lawrence, M.G., Export of Air Pollution from Southern Asia and its Large-Scale Effects. In:
34 Stohl A. (eds) *Air Pollution. The Handbook of Environmental Chemistry*, vol 4G. Springer,
35 Berlin, Heidelberg, 2004.
36
37 Lawrence and Lelieveld, Atmospheric pollutants outflow from southern Asia: a review, *Atmos.*
38 *Chem. Phys.*, 10, pp. 11017-11096, 2010.
39
40 Le Quéré, C., Andrew, R. M., Friedlingstein, P., Sitch, S., Hauck, J., Pongratz, J., Pickers, P.
41 A., Korsbakken, J. I., Peters, G. P., Canadell, J. G., Arneeth, A., Arora, V. K., Barbero, L.,
42 Bastos, A., Bopp, L., Chevallier, F., Chini, L. P., Ciais, P., Doney, S. C., Gkritzalis, T., Goll,
43 D. S., Harris, I., Haverd, V., Hoffman, F. M., Hoppema, M., Houghton, R. A., Hurtt, G., Ilyina,
44 T., Jain, A. K., Johannessen, T., Jones, C. D., Kato, E., Keeling, R. F., Goldewijk, K. K.,
45 Landschützer, P., Lefèvre, N., Lienert, S., Liu, Z., Lombardozzi, D., Metzl, N., Munro, D. R.,
46 Nabel, J. E. M. S., Nakaoka, S., Neill, C., Olsen, A., Ono, T., Patra, P., Pregon, A., Peters, W.,
47 Peylin, P., Pfeil, B., Pierrot, D., Poulter, B., Rehder, G., Resplandy, L., Robertson, E., Rocher,
48 M., Rödenbeck, C., Schuster, U., Schwinger, J., Séférian, R., Skjelvan, I., Steinhoff, T., Sutton,
49 A., Tans, P. P., Tian, H., Tilbrook, B., Tubiello, F. N., van der Laan-Luijkx, I. T., van der Werf,
50 G. R., Viovy, N., Walker, A. P., Wiltshire, A. J., Wright, R., Zaehle, S., and Zheng, B.: Global
51 Carbon Budget 2018, *Earth Syst. Sci. Data*, 10, 2141-2194, 10.5194/essd-10-2141-2018, 2018.

- 1
2 Lee, C.-L., and Brimblecombe, P.: Anthropogenic contributions to global carbonyl sulfide,
3 carbon disulfide and organosulfides fluxes, *Earth-Sci. Rev.*, 160, 1-18,
4 <https://doi.org/10.1016/j.earscirev.2016.06.005>, 2016.
5
6 ~~Lee, S. K., W. Park, M. O. Baringer, A. L. Gordon, B. Huber, and Y. Liu: Pacific origin of the~~
7 ~~abrupt increase in Indian Ocean heat content during the warming hiatus, *Nat. Geosci.*, 8, 445–~~
8 ~~449, <https://doi.org/10.1038/ngeo2438>, 2015.~~
9
10 Legrand, M., McConnell, J. R., Preunkert, S., Arienzo, M., Chellman, N., Gleason, K.,
11 Sherwen, T., Evans, M. J. and Carpenter, L. J.: Alpine ice evidence of a three-fold increase in
12 atmospheric iodine deposition since 1950 in Europe due to increasing oceanic emissions, *Proc.*
13 *Natl. Acad. Sci.*, 115(48), 12136–12141, doi:10.1073/pnas.1809867115, 2018.
14
15 Lelieveld, J., Evans, J. S., Fnais, M., Giannadaki, D., and Pozzer, A.: The contribution of
16 outdoor air pollution sources to premature mortality on a global scale, *Nature*, 525, 367-371,
17 10.1038/nature15371, 2015.
18
19 Lelieveld, J., Crutzen, P. J., Ramanathan, V., Andreae, M. O., Brenninkmeijer, C. A. M.,
20 Campos, T., Cass, G. R., Dickerson, R. R., Fischer, H., de Gouw, J. A., Hansel, A., Jefferson,
21 A., Kley, D., de Laat, A. T. J., Lal, S., Lawrence, M. G., Lobert, J. M., Mayol-Bracero, O. L.,
22 Mitra, A. P., Novakov, T., Oltmans, S. J., Prather, K. A., Reiner, T., Rodhe, H., Scheeren, H.
23 A., Sikka, D., and Williams, J.: The Indian Ocean experiment: Widespread air pollution from
24 South and Southeast Asia, *Science*, 291, 1031–1036, 2001.
25
26 Lelieveld, J., Bourtsoukidis, E., Brühl, C., Fischer, H., Fuchs, H., Harder, H., Hofzumahaus,
27 A., Holland, F., Marno, D., Neumaier, M., Pozzer, A., Schlager, H., Williams, J., Zahn, A., and
28 Ziereis, H.: The South Asian monsoon – Pollution pump and purifier, *Science*, 361, 270–273,
29 <https://doi.org/10.1126/science.aar2501>, 2018.
30
31 Lelieveld, J., K. Klingmüller, A. Pozzer, R.T. Burnett, A. Haines and V. Ramanathan: Effects
32 of fossil fuel and total anthropogenic emission removal on public health and climate. *Proc. Natl.*
33 *Acad. Sci. USA*, 116 (15), 7192-7197, doi:www.pnas.org/cgi/doi/10.1073/pnas.1819989116,
34 2019.
35
36 Lennartz, S. T., Marandino, C. A., von Hobe, M., Cortes, P., Quack, B., Simo, R., Booge, D.,
37 Pozzer, A., Steinhoff, T., Arevalo-Martinez, D. L., Kloss, C., Bracher, A., Röttgers, R., Atlas,
38 E., and Krüger, K.: Direct oceanic emissions unlikely to account for the missing source of
39 atmospheric carbonyl sulfide, *Atmos. Chem. Phys.*, 17, 385–402, [https://doi.org/10.5194/acp-](https://doi.org/10.5194/acp-17-385-2017)
40 [17-385-2017](https://doi.org/10.5194/acp-17-385-2017), 2017.
41
42 Lennartz, S. T., Marandino, C. A., von Hobe, M., Andreae, M. O., Aranami, K., Atlas, E.,
43 Berkelhammer, M., Bingemer, H., Booge, D., Cutter, G., Cortes, P., Kremser, S., Law, C. S.,
44 Marriner, A., Simó, R., Quack, B., Uher, G., Xie, H., and Xu, X.: Marine carbonyl sulfide
45 (OCS) and carbon disulfide (CS₂): a compilation of measurements in seawater and the marine
46 boundary layer, *Earth Syst. Sci. Data*, 12, 591–609, <https://doi.org/10.5194/essd-12-591-2020>,
47 2020.
48
49 Levelt, P. F., van den Oord, G. H. J., Dobber, M. R., Malkki, A., Huib, V., Johan de, V.,
50 Stammes, P., Lundell, J. O. V., and Saari, H.: The ozone monitoring instrument, *IEEE T.*
51 *Geosci. Remote Sens.*, 44, 1093–1101, <https://doi.org/10.1109/tgrs.2006.872333>, 2006.

1
2 Li, Z., Lau, W.K., Ramanathan, V., Wu, G., Ding, Y., Manoj, M.G., Liu, J., Qian, Y., Li, J.,
3 Zhou, T., Fan., J., Rosenfeld, D., Ming, Y., Wang, Y., Huang, J., Wang, B., Xu, X., Lee, S.-S.,
4 Cribb, M., Zhang, F., Yang, X., Zhao, C., Takemura, T., Wang, K., Xia, X., Yin, Y., Zhang,
5 H., Guo, J., Zhao, P., Sugimoto, N., Babu, S. S., and Brasseur, G. P.: Aerosol and monsoon
6 climate interactions over Asia, *Rev. Geophys.*, 54, 866–929, 2016.
7
8 Li, M., Zhang, Q., Kurokawa, J.-I., Woo, J.-H., He, K., Lu, Z., Ohara, T., Song, Y., Streets, D.
9 G., Carmichael, G. R., Cheng, Y., Hong, C., Huo, H., Jiang, X., Kang, S., Liu, F., Su, H., and
10 Zheng, B.: MIX: a mosaic Asian anthropogenic emission inventory under the international
11 collaboration framework of the MICS-Asia and HTAP, *Atmos. Chem. Phys.*, 17, 935–963,
12 <https://doi.org/10.5194/acp-17-935-2017>, 2017.
13
14 Li, T., Wang, B., Chang, C.P., and Y. Zhang: A theory for the Indian Ocean dipole–zonal
15 mode. *J. Atmos. Sci.*, 60(17):2119–2135, 2003.
16
17 Li, Y., Han W., A. Hu, G. A. Meehl, and F. Wang: Multidecadal changes of the upper Indian
18 Ocean heat content during 1965–2016. *J. Climate*, 31, 7863–7884,
19 <https://doi.org/10.1175/JCLI-D-18-0116.1>, 2018.
20
21 Liang, Q., Stolarski, R. S., Kawa, S. R., Nielsen, J. E., Douglass, A.R., Rodriguez, J. M., Blake,
22 D. R., Atlas, E. L., and Ott, L. E.: Finding the missing stratospheric Br_y: a global modeling
23 study of CHBr₃ and CH₂Br₂, *Atmos. Chem. Phys.*, 10, 2269–2286, [https://doi.org/10.5194/acp-](https://doi.org/10.5194/acp-10-2269-2010)
24 [10-2269-2010](https://doi.org/10.5194/acp-10-2269-2010), 2010.
25
26 [Liu, S.C.,McFarland, M., Kley, D., Zafiriou, O., Huebert, B.: Tropospheric NO_x and O₃ budgets](#)
27 [in the equatorial Pacific. *Journal of Geophysical Research* 88, 1360e1368, 1983.](#)
28
29 Liu, X., Bhartia, P. K., Chance, K., Spurr, R. J. D., and Kurosu, T. P.: Ozone profile retrievals
30 from the Ozone Monitoring Instrument, *Atmos. Chem. Phys.*, 10, 2521–2537,
31 <https://doi.org/10.5194/acp-10-2521-2010>, 2010.
32
33 Llovel, W. and Lee, T.: Importance and origin of halosteric contribution to sea level change in
34 the southeast Indian Ocean during 2005–2013. *Geophys. Res. Lett.*, 42, 1148–1157, 2015.
35
36 [Löscher, C. R.: Reviews and syntheses: Trends in primary production in the Bay of Bengal – is](#)
37 [it at a tipping point?, *Biogeosciences*, 18, 4953–4963, \[https://doi.org/10.5194/bg-18-4953-\]\(https://doi.org/10.5194/bg-18-4953-2021\)](#)
38 [2021, 2021.](#)
39
40 Lombardozzi, D, Levis, S, Bonan, G, Hess, P. G. and Sparks, J. P.: The influence of chronic
41 ozone exposure on global carbon and water cycles. *J. Climate*, 28: 292–305. DOI:
42 10.1175/JCLI-D-14-00223.1, 2015.
43
44 Lunt, M. F., Palmer, P. I., Feng, L., Taylor, C. M., Boesch, H., and Parker, R. J.: An increase
45 in methane emissions from tropical Africa between 2010 and 2016 inferred from satellite data,
46 *Atmos. Chem. Phys.*, 19, 14721–14740, <https://doi.org/10.5194/acp-19-14721-2019>, 2019.
47
48 Luo, G. and Yu, F.: A numerical evaluation of global oceanic emissions of a-pinene and
49 isoprene, *Atmos. Chem. Phys.*, 10, 2007–2015, doi:10.5194/acp-10-2007-2010, 2010.
50

1 Ma, X., Bange, H. W., Eirund, G. K., and Arévalo-Martínez, D. L.: Nitrous oxide and
2 hydroxylamine measurements in the Southwest Indian Ocean. *J. Marine Syst.*,
3 <https://doi.org/10.1016/j.jmarsys.2018.03.003>, 2018.
4
5 Maas, J., Jia, Y., Quack, B., Durgadoo, J. V., Biastoch, A., and Tegtmeier, S.: Simulations of
6 anthropogenic bromoform indicate high emissions at the coast of East Asia, *Atmos. Chem.*
7 *Phys. Discuss.*, 2020, 1-31, 10.5194/acp-2019-1004, 2020.
8
9 [Maas, J., Tegtmeier, S., Jia, Y., Quack, B., Durgadoo, J. V., and Biastoch, A.: Simulations of](https://doi.org/10.5194/acp-21-4103-2021)
10 [anthropogenic bromoform indicate high emissions at the coast of East Asia, *Atmos. Chem.*](https://doi.org/10.5194/acp-21-4103-2021)
11 [Phys., 21, 4103–4121, https://doi.org/10.5194/acp-21-4103-2021, 2021.](https://doi.org/10.5194/acp-21-4103-2021)
12
13 Madden, R.A. and P.R. Julian: Description of Global-Scale Circulation Cells in the Tropics
14 with a 40–50 Day Period. *J. Atmos. Sci.*, 29, 1109–1123, <https://doi.org/10.1175/1520->
15 [0469\(1972\)029<1109:DOGSCC>2.0.CO;2](https://doi.org/10.1175/1520-0469(1972)029<1109:DOGSCC>2.0.CO;2), 1972.
16
17 Mahajan, A. S., Plane, J. M. C., Oetjen, H., Mendes, L., Saunders, R. W., Saiz-Lopez, A., Jones,
18 C. E., Carpenter, L. J., and McFiggans, G. B.: Measurement and modelling of tropospheric
19 reactive halogen species over the tropical Atlantic Ocean, *Atmos. Chem. Phys.*, 10, 4611–4624,
20 <https://doi.org/10.5194/acp-10-4611-2010>, 2010.
21
22 Mahajan, A. S., Tinel, L., Hulswar, S., Cuevas, C. A., Wang, S., Ghude, S., et al.: Observations
23 of iodine oxide in the Indian Ocean Marine Boundary Layer: a transect from the tropics to the
24 high latitudes, *Atmos. Environ.: X*. <https://doi.org/10.1016/j.aeaoa.2019.100016>, 2019a.
25
26 Mahajan, A. S., Tinel, L., Sarkar, A., Chance, R., Carpenter, L. J., Hulswar, S., et al.:
27 Understanding Iodine Chemistry over the Northern and Equatorial Indian Ocean. *J. Geophys.*
28 *Res.*, (x), 0–3. <https://doi.org/10.1029/2018JD029063>, 2019b.
29
30 Mahajan, A.S., De Smedt, I., Biswas, M.S., Ghude, S.D., Fadnavis, S., Roy, C., van
31 Roozendaal, M.: Inter-annual variations in satellite observations of nitrogen dioxide and
32 formaldehyde over India. *Atmos. Environ.* 116, 194–201.
33 <https://doi.org/10.1016/j.atmosenv.2015.06.004>, 2015a.
34
35 Mahajan, A. S., Fadnavis, S., Thomas, M. A., Pozzoli, L., Gupta, S., Royer, S., et al.:
36 Quantifying the impacts of an updated global dimethyl sulfide climatology on cloud
37 microphysics and aerosol radiative forcing. *J. Geophys. Res.*, 120, 1–13.
38 <https://doi.org/10.1002/2014JD022687>, 2015b.
39
40 Mahowald, N. M., Hamilton, D. S., Mackey, K.R.M., Moore, J. K., Baker, A. R., Scanza, R. A.,
41 and Zhang, Y.: Aerosol trace metal leaching and impacts on marine microorganisms. *Nat.*
42 *Commun.*, 9, 2614, <https://doi.org/10.1038/s41467-018-04970-7>, 2018.
43
44 Mallik, C., Lal, S., Venkataramani, S., Naja, M., and Ojha, N.: Variability in ozone and its
45 precursors over the Bay of Bengal during post-monsoon: Transport and emission effects. *J.*
46 *Geophys. Res.*, <https://doi.org/10.1002/jgrd.50764>, 2013.
47
48 Mandal, T. K., Khan, A., Ahammed, Y. N., Tanwar, R. S., Parmar, R. S., Zalpuri, K. S., et al.:
49 Observations of trace gases and aerosols over the Indian Ocean during the monsoon transition
50 period. *J. Earth Syst. Sci.*, 115(4), 473–484, 2006.
51

1 Manö, S., and Andreae, M. O.: Emission of Methyl Bromide from Biomass Burning, *Science*,
2 263, 1255-1257, 10.1126/science.263.5151.1255, 1994.
3
4 [Marbach, T., Beirle, S., Platt, U., Hoor, P., Wittrock, F., Richter, A., Vrekoussis, M.,](#)
5 [Grzegorski, M., Burrows, J. P., and Wagner, T.: Satellite measurements of formaldehyde linked](#)
6 [to shipping emissions, *Atmos. Chem. Phys.*, 9, 8223–8234, \[https://doi.org/10.5194/acp-9-8223-\]\(https://doi.org/10.5194/acp-9-8223-2009\)](#)
7 [2009, 2009.](#)
8
9 Martino, M., Mills, G. P., Woeltjen, J., and Liss, P. S.: A new source of volatile organoiodine
10 compounds in surface seawater, *Geophys. Res. Lett.*, 36, L01609, doi:10.1029/2008GL036334,
11 2009.
12
13 Mason, R. P., and Sheu, G.-R.: Role of the ocean in the global mercury cycle, *Global*
14 *Biogeochem. Cy.*, 16, 40-41-40-14, 10.1029/2001gb001440, 2002.
15
16 Matthews, A. J., Singhruck, P. and Heywood, K. J.: Ocean temperature and salinity components
17 of the Madden–Julian oscillation observed by Argo floats. *Clim. Dynam.*, 35, 1149–1168,
18 <https://doi.org/10.1007/s00382-009-0631-7>, 2010.
19
20 Meehl, G. A., and J. M. Arblaster: Mechanisms for projected future changes in South Asian
21 monsoon precipitation. *Clim. Dynam.*, 21, 659–675, [https://doi.org/10.1007/s00382-003-0343-](https://doi.org/10.1007/s00382-003-0343-3)
22 [3](#), 2003.
23
24 Meenu, S., Rajeev, K., Parameswaran, K., and Suresh Raju, C., Characteristics of the double
25 intertropical convergence zone over the tropical Indian Ocean, *J. Geophys. Res.*, 112, D11106,
26 doi:10.1029/2006JD007950, 2007.
27
28 Mehlmann, M., Quack, B., Atlas, E., Hepach, H., and Tegtmeier, S.: Natural and anthropogenic
29 sources of bromoform and dibromomethane in the oceanographic and biogeochemical regime
30 of the subtropical North East Atlantic, *Environ. Sci. Process. Impacts*, 22, 679-707,
31 10.1039/c9em00599d, 2020.
32
33 Metzl, N.: Decadal increase of oceanic carbon dioxide in Southern Indian Ocean surface waters
34 (1991–2007), *Deep Sea Res. Part II: Topical Studies in Oceanogr.*, 56, 607-619,
35 <https://doi.org/10.1016/j.dsr2.2008.12.007>, 2009.
36
37 Mihalopoulos, N., Putaud, J. P., Nguyen, B. C., and Belviso, S.: Annual variation of
38 atmospheric carbonyl sulfide in the marine atmosphere in the Southern Indian Ocean, *J. Atmos.*
39 *Chem.*, 13, 73–82, <https://doi.org/10.1007/bf00048101>, 1991.
40
41 Mittermeier, R. A., Turner, W. R., Larsen, F. W., Brooks, T. M., Gascon, C.: Global
42 biodiversity conservation: the critical role of hotspots. *Biodiversity hotspots*, Berlin,
43 Heidelberg: Springer. pp. 3–22. doi:10.1007/978-3-642-20992-5, 2011.
44
45 Mohan, S. and Bhaskaran, P.K.: Evaluation of CMIP5 climate model projections for surface
46 wind speed over the Indian Ocean region. *Clim. Dynam.*, 53(9-10), 5415–5435, 2019.
47
48 Monks, P. S., Carpenter, L. J., Penkett, S. A., Ayers, G. P., Gillett, R. W., Galbally, I. E., and
49 Meyer, C. P.: Fundamental ozone photochemistry in the remote marine boundary layer: The
50 SOAPEX experiment, measurement and theory. *Atmos. Environ.*, 32(21), 3647-3664, 1998.
51

1 Monks, PS, Archibald, AT, Colette, A, Cooper, O, Coyle, M, Derwent, R, Fowler, D, Granier,
2 C, Law, KS, Mills, GE, Stevenson, DS, Tarasova, O, Thouret, V, von Schneidmesser, E,
3 Sommariva, R, Wild, O and Williams, ML.: Tropospheric ozone and its precursors from the
4 urban to the global scale from air quality to short-lived climate forcer. *Atmos. Chem. Phys.* 15:
5 8889–8973. DOI: 10.5194/acp-15-8889-2015, 2015.
6
7 Moorthy, K. K., Satheesh, S. K., Babu, S. S., and Dutt, C. B. S.: Integrated Campaign for
8 Aerosols, gases and Radiation Budget (ICARB): An overview, *J. Earth Syst. Sci.*, 117, 243-
9 262, 10.1007/s12040-008-0029-7, 2008.
10
11 Mungall, E. L., J. P. D. Abbatt, J. J. B. Wentzell, A. K. Y. Lee, J. L. Thomas, M. Blais, M.
12 Gosselin, L. A. Miller, T. Papakyriakou, M. D. Willis, and J. Liggio: OVOCs in the
13 summertime marine Arctic atmosphere, *Proceedings of the National Academy of Sciences*, 114
14 (24) 6203-6208; DOI: 10.1073/pnas.1620571114, 2017.
15
16 Myhre, G., D. Shindell, F.-M. Bréon, W. Collins, J. Fuglestedt, J. Huang, D. Koch, J.-F.
17 Lamarque, D. Lee, B. Mendoza, T. Nakajima, A. Robock, G. Stephens, T. Takemura and H.
18 Zhang: Anthropogenic and Natural Radiative Forcing. In: *Climate Change 2013: The Physical*
19 *Science Basis. Contribution of Working Group I to the Fifth Assessment Report of the*
20 *Intergovernmental Panel on Climate Change, 2013.*
21
22 Nair, P. R., David, L. M., Girach, I. A., and George, S. K.: Ozone in the marine boundary layer
23 of Bay of Bengal during post-winter period: Spatial pattern and role of meteorology, *Atmos.*
24 *Environ.*, 45, 4671–4681, 2011.
25
26 Naja, M., Chand, D., Sahu, L., and Lal, S.: Trace gases over marine regions around India, *Indian*
27 *J. Mar. Sci.*, 33, 95–106, 2004.
28
29 Nalini, K., Uma, K. N., Sijikumar, S., Tiwari, Y. K., and Ramachandran, R.: Satellite- and
30 ground-based measurements of CO₂ over the Indian region: its seasonal dependencies, spatial
31 variability, and model estimates, *Int. J. Remote Sens.*, 39, 7881-7900,
32 10.1080/01431161.2018.1479787, 2018.
33
34 Naqvi, S. W. A., Jayakumar, D. A., Nair, M., Kumar, M. D., and George, M. D.: Nitrous oxide
35 in the western Bay of Bengal, *Marine Chem.*, 47, 269-278, [https://doi.org/10.1016/0304-](https://doi.org/10.1016/0304-4203(94)90025-6)
36 [4203\(94\)90025-6](https://doi.org/10.1016/0304-4203(94)90025-6), 1994.
37
38 Naqvi, S. W. A., Bange, H. W., Gibb, S. W., Goyet, C., Hatton, A. D., and Upstill-Goddard, R.
39 C.: Biogeochemical ocean-atmosphere transfers in the Arabian Sea, *Progress Oceanogr.* 65,
40 116-144, <https://doi.org/10.1016/j.pocean.2005.03.005>, 2005.
41
42 Naqvi, S. W. A., Jayakumar, D.A., Narvekar, P. V., Naik, H., Sarma, V. V. S. S., D'Souza, W.,
43 Joseph, S., George, M. D.: Marine hypoxia/anoxia as a source of CH₄ and N₂O, *Biogeosciences*
44 7, 2159–2190, 2010a.
45
46 Naqvi, S. W. A., Naik, H., D'Souza, W., Narvekar, P. V., Paropkari, A. L., and Bange, H. W.:
47 Carbon and nitrogen fluxes in the northern Indian Ocean. In: Liu, K.-K., Atkinson, L.,
48 Quiñones, R., Talaue-McManus, L. (Eds.), *Carbon and Nutrient Fluxes in Continental Margins:*
49 *A Global Synthesis.* Springer-Verlag, New York, pp. 180–191, 2010b.
50

- 1 Nayak, R. K., Dadhwal, V. K., Majumdar, A., Patel, N. R., and Dutt, C. B. S.: Variability of
2 atmospheric CO₂ over India and Surrounding Oceans and control by Surface Fluxes, *Int. Arch.*
3 *Photogramm. Remote Sens. Spatial Inf. Sci.*, XXXVIII-8/W20, 96-101, 10.5194/isprsarchives-
4 XXXVIII-8-W20-96-2011, 2011.
- 5
6 Nieves, V., J. K. Willis, and W. C. Patzert: Recent hiatus caused by decadal shift in Indo-Pacific
7 heating. *Science*, 349, 532–535, <https://doi.org/10.1126/science.aaa4521>, 2015.
- 8
9 Norman, M. and Leck, C.: Distribution of marine boundary layer ammonia over the Atlantic
10 and Indian Ocean during the Aerosols 99 cruise, *J. Geophys. Res.*, 110, D16302,
11 doi:10.1029/2005JD005866, 2005.
- 12
13 Nowak, J.B., et al.: Gas-phase chemical characteristics of Asian emission plumes observed
14 during ITCT 2K2 over the eastern North Pacific Ocean, *J. Geophys. Res.* 109, D23S19.
15 doi:10.1029/2003JD004488, 2004.
- 16
17 Oetjen, H.: Measurements of halogen oxides by scattered sunlight differential optical
18 absorption spectroscopy, University of Bremen, 2009.
- 19
20 ~~Ohara, T., Akimoto, H., Kurokawa, J., Horii, N., Yamaji, K., Yan, X., and Hayasaka, T.: An~~
21 ~~Asian emission inventory of anthropogenic emission sources for the period 1980–2020, *Atmos.*~~
22 ~~*Chem. Phys.*, 7, 4419–4444, <https://doi.org/10.5194/acp-7-4419-2007>, 2007.~~
- 23 ~~Ojha, N., Naja, M., Singh, K. P., Sarangi, T., Kumar, R., Lal, S., Lawrence, M. G., Butler, T.~~
24 ~~M., and Chandola, H. C.: Variabilities in ozone at a semi-urban site in the Indo-Gangetic Plain~~
25 ~~region: Association with the meteorology and regional process, *J. Geophys. Res.*, 117, D20301,~~
26 ~~doi:10.1029/2012JD017716, 2012.~~
- 27
28 Pacyna, J. M., Pacyna, E. G.: Anthropogenic sources and global inventory of mercury
29 emissions. In: Parsons, M.B., Percival, J.B. (Eds.), *Mercury: Sources, Measurements, Cycles,*
30 *and Effects. Short Course Series, vol. 32. Mineralogical Association of Canada, 2005.*
- 31
32 Palastanga, V., van Leeuwen, P. J., Schouten, M. W., and de Ruijter, W. P. M.: Flow structure
33 and variability in the subtropical Indian Ocean: Instability of the South Indian Ocean
34 Countercurrent, *J. Geophys. Res.*, 112, C01001, doi:10.1029/2005JC003395, 2007.
- 35
36 Palmer, P. I., and Shaw, S. L.: Quantifying global marine isoprene fluxes using MODIS
37 chlorophyll observations, *Geophys. Res. Lett.*, 32, 10.1029/2005gl022592, 2005.
- 38
39 Pandey, P. C., Khare, N., and Sudhakar, M.: Oceanographic research: Indian efforts and
40 preliminary results from the Southern Ocean, *Current Sci.*, 90, 978-984, 2006.
- 41
42 Pant, V., Deshpande, C. G., and Kamra, A. K.: The concentration and number size distribution
43 measurements of the Marine Boundary Layer aerosols over the Indian Ocean, *Atmos. Res.*, 92,
44 381–393, 2009.
- 45
46 Pathak, H., Li, C., and Wassmann, R.: Greenhouse gas emissions from Indian rice fields:
47 calibration and upscaling using the DNDC model, *Biogeosciences*, 2, 113-123, 10.5194/bg-2-
48 113-2005, 2005.
- 49

1 Paytan, A., K. R. M. Mackey, Y. Chen, I. D. Lima, S. C. Doney, N. Mahowald, R. Labiosa, A.
2 F. Post: Toxicity of atmospheric aerosols on marine phytoplankton, *Proc. Natl. Acad. Sci. USA*,
3 106 (12) 4601-4605; DOI: 10.1073/pnas.0811486106, 2009.
4
5 Peters, G.P., Andrew, R.M., Canadell, J.G. et al.: Carbon dioxide emissions continue to grow
6 amidst slowly emerging climate policies. *Nat. Clim. Chang.* 10, 3–6,
7 <https://doi.org/10.1038/s41558-019-0659-6>, 2020.
8
9 Pfannerstill, E. Y., Wang, N., Edtbauer, A., Bourtsoukidis, E., Crowley, J. N., Dienhart, D.,
10 Eger, P. G., Ernle, L., Fischer, H., Hottmann, B., Paris, J.-D., Stöner, C., Tadic, I., Walter, D.,
11 Lelieveld, J., and Williams, J.: Shipborne measurements of total OH reactivity around the
12 Arabian Peninsula and its role in ozone chemistry, *Atmos. Chem. Phys.*, 19, 11501–11523,
13 <https://doi.org/10.5194/acp-19-11501-2019>, 2019.
14
15 [Phillips, H. E., Tandon, A., Furue, R., Hood, R., Ummenhofer, C., Benthuyzen, J., Menezes,](https://doi.org/10.5194/os-2021-1)
16 [V., Hu, S., Webber, B., Sanchez-Franks, A., Cherian, D., Shroyer, E., Feng, M., Wijeskera, H.,](https://doi.org/10.5194/os-2021-1)
17 [Chatterjee, A., Yu, L., Hermes, J., Murtugudde, R., Tozuka, T., Su, D., Singh, A., Centurioni,](https://doi.org/10.5194/os-2021-1)
18 [L., Prakash, S., and Wiggert, J.: Progress in understanding of Indian Ocean circulation,](https://doi.org/10.5194/os-2021-1)
19 [variability, air-sea exchange and impacts on biogeochemistry, *Ocean Sci. Discuss.* \[preprint\],](https://doi.org/10.5194/os-2021-1)
20 <https://doi.org/10.5194/os-2021-1>, in review, 2021.
21
22 [Pitts, B. J. F., and Pitts, J. N.: Chemistry of the Upper and Lower Atmosphere. Academic Press,](#)
23 [California, 2000](#)
24
25 Portmann, R.W., J.S. Daniel, and A.R. Ravishankara: Stratospheric ozone depletion due to
26 nitrous oxide: influences of other gases. *Philosophical Transactions of the Royal Society*
27 *London B Biological Sciences* 367 (1593): 1256–1264. <https://doi.org/10.1098/rstb.2011.0377>,
28 2012.
29
30 Prasanna Kumar, S., Muraleedharan, P. M., Prasad, T. G., Gauns, M., Ramaiah, N., de Souza,
31 S. N., Sardesai, S., and Madhupratap, M.: Why is the Bay of Bengal less productive during
32 summer monsoon compared to the Arabian Sea? *Geophys. Res. Lett.*, 29(24), 2235,
33 doi:10.1029/2002GL016013, 2002.
34
35 ~~Prather, M., C. Holmes, and J. Hsu: Reactive greenhouse gas scenarios: Systematic exploration~~
36 ~~of uncertainties and the role of atmospheric chemistry. *Geophys. Res. Lett.*, 39, L09803, 2012.~~
37
38 Prather, M. J., Hsu, J., DeLuca, N. M., Jackman, C. H., Oman, L. D., Douglass, A. R., Fleming,
39 E. L., Strahan, S. E., Steenrod, S. D., Søvde, O. A., Isaksen, I. S. A., Froidevaux, L., and Funke,
40 B: Measuring and modeling the lifetime of nitrous oxide including its variability. *J. Geophys.*
41 *Res.*, 120, 5693– 5705. doi: 10.1002/2015JD023267, 2015.
42
43 Quack, B., Atlas, E., Petrick, G., and Wallace, D.: Bromoform and dibromomethane above the
44 Mauritanian upwelling: Atmospheric distributions and oceanic emissions, *J. Geophys.*
45 *Res.*, 112, D09312, doi:10.1029/2006JD007614, 2007.
46
47 Quartly, G. D., J. J. H. Buck, M. A. Srokosz, and A. C. Coward: Eddies around Madagascar—
48 The retroflection reconsidered, *J. Mar. Syst.*, 63(3–4), 115–129,
49 doi:10.1016/j.jmarsys.2006.06.001, 2006.
50

1 Quinn, P. K., Coffman, D. J., Johnson, J. E., Upchurch, L. M., and Bates, T. S.: Small fraction
2 of marine cloud condensation nuclei made up of sea spray aerosol. *Nat. Geosci.*, 10(9), 674–
3 679, 2017.

4

5 Raes, E. J., Bodrossy, L., Van de Kamp, J., Holmes, B., Hardman-Mountford, N., Thompson,
6 P. A., McInnes, A. S., and Waite, A. M.: Reduction of the Powerful Greenhouse Gas N₂O in
7 the South-Eastern Indian Ocean, *PLOS ONE*, 11, e0145996, 10.1371/journal.pone.0145996,
8 2016.

9

10 Rahav, E., Belkin, N., Paytan, A., and Herut, B.: Phytoplankton and Bacterial Response to
11 Desert Dust Deposition in the Coastal Waters of the Southeastern Mediterranean Sea: A Four-
12 Year In Situ Survey. *Atmosphere*, 9, 305, 2018.

13

14 Rajak, R. and Chattopadhyay, A., Short and long-term exposure to ambient air pollution and
15 impact on health in India: a systematic review, *Int. J. Environ. Health Res.*,
16 10.1080/09603123.2019.1612042, 2019.

17

18 Ramanathan, V., Crutzen, P. J., Mitra, A. P., and Sikka, D.: The Indian Ocean Experiment and
19 the Asian Brown Cloud, *Curr. Sci. India*, 83, 947–955, 2002.

20

21 Ramanathan, V., C. Chung, D. Kim, T. Bettge, L. Buja, J. T. Kiehl, W. M. Washington, Q. Fu,
22 D. R. Sikka, M. Wild: Atmospheric brown clouds: Impacts on South Asian climate and
23 hydrological cycle, *Proc. Natl. Acad. Sci. USA*, 102 (15) 5326-5333; DOI:
24 10.1073/pnas.0500656102, 2005.

25

26 Randel, W. J., Park, M., Emmons, L., Kinnison, D., Bernath, P., Walker, K. A., Boone, C., and
27 Pumphrey, H.: Asian monsoon transport of pollution to the stratosphere, *Science*, 328, 611–
28 613, doi:10.1126/science.1182274, 2010.

29

30 ~~Rao, S.A., Dhakate, A.R., Saha, S.K., Mahapatra, S., Chaudhari, H.S., Pokhrel, S., and Sahu,~~
31 ~~S. K.: Why is Indian Ocean warming consistently? *Clim. Change* 110:709–719,~~
32 ~~doi.org/10.1007/s10584-011-0121-x, 2012.~~

33

34 Rao, R. R., and Sivakumar, R.: Seasonal variability of sea surface salinity and salt budget of
35 the mixed layer of the north Indian Ocean, *J. Geophys. Res.*, 108(C1), 3009,
36 doi:10.1029/2001JC000907, 2003.

37

38 Raut, N., B. K. Sitaula, L. R. Bakken, R. M. Bajracharya, and P. Dörsch.: Higher N₂O emission
39 by intensified crop production in South Asia. *Global Ecology and Conservation* 4:176–84.
40 doi:10.1016/j.gecco.2015.06.004, 2015.

41

42 Ravishankara, A., J. S. Daniel, and R. W. Portmann: Nitrous oxide (N₂O): The dominant ozone-
43 depleting substance emitted in the 21st century, *Science*, 326(5949), 123–125,
44 doi:10.1126/science.1176985, 2009.

45

46 Rayman, M. P.: The importance of selenium to human health. *Lancet*, 356, 233–241, 2000.

47

48 Read, K., A. Mahajan, L. Carpenter, M. J. Evans, B. V. E. Faria, D. E. Heard, J. R. Hopkins, J.
49 D. Lee, S. J. Moller, A. C. Lewis, L. Mendes, J. B. McQuaid, H. Oetjen, A. Saiz-Lopez, M. J.
50 Pilling, and J. M. C. Plane: Extensive halogen-mediated ozone destruction over the tropical
51 Atlantic Ocean. *Nature* 453, 1232–1235, <https://doi.org/10.1038/nature07035>, 2008.

1
2 Reppin, J., F. Schott, and J. Fischer: Equatorial currents and transports in the upper central
3 Indian Ocean: Annual cycle and interannual variability, *J. Geophys. Res.*, 104(C7), 15,495 –
4 15,514, 1999.
5
6 Richter, U. and Wallace, D. W. R.: Production of methyl iodide in the tropical Atlantic Ocean,
7 *Geophys. Res. Lett.*, 31(23), 2004.
8
9 Richter, I., and S.P. Xie: Muted precipitation increase in global warming simulations: a surface
10 evaporation perspective. *J. Geophys. Res.*, 113:D24118, doi.org/10.1029/2008J D0105 61,
11 2008.
12
13 Ridderinkhof, H., and W. P. M. de Ruijter: Moored current observations in the Mozambique
14 Channel, *Deep Sea Res. Part II*, 50, 1933–1955, 2003.
15
16 [Rixen, T., Cowie, G., Gaye, B., Goes, J., do Rosário Gomes, H., Hood, R. R., Lachkar, Z., Schmidt,
17 H., Segschneider, J., and Singh, A.: Reviews and syntheses: Present, past, and future of the oxygen
18 minimum zone in the northern Indian Ocean, *Biogeosciences*, 17, 6051–6080,
19 <https://doi.org/10.5194/bg-17-6051-2020>, 2020.](https://doi.org/10.5194/bg-17-6051-2020)
20
21 Rixen, T., Goyet, C., and Ittekkot, V.: Diatoms and their influence on the biologically mediated
22 uptake of atmospheric CO₂ in the Arabian Sea upwelling system, *Biogeosciences*, 3, 1–13,
23 <https://doi.org/10.5194/bg-3-1-2006>, 2006.
24
25 Rodríguez-Ros, P., Cortés, P., Robinson, C. M., Nunes, S., Hassler, C., Royer, S. J., Estrada,
26 M., Sala, M. M. and Simó, R.: Distribution and drivers of marine isoprene concentration across
27 the Southern Ocean, *Atmosphere (Basel)*, 11(6), 1–19, doi:10.3390/atmos11060556, 2020.
28
29 [Roser, M., Ritchie H., and Ortiz-Ospina, E.: World Population Growth, published online at
30 OurWorldInData.org., 2013.](https://www.ourworldindata.org/)
31
32 Roxy, M. K., Raghu Murtugudde, A. M., Valsala, V., Panickal, S., Prasanna Kumar, S.,
33 Ravichandran, M., et al.: A reduction in marine primary productivity driven by rapid warming
34 over the tropical Indian Ocean. *Geophys. Res. Lett.*, 43, 826–833. doi: 10.1002/2015gl066979,
35 2016.
36
37 Roxy M. K., Ritika K., Terray P., Murtugudde R., Ashok K., Goswami B. N.: Drying of Indian
38 subcontinent by rapid Indian Ocean warming and a weakening land-sea thermal gradient, *Nat.*
39 *Commun.*, 6:7423. doi.org/10.1038/ncomm s8423, 2015.
40
41 Roxy, M. K., Ritika, K., Terray, P. and Masson, S.: The curious case of Indian Ocean warming.
42 *J. Clim.* 27, 8501–8509, 2014.
43
44 Roy, R., Pratihary, A., Narvenkar, G., Mochemadkar, S., Gauns, M., and Naqvi, S. W. A.: The
45 relationship between volatile halocarbons and phytoplankton pigments during a
46 *Trichodesmium* bloom in the coastal eastern Arabian Sea, *Estuarine, Coastal and Shelf Science*,
47 95, 110–118, <https://doi.org/10.1016/j.ecss.2011.08.025>, 2011.
48
49 Saha A., Ghosh S., Sahana A. S., and E. P. Rao: Failure of CMIP5 climate models in simulating
50 post-1950 decreasing trend of Indian monsoon, *Geophys. Res. Lett.*, 41:7323–7330.
51 doi.org/10.1002/2014G L0615 73, 2014.

1
2 [Sahu, L. K., Lal, S., and Venkataramani, S.: Seasonality in the latitudinal distributions of](#)
3 [NMHCs over the Bay of Bengal, *Atmos. Env.*, 45, 2356-2366,](#)
4 <https://doi.org/10.1016/j.atmosenv.2011.02.021>, 2011.
5
6 [Sahu, L. K., Lal, S., and Venkataramani, S.: Impact of monsoon circulations on oceanic](#)
7 [emissions of light alkenes over Bay of Bengal, *Global Biogeochem. Cycles*, 24, GB4028,](#)
8 [doi:10.1029/2009GB003766](https://doi.org/10.1029/2009GB003766), 2010.
9
10 Sahu, L.K., Lal, S., and Venkataramani, S.: Distributions of O₃, CO and hydrocarbons over the
11 Bay of Bengal: a study to assess the role of transport from southern India and marine regions
12 during September-October 2002, *Atmos. Environ.*, 40, 4633–4645, 2006.
13
14 Saiz-Lopez, A., Fernandez, R. P., Ordóñez, C., Kinnison, D. E., Gómez Martín, J. C.,
15 Lamarque, J.-F. and Tilmes, S.: Iodine chemistry in the troposphere and its effect on ozone,
16 *Atmos. Chem. Phys.*, 14(23), 13119–13143, doi:10.5194/acp-14-13119-2014, 2014.
17
18 Saiz-Lopez, A., Baidar, S., Cuevas, C. A., Koenig, T. K., Fernandez, R. P., Dix, B., Kinnison,
19 D. E., Lamarque, J., Rodriguez-Lloveras, X., Campos, T. L. and Volkamer, R.: Injection of
20 iodine to the stratosphere, *Geophys. Res. Lett.*, 42, 6852–6859, doi:10.1002/2015GL064796,
21 2015.
22
23 Saji, N. H., Goswami, B. N., Vinayachandran, P. N., and Yamagata, T.: A dipole mode in the
24 tropical Indian Ocean, *Nature*, volume 401, 360–363, 1999.
25
26 Sánchez-Pérez, E. D., Marín, I., Nunes, S., Fernández-González, L., Peters, F., Pujo-Pay, M.,
27 Conan, P., Marrasé, C.: Aerosol inputs affect the optical signatures of dissolved organic matter
28 in NW Mediterranean coastal waters, *Scientia Marina* 80(4), 437-446,
29 <https://doi.org/10.3989/scimar.04318.20B>, 2016.
30
31 Sardesai, S., Ramaiah, N., Prasanna Kumar, S. and de Sousa, S. N.: Influence of environmental
32 forcings on the seasonality of dissolved oxygen and nutrients in the Bay of Bengal, *J. Marine*
33 *Res.*, 65, 301–316, 2007.
34
35 [Sarma, V. V. S. S., Swathi, P. S., Kumar, M. D., Prasannakumar, S., Bhattathiri, P. M. A.,](#)
36 [Madhupratap, M., Ramaswamy, V., Sarin, M. M., Gauns, M., Ramaiah, N., Sardesai, S., and](#)
37 [de Sousa, S. N.: Carbon budget in the Eastern and Central Arabian Sea: an Indian JGOFS](#)
38 [synthesis, *Global Biogeochem. Cy.*, 17, 1102, doi:10.1029/2002GB001978](#), 2003.
39
40 Sarma, V. V. S. S., Kumar, N. A., Prasad, V. R., Venkataramana, V., Appalanaidu, S., Sridevi,
41 B., Kumar, B. S. K., Bharati, M. D., Subbaiah, C. V., Acharyya, T., Rao, G. D., Viswanadham,
42 R., Gawade, L., Manjary, D. T., Kumar, P. P., Rajeev, K., Reddy, N. P. C., Sarma, V. V.,
43 Kumar, M. D., Sadharam, Y., and Murty, T. V. R.: High CO₂ emissions from the tropical
44 Godavari estuary (India) associated with monsoon river discharges, *Geophys. Res. Lett.*, 38,
45 10.1029/2011gl046928, 2011.
46
47 [Sarma, V. V. S. S., Lenton, A., Law, R. M., Metzl, N., Patra, P. K., Doney, S., Lima, I. D.,](#)
48 [Dlugokencky, E., Ramonet, M., and Valsala, V., \(2013\), Sea-air CO₂ fluxes in the Indian Ocean](#)
49 [between 1990 and 2009, \(2013\): *Biogeosciences*, 10, 7035-7052, doi:10.5194/bg-10-7035-](#)
50 [2013.](#)
51

1 Sarma, V. V. S. S., Swathi, P. S., Kumar, M. D., Prasannakumar, S., Bhattathiri, P. M. A.,
2 Madhupratap, M., Ramaswamy, V., Sarin, M. M., Gauns, M., Ramaiah, N., Sardesai, S., and
3 de Sousa, S. N.: Carbon budget in the Eastern and Central Arabian Sea: an Indian JGOFS
4 synthesis, *Global Biogeochem. Cy.*, 17, 1102, doi:10.1029/2002GB001978, 2003.
5
6 Saunois, M., Bousquet, P., Poulter, B., Pregon, A., Ciais, P., Canadell, J. G., Dlugokencky, E.
7 J., Etiope, G., Bastviken, D., Houweling, S., Janssens-Maenhout, G., Tubiello, F. N., Castaldi,
8 S., Jackson, R. B., Alexe, M., Arora, V. K., Beerling, D. J., Bergamaschi, P., Blake, D. R.,
9 Brailsford, G., Brovkin, V., Bruhwiler, L., Crevoisier, C., Crill, P., Covey, K., Curry, C.,
10 Frankenberg, C., Gedney, N., Höglund-Isaksson, L., Ishizawa, M., Ito, A., Joos, F., Kim, H. S.,
11 Kleinen, T., Krummel, P., Lamarque, J. F., Langenfelds, R., Locatelli, R., Machida, T.,
12 Maksyutov, S., McDonald, K. C., Marshall, J., Melton, J. R., Morino, I., Naik, V., O'Doherty,
13 S., Parmentier, F. J. W., Patra, P. K., Peng, C., Peng, S., Peters, G. P., Pison, I., Prigent, C.,
14 Prinn, R., Ramonet, M., Riley, W. J., Saito, M., Santini, M., Schroeder, R., Simpson, I. J.,
15 Spahni, R., Steele, P., Takizawa, A., Thornton, B. F., Tian, H., Tohjima, Y., Viovy, N.,
16 Voulgarakis, A., van Weele, M., van der Werf, G. R., Weiss, R., Wiedinmyer, C., Wilton, D.
17 J., Wiltshire, A., Worthy, D., Wunch, D., Xu, X., Yoshida, Y., Zhang, B., Zhang, Z., and Zhu,
18 Q.: The global methane budget 2000–2012, *Earth Syst. Sci. Data*, 8, 697-751, 10.5194/essd-8-
19 697-2016, 2016.
20
21 Savoie, D.L., and Prospero, J.M.: Comparison of oceanic and continental sources of non-sea-
22 salt sulphate over the Pacific Ocean, *Nature*, 339, 685–687, 1989.
23
24 Sciare, J., Mihalopoulos, N., Dentener, F. J., and Sciare, L.: Interannual variability of
25 atmospheric dimethylsulfide in the southern Indian Ocean. *J. Geophys. Res.*, 105(D21), 26369–
26 26377, 2000.
27
28 Schott, F., and J. P. McCreary, The monsoon circulation of the Indian Ocean, *Prog. Oceanogr.*,
29 51, 1– 123, 2001.
30
31 Schott, F. A., Xie, S.-P., and McCreary, J. P., Indian Ocean circulation and climate variability,
32 *Rev. Geophys.*, 47, RG1002, doi:10.1029/2007RG000245, 2009.
33
34 Schouten, M. W., W. P. M. de Ruijter, P. J. van Leeuwen, and H. Ridderinkhof: Eddies and
35 variability in the Mozambique Channel, *Deep Sea Res. Part II*, 50, 1987–2003, 2003.
36
37 Seinfeld, J. H., and S. N. Pandis: *Atmospheric Chemistry and Physics: From Air Pollution to*
38 *Climate Change*, 2nd ed., John Wiley&Sons, 2006.
39
40 Selin, N. E., Jacob, D. J., Park, R. J., Yantosca, R. M., Strode, S., Jaeglé, L., and Jaffe, D.:
41 Chemical cycling and deposition of atmospheric mercury: Global constraints from
42 observations, *J. Geophys. Res.*, 112, D02308, doi:10.1029/2006JD007450, 2007.
43
44 Sharma, S. K., Singh, A. K., Saud, T., Mandal, T. K., Saxena, M., Singh, S., et al.: Measurement
45 of ambient NH₃ over Bay of Bengal during W-ICARB campaign. *Annales Geophysicae*, 30(2),
46 371–377, <https://doi.org/10.5194/angeo-30-371-2012>, 2012.
47
48 Shaw, S. L., Chisholm, S. W., and Prinn, R. G.: Isoprene production by *Prochlorococcus*, a
49 marine cyanobacterium, and other phytoplankton, *Mar. Chem.*, 80, 227–245,
50 doi:10.1016/S0304-4203(02)00101-9, 2003.
51

1 Shechner, M. and Tas, E.: Ozone Formation Induced by the Impact of Reactive Bromine and
2 Iodine Species on Photochemistry in a Polluted Marine Environment, *Environ. Sci. Technol.*,
3 51, 24, 14030–14037, <https://doi.org/10.1021/acs.est.7b02860>, 2017.
4
5 Siedler, G., M. Rouault, and J. R. E. Lutjeharms: Structure and origin of the subtropical South
6 Indian Ocean Countercurrent, *Geophys. Res. Lett.*, 33, L24609, doi:10.1029/2006GL027399,
7 2006.
8
9 Singh, A., Ramesh, R.: Environmental controls on new and primary production in the northern
10 Indian ocean. *Prog. Oceanogr.* 131, 138–145, 2015.
11
12 Singh D., Ghosh S., Roxy M. K., and McDermid, S.: Indian summer monsoon: extreme events,
13 historical changes, and role of anthropogenic forcings. *Wiley Interdisc. Rev. Clim. Change*,
14 doi.org/10.1002/wcc.571, 2019a.
15
16 [Singh, H.B., Kanakidou, M., Crutzen, P.J., Jacob, D.J.: High concentrations and
17 photochemical fate of oxygenated hydrocarbons in the global troposphere, *Nature*, 378, 50–
18 54, 1995.](#)
19
20 Singh, K., Panda, J., and Kant, S.: A study on variability in rainfall over India contributed by
21 cyclonic disturbances in warming climate scenario, *Int. J. Climatology*, doi: 10.1002/joc.6392,
22 2019b.
23
24 Singh, K., Panda, J., Osuri, K.K. and Vissa, N.K.: Progress in tropical cyclone predictability
25 and present status in the North Indian Ocean region. In: Lupo, A.R. (Ed.) *Tropical Cyclone
26 Dynamics, Prediction, and Detection*. London: Intech Open, <https://doi.org/10.5772/64333>,
27 2016.
28
29 Simpson, M. D. and Raman, S.: Role of the land plume in the transport of ozone over the ocean
30 during INDOEX (1999), *Bound. Lay. Meteorol.*, 111, 133–152, 2004.
31
32 Sprovieri, F., Pirrone, N., Bencardino, M., D'Amore, F., Carbone, F., Cinnirella, S., Mannarino,
33 V., Landis, M., Ebinghaus, R., Weigelt, A., Brunke, E.-G., Labuschagne, C., Martin, L.,
34 Munthe, J., Wängberg, I., Artaxo, P., Morais, F., Barbosa, H. D. M. J., Brito, J., Cairns, W.,
35 Barbante, C., Diéguez, M. D. C., Garcia, P. E., Dommergue, A., Angot, H., Magand, O., Skov,
36 H., Horvat, M., Kotnik, J., Read, K. A., Neves, L. M., Gawlik, B. M., Sena, F., Mashyanov, N.,
37 Obolkin, V., Wip, D., Feng, X. B., Zhang, H., Fu, X., Ramachandran, R., Cossa, D., Knoery,
38 J., Maruszak, N., Nerentorp, M., and Norstrom, C.: Atmospheric mercury concentrations
39 observed at ground-based monitoring sites globally distributed in the framework of the GMOS
40 network, *Atmos. Chem. Phys.*, 16, 11915–11935, <https://doi.org/10.5194/acp-16-11915-2016>,
41 2016.
42
43 [Sreeush M. G., R. Saran, V. Valsala, S. Pentakota, K.V. S.R. Prasad, R. Murtugudde \(2019\):
44 Variability, trend and controlling factors of Ocean acidification over Western Arabian Sea
45 upwelling region, *Marine Chemistry*, doi/10.1016/j.marchem.2018.12.002.](#)
46
47 Srivastava, S., Lal, S., Venkataramani, S., Gupta, S., and Acharya, Y. B.: Vertical distribution
48 of ozone in the lower troposphere over the Bay of Bengal and the Arabian Sea during ICARB-
49 2006: Effects of continental outflow, *J. Geophys. Res.*, 116, D13301,
50 doi:10.1029/2010JD015298, 2011.
51

1 Srivastava, S., Lal, S., Venkataramani, S., Gupta, S., and Sheel, V.: Surface distributions of O₃,
2 CO and hydrocarbons over the Bay of Bengal and the Arabian Sea during pre-monsoon season,
3 Atmospheric Environment, 47, 459-467, <https://doi.org/10.1016/j.atmosenv.2011.10.023>,
4 2012a.
5
6 Srivastava, S. Lal, S. Venkataramani, S., Guha, I., and Bala Subrahmanyam, D.: Airborne
7 measurements of O₃, CO, CH₄ and NMHCs over the Bay of Bengal during winter, Atmos.
8 Environ., 59, 2012, 597-609, <https://doi.org/10.1016/j.atmosenv.2012.04.054>, 2012b.
9
10 Stemmler, I., Hense, I., and Quack, B.: Marine sources of bromoform in the global open ocean
11 – global patterns and emissions, Biogeosciences, 12, 1967–1981, [https://doi.org/10.5194/bg-](https://doi.org/10.5194/bg-12-1967-2015)
12 12-1967-2015, 2015.
13
14 Streets, D. G., Hao, J., Wu, Y., Jiang, J., Chan, M., Tian, H., and Feng, X.: Anthropogenic
15 mercury emissions in China, Atmos. Environ., 39, 7789-7806,
16 <https://doi.org/10.1016/j.atmosenv.2005.08.029>, 2005.
17
18 Stuecker, M. F., Timmermann, A., Jin, F. F., Chikamoto, Y., Zhang, W., Wittenberg, A. T.,
19 Widiastih, E., and Zhao, S., Revisiting ENSO/Indian Ocean Dipole phase relationships.
20 Geophys. Res. Lett., 44, 2481–2492. <https://doi.org/10.1002/2016GL072308>, 2017.
21
22 Sudheesh, V., Gupta, G. V. M., Sudharma, K. V., Naik, H., Shenoy, D. M., Sudhakar, M., and
23 Naqvi, S. W. A.: Upwelling intensity modulates N₂O concentrations over the western Indian
24 shelf, J. Geophys. Res., 121, 8551-8565, 10.1002/2016jc012166, 2016.
25
26 Suntharalingam, P., Kettle, A. J., Montzka, S. M., and Jacob, D. J.: Global 3-D model analysis
27 of the seasonal cycle of atmospheric carbonyl sulfide: Implications for terrestrial vegetation
28 uptake, Geophys. Res. Lett., 35, 10.1029/2008gl034332, 2008.
29
30 Suntharalingam, P., Zamora, L. M., Bange, H. W., Bikkina, S., Buitenhuis, E., Kanakidou, M.,
31 Lamarque, J.-F., Landolfi, A., Resplandy, L., Sarin, M. M., Seitzinger, S., and Singh, A.:
32 Anthropogenic nitrogen inputs and impacts on oceanic N₂O fluxes in the northern Indian
33 Ocean: The need for an integrated observation and modelling approach, Deep Sea Research
34 Part II: Topical Studies in Oceanogr., 166, 104-113, <https://doi.org/10.1016/j.dsr2.2019.03.007>,
35 2019.
36
37 Surratt, J. D., Chan, A. W. H., Eddingsaas, N. C., Chan, M., Loza, C. L., Kwan, A. J., Hersey,
38 S. P., Flagan, R. C., Wennberg, P. O., and Seinfeld, J. H.: Reactive intermediates revealed in
39 secondary organic aerosol formation from isoprene, Proc. Natl. Acad. Sci., 107, 6640-6645,
40 10.1073/pnas.0911114107, 2010.
41
42 ~~Swapna P., Krishnan R., and Wallace J.: Indian ocean and monsoon coupled interactions in a~~
43 ~~warming environment, Clim. Dynam., 42 (2014), pp. 2439-2454, 2014.~~
44
45 Tadic, I., Crowley, J. N., Dienhart, D., Eger, P., Harder, H., Hottmann, B., Martinez, M.,
46 Parchatka, U., Paris, J.-D., Pozzer, A., Rohloff, R., Schuladen, J., Shenolikar, J., Tauer, S.,
47 Lelieveld, J., and Fischer, H.: Net ozone production and its relationship to NO_x and VOCs in
48 the marine boundary layer around the Arabian Peninsula, Atmos. Chem. Phys. Discuss.,
49 <https://doi.org/10.5194/acp-2019-1031>, in review, 2019.
50

1 Tegtmeier, S., Krüger, K., Quack, B., Atlas, E. L., Pisso, I., Stohl, A., and Yang, X.: Emission
2 and transport of bromocarbons: from the West Pacific ocean into the stratosphere, *Atmos.*
3 *Chem. Phys.*, 12, 10633–10648, <https://doi.org/10.5194/acp-12-10633-2012>, 2012.
4
5 Tegtmeier, S., Atlas, E., Quack, B., Ziska, F., and Krüger, K.: Variability and past long-term
6 changes of brominated very short-lived substances at the tropical tropopause, *Atmos. Chem.*
7 *Phys.*, 20, 7103–7123, <https://doi.org/10.5194/acp-20-7103-2020>, 2020.
8
9 Tian, H., et al., Global methane and nitrous oxide emissions from terrestrial ecosystems due to
10 multiple environmental changes. *Ecosyst. Health*, 1(1):4. [http://dx.doi.org/10.1890/EHS14-](http://dx.doi.org/10.1890/EHS14-0015.1)
11 [0015.1](http://dx.doi.org/10.1890/EHS14-0015.1), 2015.
12
13 Toihir, Abdoulwahab M. et al. Studies on CO variation and trends over South Africa and the
14 Indian Ocean using TES satellite data. *S. Afr. j. sci*, 111, 9-10, 01-09,
15 <http://dx.doi.org/10.17159/SAJS.2015/20140174>, 2015.
16
17 Tomsche, L., Pozzer, A., Ojha, N., Parchatka, U., Lelieveld, J., and Fischer, H.: Upper
18 tropospheric CH₄ and CO affected by the South Asian summer monsoon during the Oxidation
19 Mechanism Observations mission, *Atmos. Chem. Phys.*, 19, 1915–1939,
20 <https://doi.org/10.5194/acp-19-1915-2019>, 2019.
21
22 Tokarczyk, R. and Moore, R. M.: Production of volatile organohalo- gens by phytoplankton
23 cultures, *Geophys. Res. Lett.*, 21, 285– 288, <https://doi.org/10.1029/94GL00009>, 1994.
24
25 Tournadre, J.: Anthropogenic pressure on the open ocean: The growth of ship traffic revealed
26 by altimeter data analysis, *Geophys. Res. Lett.*, 41, 7924-7932, [10.1002/2014gl061786](https://doi.org/10.1002/2014gl061786), 2014.
27
28 Tripathi, N., Sahu, L. K., Singh, A., Yadav, R. and Karati, K. K.: High Levels of Isoprene in
29 the Marine Boundary Layer of the Arabian Sea during Spring Inter-Monsoon: Role of
30 Phytoplankton Blooms, *ACS Earth Sp. Chem.*, 4(4), 583–590,
31 [doi:10.1021/acsearthspacechem.9b00325](https://doi.org/10.1021/acsearthspacechem.9b00325), 2020.
32
33 [Tripathi, N., Sahu, L. K., Singh, A., Yadav, R., Patel, A., Patel, K., Patel, A., and Patel, K.:
34 Elevated levels of biogenic nonmethane hydrocarbons in the marine boundary layer of the
35 Arabian Sea during the intermonsoon, *J. Geophys. Res.: Atmos.*, 124, e2020JD032869.
36 <https://doi.org/10.1029/2020JD032869>, 2020.
37
38 UN-Environment, 2019. Global Mercury Assessment 2018. UN-Environment Programme,
39 Chemicals and Health Branch, Geneva, Switzerland. 59 pp., 2019.
40
41 \[Valsala, V., S. Maksyutov, \\(2013\\), Interannual variability of the air–sea CO₂ flux in the north
42 Indian Ocean, *Ocean Dynamics*, DOI:10.1007/s10236-012-0588-7, 1-14.
43
44 \\[Valsala, V., S. Maksyutov, and R. G. Murtugudde, \\\(2012\\\), A window for car-
45 bon uptake in the southern subtropical Indian Ocean, *Geophys. Res. Lett.*, doi:10.1029/2012GL052857.
46
47 \\\[Valsala, V., and R. Murtugudde, \\\\(2015\\\\), Mesoscale and Intraseasonal Air-Sea CO₂ C₂
48 Exchanges in the Western Arabian Sea during Boreal Summer, *Deep Sea Research-I*,
49 \\\\[doi:10.1016/j.dsr.2015.06.001\\\\]\\\\(https://doi.org/10.1016/j.dsr.2015.06.001\\\\).
50\\\]\\\(https://doi.org/10.1016/j.dsr.2015.06.001\\\)\\]\\(https://doi.org/10.1029/2012GL052857\\)\]\(https://doi.org/10.1007/s10236-012-0588-7\)](https://doi.org/10.1029/2020JD032869)

1 [Valsala, V., M. G. Sreeush, and K. Chakraborty, \(2020\), IOD impacts on Indian the Ocean](#)
2 [Carbon Cycle, Journal of Geophysical Research, <https://doi.org/10.1029/2020JC016485>.](#)
3
4 Van Damme, M., Clarisse, L., Whitburn, S., Hadji-Lazaro, J., Hurtmans, D., Clerbaux, C., and
5 Coheur, P.-F.: Industrial and agricultural ammonia point sources exposed, *Nature*, 564, 99-103,
6 10.1038/s41586-018-0747-1, 2018.
7
8 Vecchi, G. A., S.-P. Xie, and A. S. Fischer: Ocean-atmosphere co-variability in the western
9 Arabian Sea, *J. Climate*, 17, 1213–1224, 2004.
10
11 [Verreyken, B., Amelynck, C., Schoon, N., Müller, J.-F., Brioude, J., Kumps, N., Hermans, C.,](#)
12 [Metzger, J.-M., Colomb, A., and Stavrakou, T.: Measurement report: Source apportionment of](#)
13 [volatile organic compounds at the remote high-altitude Maïdo observatory, *Atmos. Chem.*](#)
14 [*Phys.*, 21, 12965–12988, <https://doi.org/10.5194/acp-21-12965-2021>, 2021.](#)
15
16 Verver, G. H. L., Sikka, D. R., Lobert, J. M., Stossmeister, G., and Zachariasse, M.: Overview
17 of the meteorological conditions and atmospheric transport processes during INDOEX 1999, *J.*
18 *Geophys. Res.*, 106, 28399–28413, 2001.
19
20 Wai, K. M., Wu, S., Kumar, A., and Liao, H.: Seasonal variability and long-term evolution of
21 tropospheric composition in the tropics and Southern Hemisphere, *Atmos. Chem. Phys.*, 14,
22 4859–4874, <https://doi.org/10.5194/acp-14-4859-2014>, 2014.
23
24 Waliser, D. E., Intraseasonal variability. *The Asian Monsoon*, B. Wang, Ed., Springer, 203–
25 258, 2006.
26
27 Waliser, D. E., and C. Gautier: A Satellite-derived Climatology of the ITCZ. *J. Climate*, 6,
28 2162–2174, [https://doi.org/10.1175/1520-0442\(1993\)006<2162:ASDCOT>2.0.CO;2](https://doi.org/10.1175/1520-0442(1993)006<2162:ASDCOT>2.0.CO;2), 1993.
29
30 Wang, S., Kinnison, D., Montzka, S. A., Apel, E. C., Hornbrook, R. S., Hills, A. J., et al., Ocean
31 biogeochemistry control on the marine emissions of brominated very short-lived ozone-
32 depleting substances: a machine-learning approach. *J. Geophys. Res.*, 124, 12319– 12339.
33 <https://doi.org/10.1029/2019JD031288>, 2019.
34
35 Wang, R., Balkanski, Y., Bopp, L., Aumont, O., Boucher, O., Ciais, P., Gehlen, M., Peñuelas,
36 J., Ethé, C., Hauglustaine, D., Li, B., Liu, J., Zhou, F., Tao, S.: Influence of anthropogenic
37 aerosol deposition on the relationship between oceanic productivity and warming, *Geophys.*
38 *Res. Lett.*, 42, 10,745– 10,754, doi:10.1002/2015GL066753, 2015.
39
40 Warneck, P.: The relative importance of various pathways for the oxidation of sulfur dioxide
41 and nitrogen dioxide in sunlit continental fair weather clouds, *Phys. Chem. Chem. Phys.*, 1,
42 5471–5483, 1999.
43
44 Watts, S. F.: The mass budgets of carbonyl sulfide, dimethyl sulfide, carbon disulfide and
45 hydrogen sulfide, *Atmos. Environ.*, 34, 761–779, 2000.
46
47 Webster, P. J., Moore, A. M., Loschnigg, J. P. and Leben, R. R. Coupled oceanic-atmospheric
48 dynamics in the Indian Ocean during 1997–98. *Nature*, 401, 356–360, 1999.
49
50 [Williams, J., Custer, T., Riede, H., Sander, R., Jöckel, P., Hoor, P., Pozzer, A., Wong-](#)
51 [Zehnpfennig, S., Hosaynali-Beygi, Z., Fischer, H., Gros, V., Colomb, A., Bonsang, B., Yassaa,](#)

1 [N., Peeken, I., Atlas, E.L., Waluda, C.M., van Aardenne, J.A., Lelieveld, J.: Assessing the effect](#)
2 [of marine isoprene and ship emissions on ozone, using modeling and measurements from the](#)
3 [South Atlantic Ocean, Environ. Chem., 7, 171–182, doi: 10.1071/EN09154, 2010.](#)

4
5 Williams, J., Fischer, H., Wong, S., Crutzen, P. J., Scheele, M. P., and Lelieveld, J.: Near
6 equatorial CO and O₃ profiles over the Indian Ocean during the winter monsoon: High O₃ levels
7 in the middle troposphere and interhemispheric exchange, *J. Geophys. Res.*, 107, 8007,
8 doi:10.1029/2001JD001126, 2002.

9
10 Wurl, O., Wurl, E., Miller, L., Johnson, K., and Vagle, S.: Formation and global distribution of
11 sea-surface microlayers, *Biogeosciences*, 8, 121–135, doi:10.5194/bg-8-121-2011, 2011.

12
13 Yamamoto, H., Yokouchi, Y., Otsuki, A., and Itoh, H.: Depth profiles of volatile halogenated
14 hydrocarbons in seawater in the Bay of Bengal, *Chemosphere*, 45, 371–377,
15 [https://doi.org/10.1016/S0045-6535\(00\)00541-5](https://doi.org/10.1016/S0045-6535(00)00541-5), 2001.

16
17 [Yang, J., Zhao, W., Wei, L., Zhang, Q., Zhao, Y., Hu, W., Wu, L., Li, X., Pavuluri, C. M., Pan,](#)
18 [X., Sun, Y., Wang, Z., Liu, C.-Q., Kawamura, K., and Fu, P.: Molecular and spatial](#)
19 [distributions of dicarboxylic acids, oxocarboxylic acids, and \$\alpha\$ -dicarbonyls in marine aerosols](#)
20 [from the South China Sea to the eastern Indian Ocean, Atmos. Chem. Phys., 20, 6841–6860,](#)
21 <https://doi.org/10.5194/acp-20-6841-2020>, 2020.

22
23 Yao, S.L., G. Huang, R.-G. Wu, X. Qu, and D. Chen: Inhomogeneous warming of the tropical
24 Indian Ocean in the CMIP5 model simulations during 1900–2005 and associated mechanisms,
25 *Clim. Dynam.*, 2016.

26
27 Ye, H., Sheng, J., Tang, D., Morozov, E., Kalhor, M. A., Wang, S., and Xu, H.: Examining
28 the Impact of Tropical Cyclones on Air-Sea CO₂ Exchanges in the Bay of Bengal Based on
29 Satellite Data and In Situ Observations, *J. Geophys. Res.*, 124, 555–576,
30 10.1029/2018jc014533, 2019.

31
32 Yoder, J. A., McClain, C. R., Feldman, G. C., and Esaias, W. E.: Annual cycles of
33 phytoplankton chlorophyll concentrations in the global ocean: A satellite view, *Global*
34 *Biogeochem. Cy.*, 7, 181–193, 10.1029/93gb02358, 1993.

35
36 Yoshida, Y., Ota, Y., Eguchi, N., Kikuchi, N., Nobuta, K., Tran, H., Morino, I., and Yokota,
37 T.: Retrieval algorithm for CO₂ and CH₄ column abundances from short-wavelength infrared
38 spectral observations by the Greenhouse gases observing satellite, *Atmos. Meas. Tech.*, 4, 717–
39 734, doi:10.5194/amt-4-717-2011, 2011.

40
41 Yu, L.: Global variations in oceanic evaporation (1958–2005): the role of the changing wind
42 speed. *J. Climate*, 20:5376–5390, 2007.

43
44 Zavarisky, A., Goddijn-Murphy, L., Steinhoff, T., and Marandino, C. A.: Bubble-Mediated Gas
45 Transfer and Gas Transfer Suppression of DMS and CO₂, *J. Geophys. Res.*, 123, 6624–6647,
46 10.1029/2017jd028071, 2018a.

47
48 Zavarisky, A., Booge, D., Fiehn, A., Krüger, K., Atlas, E., and Marandino, C.: The Influence of
49 Air-Sea Fluxes on Atmospheric Aerosols During the Summer Monsoon Over the Tropical
50 Indian Ocean, *Geophys. Res. Lett.*, 45, 418–426, 10.1002/2017gl076410, 2018b.

51

1 Zhang, N., Feng, M., Du, Y., Lan, J., Wijffels, S.E.: Seasonal and interannual variations of
2 mixed layer salinity in the southeast tropical Indian Ocean. *J. Geophys. Res.*, 121(7):4716–
3 4731, 2016.

4
5 Zheng, B., Tong, D., Li, M., Liu, F., Hong, C., Geng, G., Li, H., Li, X., Peng, L., Qi, J., Yan,
6 L., Zhang, Y., Zhao, H., Zheng, Y., He, K., and Zhang, Q.: Trends in China's anthropogenic
7 emissions since 2010 as the consequence of clean air actions, *Atmos. Chem. Phys.*, 18, 14095–
8 14111, <https://doi.org/10.5194/acp-18-14095-2018>, 2018.

9
10 Zhou, S., Gonzalez, L., Leithead, A., Finewax, Z., Thalman, R., Vlasenko, A., Vagle, S., Miller,
11 L. A., Li, S.-M., Bureekul, S., Furutani, H., Uematsu, M., Volkamer, R., and Abbatt, J.:
12 Formation of gas-phase carbonyls from heterogeneous oxidation of polyunsaturated fatty acids
13 at the air–water interface and of the sea surface microlayer, *Atmos. Chem. Phys.*, 14, 1371–
14 1384, <https://doi.org/10.5194/acp-14-1371-2014>, 2014.

15
16 Zhou, M., Langerock, B., Vigouroux, C., Sha, M. K., Ramonet, M., Delmotte, M., Mahieu, E.,
17 Bader, W., Hermans, C., Kumps, N., Metzger, J.-M., Duflot, V., Wang, Z., Palm, M., and De
18 Mazière, M.: Atmospheric CO and CH₄ time series and seasonal variations on Reunion Island
19 from ground-based in situ and FTIR (NDACC and TCCON) measurements, *Atmos. Chem.*
20 *Phys.*, 18, 13881–13901, <https://doi.org/10.5194/acp-18-13881-2018>, 2018.

21
22 Ziska, F., Quack, B., Abrahamsson, K., Archer, S. D., Atlas, E., Bell, T., Butler, J. H.,
23 Carpenter, L. J., Jones, C. E., Harris, N. R. P., Hepach, H., Heumann, K. G., Hughes, C., Kuss,
24 J., Krüger, K., Liss, P., Moore, R. M., Orlikowska, A., Raimund, S., Reeves, C. E.,
25 Reifenhäuser, W., Robinson, A. D., Schall, C., Tanhua, T., Tegtmeier, S., Turner, S., Wang, L.,
26 Wallace, D., Williams, J., Yamamoto, H., Yvon-Lewis, S., and Yokouchi, Y.: Global sea-to-
27 air flux climatology for bromoform, dibromomethane and methyl iodide, *Atmos. Chem. Phys.*,
28 13, 8915–8934, <https://doi.org/10.5194/acp-13-8915-2013>, 2013.

29
30 Zou, L.W., Zhou, T.J., Near future (2016–2040) summer precipitation changes over China as
31 projected by a regional climate model (RCM) under the RCP8.5 emissions scenario:
32 comparison between RCM downscaling and the driving GCM. *Adv. Atmos. Sci.*, 30:806–818,
33 2013.

34 35 36 37 38 Supplemental material

39 40 A) Atmospheric intraseasonal and interannual variability

41
42 Intraseasonal variability can impact atmospheric transport patterns over the Indian Ocean with
43 the dominant mode being the eastward propagating Madden-Julian Oscillation (MJO).
44 Equatorially trapped, baroclinic oscillations in the tropical wind field propagate slowly
45 eastward across the Indian Ocean, Maritime Continent, and West Pacific with an intraseasonal
46 cycle of 30–60 days (Madden and Julian, 1972). A typical MJO event exhibits large-scale
47 convection anomalies where enhanced convection and rainfall develop over the western Indian
48 Ocean with suppressed convection further east over the western Pacific (Zhang, 2005). The
49 eastward propagation of the convection and circulation anomalies depends on the season and is
50 strongest during the winter monsoon. The summer monsoon shows a north-eastward
51 propagation of the anomalies into Southeast Asia in addition to the eastward propagation along

1 the equator (Waliser, 2006). Among the many impacts of the MJO, strong interactions with
2 ocean surface fluxes of mass, heat, and momentum have been observed (e.g., Matthews et al.,
3 2010).

4 Similarly, modes of tropical interannual variability, such as the irregular oscillation of sea
5 surface temperatures known as the Indian Ocean Dipole (IOD), play a role for Indian Ocean
6 meteorology. The positive phase of the IOD is characterised by positive sea surface temperature
7 anomalies in the western part of the Indian Ocean accompanied by negative anomalies in
8 eastern part (Saji et al., 1999). The initial cooling off the coast of Sumatra–Java leads to a
9 positive feedback mechanism via suppressed local convection, anomalous easterly winds, a
10 shoaling thermocline and stronger upwelling, which in turn reinforce the initial cooling with a
11 peak from September to November (Cai et al., 2014). Extreme positive IOD events can also
12 impact the equatorial ocean by inducing a north-westward extension of the south-easterly trades
13 and drying along the equatorial Indian Ocean (Webster et al., 1999).

14 The dominant mode of interannual climate variability of the Pacific, the El Niño–Southern
15 Oscillation (ENSO), can also impact Indian Ocean sea surface temperatures via anomalous
16 wind stress forcing (Latif and Barnett, 1995). In addition, ENSO modulates the depth of the
17 Indian Ocean thermocline and contributes to changes in salinity due to shifts in rainfall and
18 evaporation. The potential impact of ENSO on the IOD is currently under discussion (Stuecker
19 et al., 2017 and references therein).

20 **B.) Regional Oceanic Transport**

21 **Southern Indian Ocean**

22 The South Equatorial Current (SEC) in the Indian Ocean carries water masses entering through
23 the Indonesian passages, with a relative salinity minimum in the Indian Ocean environment,
24 via broad zonal inflow westward. Driven by the sSoutheast tTrades, the SEC supplies the
25 western boundary currents east of Madagascar. Part of the throughflow water in the SEC forms
26 the northern East Madagascar Current (EMC), which partly passes in southward moving eddies
27 through the Mozambique Channel and merges into the Agulhas (Ridderinkhof and de Ruijter,
28 2003; Schouten et al., 2003).

29 Data from satellite altimetry suggest that the eastward South Indian Countercurrent (SICC) is
30 already present in the Mozambique Basin, southwest of Madagascar (Siedler et al., 2006). The
31 eastward frontal SICC coincides with the thermohaline front that separates the saline
32 subtropical surface water from the fresher tropical surface water in the EMC in summer
33 (Palastanga et al., 2007). The variability of SST and salinity is high in the warm waters south
34 to south-east of Madagascar, likely due to eddy activity and upwelling. There is year-round
35 coastal upwelling along the southern stretch of the oligotrophic EMC and in the shallower
36 region just to the south of Madagascar, which leads to enhanced phytoplankton growth (Quartly
37 et al., 2006). All productivity further from the island in bands of relatively high variability along
38 25°S and along the EMC are due to a combination of local upwelling caused by eddies and,
39 more importantly, the advection of upwelled coastal waters around eddy features. The
40 anticyclones moving through the region wrap both the warm EMC waters and the nutrient-rich
41 upwelled waters into well-defined arcs. Occasionally strands of chlorophyll-rich water can
42 stretch 500 km or more eastward, which are caused by the combined effects of both cyclonic
43 and anticyclonic eddies (Quartly et al., 2006). The southward flowing EMC, as part of the
44 bifurcated SEC, and the SEC form the western and northern boundary currents of the South
45 Indian subtropical gyre, where saline surface water is formed, as there is more evaporation than
46 precipitation in this region (Schott et al., 2009). The south-eastern Indian Ocean shows the
47 strongest interannual to decadal variability of upper-ocean salinity in the Indian Ocean.
48 Seasonality of the mixed layer salinity in the south-eastern tropical Indian Ocean is influenced

1 by the annual cycles of the Indonesian Throughflow and the Leeuwin Current transports,
2 freshwater forcing, and eddy fluxes (Zhang et al., 2016).

3 Open ocean upwelling associated with the Seychelles dome, a thermocline ridge in the southern
4 tropical gyre can occur between 5 and 10°S, along the northern edge of the southeast trades,
5 where Ekman divergence occasionally appears to be strong enough to upwell subsurface waters
6 into the mixed layer (Schott et al., 2009). In this region, the South Equatorial Countercurrent
7 (SECC) flows eastward year-round, fed by the East African Coastal Current (EACC) and
8 forming the northern flank of the southern Indian Ocean tropical gyre. Low sea surface height
9 is the signature of the Indian Ocean's tropical gyre, bounded in the north by the SECC, to the
10 south by the SEC, and at the western boundary by the EACC.

11 12 **Northern Indian Ocean**

13 During the summer monsoon, the northward flowing Somali Current is supplied by the SEC
14 and EACC. Once the Somali Current crosses the equator, a part of it turns offshore around 4°N
15 and another part returns across the equator as a part of the southern gyre. A northern gyre occurs
16 north of the Equator and occasionally a third gyre can be observed in many summer monsoons
17 (Schott et al., 2009). These gyres influence the stability of the atmospheric planetary boundary
18 layer, impacting surface wind stress and heat fluxes (Vecchi et al., 2004). Furthermore, the
19 Southwest Monsoon Current flows towards the east, south of Sri Lanka, then turns to flow
20 toward the north, bringing saltier Arabian Sea water into the Bay of Bengal (Jensen, 2003). In
21 contrast, the Somali Current flows southward during the winter monsoon to meet the northward
22 flowing EACC. They supply water for the eastward flowing SECC. The Northeast Monsoon
23 Current flows toward the west, bringing fresher Bay of Bengal water into the Arabian Sea
24 (Schott et al., 2009). In addition, model studies have suggested that Bay of Bengal water flows
25 across the equator in the eastern basin in the winter monsoon (Han and McCreary, 2001; Jensen,
26 2003).

27 Unique to the Indian Ocean are strong eastward ocean surface jets during the inter-monsoon
28 period, called Wyrтки Jets. They are produced by the semi-annual westerly equatorial winds and
29 are important because they carry warm upper layer waters toward the east, which increases sea
30 level and mixed layer depth in the east and decreases them in the west. These semi-annual
31 westerlies are the reason for another unique Indian Ocean feature, namely the eastward
32 Equatorial Undercurrent that is only present for a part of the year (i.e. February – June) when
33 the winds have an easterly component (Schott et al., 2009; Reppin et al., 1999).

34